R-07-20

Updated strategy and test of new concepts for groundwater flow modelling in Forsmark in preparation of site descriptive modelling stage 2.2

Sven Follin, SF GeoLogic AB

Per-Olof Johansson, Artesia Grundvattenkonsult AB

Jakob Levén, Geosigma AB

Lee Hartley, David Holton
Rachel McCarthy, David Roberts
Serco Assurance

January 2007

Svensk Kärnbränslehantering AB
Swedish Nuclear Fuel
and Waste Management Co
Box 5864
SE-102 40 Stockholm Sweden
Tel 08-459 84 00
+46 8 459 84 00
Fax 08-661 57 19
+46 8 661 57 19

ISSN 1402-3091
SKB Rapport R-07-20

Updated strategy and test of new concepts for groundwater flow modelling in Forsmark in preparation of site descriptive modelling stage 2.2

Sven Follin, SF GeoLogic AB

Per-Olof Johansson, Artesia Grundvattenkonsult AB

Jakob Levén, Geosigma AB

Lee Hartley, David Holton
Rachel McCarthy, David Roberts
Serco Assurance

January 2007

Keywords: Hydrogeology, Groundwater head, Hydrogeochemistry, Interference test, Numerical modelling.

Abstract

As part of the preliminary Site Descriptive Modelling (SDM version 1.2) for the Initial Site Investigation (ISI) stage at Forsmark, Simpevarp and Laxemar, a methodology was developed for constructing hydrogeological models of the crystalline bedrock. The methodology achieved reasonable success given the restricted amounts and types of data available at the time. Notwithstanding, several issues of concern have surfaced following the reviews of the preliminary site descriptions of the three sites. Possible solutions to parts of the problems have been discussed internally for a longer time and an integrated view and strategy forward has been formulated. The "new strategy" is not a complete shift in methodology, however, but a refocusing on and clarification of the key aspects that the hydrogeological SDM needs to accomplish. In broad terms the basic principle of the "new strategy" suggested is to develop an overall conceptual model that first establishes the major flowing deformation zones, and then gradually approaches determination of the hydraulic properties of the bedrock outside these zones in the potential repository volume. On each scale, the focus of the description should be on features/structures of significance on that scale. Clearly, a detailed (although statistical) description of the repository and canister deposition hole scale is the end goal, but this approach (which also is more the traditional approach in hydrogeology) is judged to provide a much better motivated overall geometrical description. Furthermore, the "new strategy" puts more emphasis on field testing (e.g. interference tests) and data analyses and less on numerical simulation and calibration. That is, before extensive (and costly) simulations and model calibrations are made it needs to be clearly understood what could be the potential gains of carrying them out.

This report presents the conceptual model development for Forsmark in preparation of the site descriptive modelling in stage 2.2. Four 'pre-modelling' exercises have been performed to develop and test the methodology issues. These exercises are not directly aimed at a model update, but more intended to provide some insight into new aspects of the modelling methodology and the use of field data, and therefore provide background support also for the upcoming final SDM. Some of the issues treated for the SDM of the Forsmark site are also of interest for the SDM of the Laxemar site.

Sammanfattning

Inom ramen för de preliminära platsbeskrivningarna av förhållandena i Simpevarp, Forsmark och Laxemar (’SDM version 1.2’) utvecklades en metodik för hydrogeologisk modellering av kristallint berg. Metodiken fungerade förhållandevis väl med tanke på den tämligen begränsade tillgången på data efter det inledande platsundersökningsskedet. De granskningar som utförts, såväl internt som externt, har emellertid ställt flera berättigade frågor. Möjliga lösningar har diskuterats en längre tid och en integrerad syn och strategi inför det kompletta platsundersökningsskedet har presenterats. Den ”nya strategin” innebär inte att metodiken är helt och hållet utbytt, utan är snarare en fokusering på och förtydligande av de nyckelfrågor som den hydrogeologiska delen av platsbeskrivningen måste svara på. I stora drag handlar den ”nya strategin” om att utveckla en övergripande konceptuell modell som börjar med att först beskriva de viktigaste vattenförande sprickzonerna och därefter successivt närma sig karaktäriseringen av de hydrauliska egenskaperna i berggrunden mellan dessa zoner i det tilltänkta förvarsområdet. I varje skala skall den konceptuella modellen fokusera sig på att beskriva de viktigaste strukturerna i den aktuella skalan. Alldeles uppenbart är huvudmålet att uppnå en (statistsik) beskrivning av de hydrogeologiska förhållandena i förvarsområdet närmast kapselpositionerna. I sak är det ingenting nytt, men synsättet att fokusera den hydrogeologiska modelleringen på de viktigaste strukturerna i varje skala bedöms leda till en bättre motiverad geometrisk beskrivning. Vidare betonar den ”nya strategin” betydelsen av fältundersökningar, t ex interferenstester, och dataanalyser framför numeriska simuleringar och kalibrering. Med andra ord, innan omfattande (och dyra) simuleringar och modellkalibreringar görs måste syftet med dessa och vilka resultat som förväntas vara fullständigt klarlagt.

Föreliggande rapport presenterar utvecklingen av den konceptuella modellen för Forsmark och statusen av densamma inför platsmodelleringssteget 2.2. Fyra ”förmodelleringsövningar” har genomförts i syfte att utveckla och testa olika koncept och modelleringsmetodiker. Modelleringsövningarna ska betraktas som ett hjälpmedel till den slutliga platsbeskrivningen för Forsmark. Tonvikten i de numeriska simuleringarna ligger på att testa den konceptuella modellens utveckling och hur man bäst ska kunna representera de fältdata som ligger till grund för denna. Några av de frågor som hanteras i denna rapport bedöms också vara av intresse för platsbeskrivningen i Laxemar.

Contents

1 Introduction

1.1 Background

As part of the preliminary Site Descriptive Modelling (SDM) for the Initial Site Investigation (ISI) stage at Forsmark, Simpevarp and Laxemar, a methodology was developed for constructing hydrogeological models of the crystalline bedrock. The methodology combined a deterministic representation of the major deformation zones (DZ) with a stochastic representation of the less fractured bedrock outside these zones using a Discrete Fracture Network (DFN) concept.

The DZ and DFN models were parameterised hydraulically with data from single-hole Posiva Flow Log (PFL-f and PFL-s) pumping tests and single-hole Pipe String System (PSS 5 m, 20 m and 100 m) injection tests, see /Follin et al. 2005/ and /Hartley et al. 2005/. The hydrogeological descriptions of the major deformation zones and the less fractured bedrock outside these zones were referred to as Hydraulic Conductor Domains (HCD) and Hydraulic Rock Domains (HRD), respectively.

The HCD and HRD formed the basis for constructing regional-scale Equivalent Continuum Porous Medium (ECPM) flow models, which were used to simulate the palaeo-hydrogeological-hydrogeochemical evolution over the last 10,000 years (Holocene), as a coupled process between groundwater flow and the hydrodynamic transport of several reference waters including the process of rock-matrix diffusion. Results obtained from these simulations included a prediction of hydrogeochemical constituents (e.g. major ions and environmental isotopes) for the present-day situation along boreholes which could be compared with corresponding groundwater samples acquired from the sites. By comparing the model predictions with measurements the models developed could be partially calibrated to improve model parameterisation, improve our understanding of the hydrogeological system, and help build confidence in the conceptual models developed for the sites.

The methodology achieved reasonable success given the restricted amounts and types of data available at the time. Notwithstanding, several issues of concern have surfaced following the reviews of the preliminary site descriptions of the three sites conducted internally by SKB's modelling teams /SKB 2005a/, by SKB's external review group (SIERG) and by the SKI's international review group (INSITE) /SKI 2005/. Moreover, the safety implications of the preliminary site descriptions have been assessed in the Preliminary Safety Evaluations (PSE) /SKB 2005b/ and in SR-Can /SKB 2006b/.

The issues raised both internally and externally, as well as the feedback obtained from the Safety Assessment work are essentially in agreement. In short the main concerns are:

- There is a need to extend the discussion on the applicable conceptual model in the context of the data found. Issues that should be discussed include is there an indication that deformation zones are more conductive than the surrounding bedrock? Is there any data support for dividing HRDs into different sub domains? What is the statistical significance of potential depth dependence?
- Design and Safety Assessment need detailed information (repository and canister scale information). Thus, using better-motivated conceptual models, there is also a need to provide more robust estimates of the hydraulic and transport properties of HRDs in the repository volume. It needs to be more firmly assessed to what extent model properties are based on "hard to verify" assumptions about DFN-properties (connectivity, size vs transmissivity correlation), extrapolation of data over unexplored volumes and what is more insensitive to these assumptions. An approach starting from simple descriptions and gradually testing the significance of more complex hypotheses should be tried.

- Matching hydrogeology and hydrogeochemistry is important a potentially powerful means of enhancing confidence in the modelling. However, a realistic expectation on what can be achieved – and what us unattainable is needed. There is a need to more critically assess the significance of calibration against existing hydrogeochemical data. Is the "mixing" process correctly modelled, given the fact that many species dissolved in the groundwater are not conservative tracers? Are the hydrogeochemical data really sensitive to the hydrogeological parameters and are there other, not tested assumptions, which would have a larger impact? That is, are shown fits with chemical data more coincidental than actual proofs?
- There is also a need to explore possibilities to carry out additional measurements, possible tracer tests, in order to at least partially validate the hard to prove assumptions in the up-scaling using the DFN-approach. However, the need for such experiments must also be related to the realism in actually carrying them out. For example, testing the DFN-model in a multi-hole interference and tracer test is only realistically performed from the underground. There will be remaining uncertainties – and thus also different alternative interpretations – after the conclusion of the surface based investigations.
- Finally, there is also a need to revise the presentation of the hydrogeological modelling in the SDM such that it is clear what is the resulting hydrogeological description and what are analyses (including simulations) made in support of this description.

These issues will require satisfactory resolution as the site investigation work moves towards completion. In particular, the use of the integrated hydrogeological, hydrogeochemical and transport modelling has identified the need for more robust discipline consistent and 'partially validated' models to be produced by the final Site Descriptive Modelling (SDM stage 2.3) for the Complete Site Investigation (CSI) stage.

Possible solutions to parts of the problems have been discussed internally for a longer time and an integrated view and strategy forward has been formulated and presented to INSITE's experts on flow and transport at a meeting 2006-06-16. The "new strategy" is not a complete shift in methodology, however, but a refocusing and clarification of the key aspects of the hydrogeological SDM:

- assessing the current understanding of the hydrogeology at the analysed site, and
- providing the hydrogeological input descriptions needed for the end users, Design, Safety Assessment and Environmental Impact Assessment. The input descriptions should especially focus on properties in the potential repository volumes of the explored sites and assess the distribution flow paths at potential repository depth.

In broad terms the basic principle of the "new strategy" suggested is to develop an overall conceptual model that first establishes the major flowing deformation zones, and then gradually approaches determination of the hydraulic properties of the bedrock outside these zones in the potential repository volume. On each scale, the focus of the description should be on features/structures of significance on that scale. Clearly, a detailed (although statistical) description of the repository and canister deposition hole scale is the end goal, but this approach (which also is more the traditional approach in hydrogeology) is judged to provide a much better motivated overall geometrical description.

Furthermore, the "new strategy" puts more emphasis on field testing (e.g. interference tests) and data analyses and less on numerical simulation and calibration. That is, before extensive (and costly) simulations and model calibrations are made it needs to be clearly understood what could be the potential gains of carrying them out.

Figure 1-1 outlines the modelling steps associated with the "new strategy". In the work presented here we focus on developing the contents of Step 1 and Step 2. In the hydrogeological reporting for Forsmark stage 2.2 these two steps will be revisited (e.g. updated with regard to Data Freeze 2.2) and accompanied by work associated with Step 3 and Step 4. In the final hydrogeological reporting for Forsmark, i.e. SDM stage 2.3, all steps will be revisited (e.g. updated with regard to Data Freeze 2.3) although the focus will be put on Step 4 and Step 5.

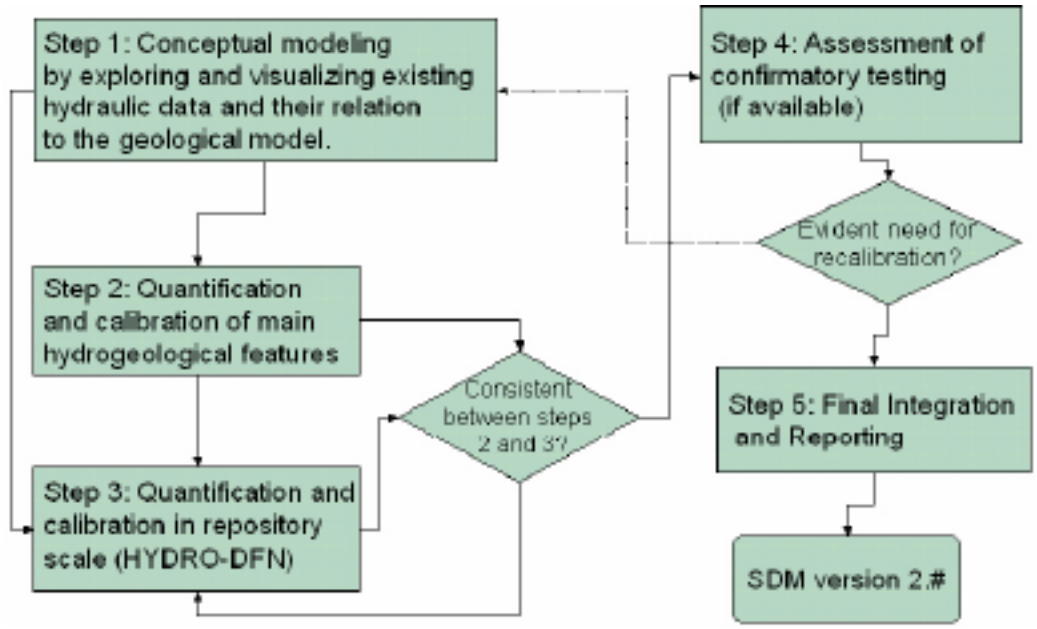

Figure 1-1. *Overall flow chart of the hydrogeological modelling suggested for the final Site Descriptive Modelling (SDM stage 2.3) of the Complete Site Investigation (CSI) stage.*

1.2 Scope and objectives

For the Complete Site Investigation (CSI) programme stages 2.1–2.3, new types of hydrogeological data will be available and in greater amounts, and hence the methodology needs to advance to integrate this new information. The integration of the new types of hydrogeological data is under development and the work presented in this report demonstrates the procedure, which will be used in the final SDM.

Four types of data are planned to be used in the hydrogeological modelling for the final SDM in Forsmark, see Figure 1-2:

- Item A – modelling the hydrogeological DFN (Hydro-DFN) properties of the less fractured bedrock outside the deterministically modelled deformation zones using geometrical and hydraulic data from single-hole investigations and tests.
- Item B – modelling the interplay between surface hydrology and near-surface and bedrock hydrogeology; that is, recharge and discharge.
- Item C – modelling the palaeo-hydrogeological-hydrogeochemical evolution in the bedrock during the Holocene using an ECPM model formulation for advective flow in the interconnected network of open fractures and diffusion into the fractured matrix outside it.
- Item D – modelling the test responses of large-scale interference tests; that is, matching the hydraulic diffusivities deduced from a large number of observation intervals..

In operation, four ‘pre-modelling’ exercises have been performed to develop and test the methodology issues in time for the upcoming hydrogeological modelling studies stages 2.2 and 2.3. These exercises are not directly aimed at a model update, but more intended to provide some insight in to new aspects of the modelling methodology and the use of field data, and therefore provide background support also for the upcoming final SDM. Some of the issues will also be of interest for the SDM of the Laxemar site.

Three of the four ‘pre-modelling’ exercises are treated in the work reported here, whereas the fourth exercise is treated in the work by /Follin et al. 2007/.

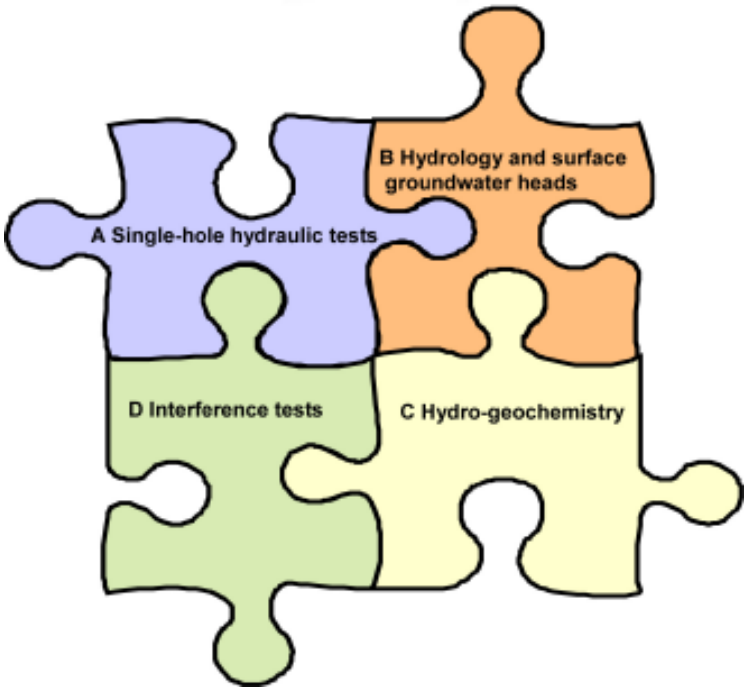

Figure 1-2. *Four key types of data are planned to be used in the hydrogeological modelling for the final SDM in Forsmark. The integration of the four types of data is under development and the work presented in this report demonstrates the procedure, which will be used in the final SDM.*

1.2.1 Sensitivity of Poissonian DFN models to parameter heterogeneity

A provisional application of the Hydro-DFN modelling approach suggested for Forsmark was presented in the hydrogeological background reports of the preliminary SDM, see /Follin et al. 2005/ and /Hartley et al. 2005/. The modelling approach is based on two important geometrical assumptions:

- a Poisson process for the locations of the fractures centres in space, and
- a power-law frequency distribution for the fracture sizes.

The rationale for invoking these two assumptions are discussed in the preliminary geological DFN background reports of the preliminary SDM, see /La Pointe et al. 2005, Darcel et al. 2006/.
An important mathematical implication is that the fracture intensity is also power-law distributed, i.e. size and intensity are correlated. Fracture intensity can be expressed in several ways depending on the number of Euclidian dimensions considered. In three dimensions, intensity means fracture surface area per unit volume of rock, commonly denoted by P_{32}. The fracture surface area per unit volume of rock is linearly proportional to the one-dimensional entity known as fracture frequency, commonly denoted by P_{10}. The proportionality factor between P_{10} and P_{32} is one of many factors addressed in structural analysis of borehole fracture data. The possibility of the Posiva Flow Log to detect individual flowing fractures provides a tool for the important assessment of the frequency (and orientation) of flowing features, i.e. $P_{10,PFL}$. A vital notion suggested by /Follin et al. 2005/ is that flow can only occur in *connected open fractures*, *cof*, which implies that $P_{32,cof} \propto P_{10,PFL}$. This concept is the basis for the DFN modelling conducted for SDM stage 2.3.

Hydrogeological DFN (Hydro-DFN) modelling constitutes a cornerstone for Design and Safety Assessment. Hydro-DFN modelling entails a great deal of structural geology, vector algebra, percolation theory, statistical-numerical simulation techniques as well as detailed knowledge about the hydraulic test methods used. It is recognised that most reviewers found the Hydro-DFN section in the preliminary SDM /SKB 2005a/ to be one of the most difficult to read. The objective of the Hydro-DFN 'pre-modelling' exercise is to investigate the sensitivity of the *connected open fracture surface area per unit volume of rock*, i.e. $P_{32,cof}$, to the observed heterogeneities in:

- the Fisher orientation model concentration factor, κ (kappa),
- the power-law size distribution (shape and location) parameters, k_r and r_0, and
- the fracture intensity of *open* fractures, $P_{32,open}$ ($r \geq r_0$).

It is repeated that the Hydro-DFN 'pre-modelling' exercise is treated in /Follin et al. 2007/, i.e. outside the work reported here.

1.2.2 Hydraulic cage modelling

The objective of this task is to match the point-water heads observed in the uppermost part of the bedrock and the generic head condition in the Quaternary deposit using the representative case equivalent continuum porous medium (ECPM) flow model from SR-Can F1.2 /Hartley et al. 2006a/ as a start and then introduce a high transmissive near-surface stratum. The strands of evidence for assuming such a model simplification is treated in Chapter 2 and the numerical modelling undertaken in the work reported here is presented in Chapter 3.

1.2.3 Palaeo-hydrogeological-hydrogeochemical modelling

The objective of this task is to match the hydrogeochemistry data from Data Freeze 2.1 using the modified flow model derived in the hydraulic cage modelling presented in Chapter 3. Of particular interest here is the matching of near-surface hydrogeochemistry data and data from the matrix as acquired in borehole KFM06A. The numerical modelling undertaken in the work reported here is presented in Chapter 4.

1.2.4 Interference test modelling

The objective of this task is to test the calibrated flow model derived in Chapters 3 and 4 with regard to the responses observed during 'Jakob's Interference Test' (explained in Section 2.1.4). The simulation results of this test are fairly preliminary since there are several structures present in the representative case equivalent continuum porous medium (ECPM) flow model from SR-Can F1.2 that are not included in the deformation model presented in stage 2.1 /SKB 2006a/. That is, the F1.2 deformation model does not reflect some of the structural components required to match the cross-hole test responses observed. Notwithstanding, the numerical modelling undertaken in the work reported here is presented in Chapter 5.

1.3 This report

This report is divided into two main parts. Part 1 presents a summary of the conceptual model development for Forsmark based on hydrogeological field observations up to Data Freeze 2.1. To a limit extent data gathered between Data Freeze 2.1 and Data Freeze 2.2 have been incorporated. Part 2 describes numerical modelling to illustrate this conceptual model and test it against field data available up to Data Freeze 2.1. The main objective is to test the main principles outlined in the conceptual model development and check for inconsistencies and possible model improvements in preparation for Forsmark stage 2.2. Part 1 is wholly covered by Chapter 2. Part 2 is treated in Chapters 3 through 5.

The data collection and conceptual model development up to Data Freeze 2.1 is previously described in /SKB 2006a/. A key component of the 2.1 conceptual model development is the notion of a 'hydraulic cage'. This notion refers to the particular hydraulic behaviour observed in the uppermost part of the bedrock, where the hydraulic gradient is found to be quite low and non-correlated with topography. It is suggested that this phenomenon results from a dense lattice of interconnected, transmissive structures occurring in the uppermost c. 150 m of the bedrock inside the tectonic lens. Presumably, the 'hydraulic cage' phenomenon is centred on the area where the gently-dipping deformation zone ZFMNE00A2 is outcropping, which is in the north-western part of the candidate area. Many of the structures forming this lattice can be associated with outcropping deformation zones but another key component of this lattice is the often high yielding horizontal fractures/sheet joints associated with stress release in the uppermost part of the bedrock. Chapter 2 is written with a particular focus on the different strands of field evidence that support the 'hydraulic cage' concept.

Chapter 3 describes a model that considers how near-surface groundwater head data can be used to calibrate the near-surface hydrogeology.

The modelling of the evolution of the hydrogeochemistry using data acquired in deformation zones was demonstrated in the background reports to the preliminary SDM /SKB 2005a/, see /Follin et al. 2005/ and /Hartley et al. 2005/. In Chapter 4 we look at the implications of the new conceptual model in hydrogeology for hydrogeochemistry. A major difference with regard to the modelling conducted in preparation for the preliminary SDM is the extended hydrogeochemical data set from Data Freeze 2.1, in particular the pore water chemistry.

The ongoing development of the flow model to encompass a new type of hydraulic information from large-scale interference tests for calibrating numerical flow models is reported in Chapter 5.

It is noted that the conclusions drawn in the work presented here are presented at the end of each chapter dealing with the numerical modelling of the 'pre-modelling' exercises, respectively. That is, there is not a separate chapter with overall, main conclusions since many input data sets, which govern the model set-up, will change in due time in time for the hydrogeological modelling for Forsmark stage 2.2, e.g. the deformation zone model.

1.4 Limitations

The focus of the work reported here is put on the conceptual model development and the ongoing development of the numerical modelling of items B–D. The reader is kindly referred to the hydrogeological background reports of the preliminary SDM for Forsmark /SKB 2005a/, i.e. /Follin et al. 2005/ and /Hartley et al. 2005/, and to the hydrogeological background report of the preliminary safety assessment for Forsmark (SR-Can) /SKB 2006b/, i.e. /Hartley et al. 2006a/, for a detailed description of:

- the geometry of the deformation zone model,
- the motives for the size of the model domain chosen,
- the initial and boundary conditions chosen, and
- the hydraulic properties of the DFN, the deformation zones, and the Quaternary deposits used in stage 1.2.

The numerical modelling exercises were all based on the representative case equivalent continuum porous medium (ECPM) flow model from SR-Can F1.2 /Hartley et al. 2006a/, with appropriate changes based on new information.

1.5 Hydrogeological reports for Forsmark stage 2.2

Two hydrogeological reports dealing with bedrock hydrogeology are envisaged for Forsmark stage 2.2. The first report presents the hydraulic data acquired in cored and percussion-drilled boreholes up to Data Freeze 2.2. The objective is to describe the hydrogeological properties of the near-surface bedrock, the deformation zones and the sparsely fractured bedrock outside (between) these zones.

The second report mimics the structure of the work presented here; that is, it is divided into two parts, where Part 1 presents a summary of the conceptual model development for Forsmark based on hydrogeological field observations up to Data Freeze 2.2, and Part 2 describes numerical modelling to illustrate this conceptual model and test it against field data available up to Data Freeze 2.2. Again, the main objective of the numerical modelling is to test the main principles outlined in the conceptual model development and check for inconsistencies and model improvements.

2 Summary of the conceptual model development prior to Data Freeze 2.2

2.1 Boreholes and hydraulic borehole investigations

The geological and hydraulic data acquired from the geological mapping and hydraulic testing of boreholes constitute cornerstones in the development of the hydrogeological conceptual model. Below follows a brief summary of the drilling campaigns and the different hydraulic borehole investigations carried out in Forsmark. Data from Data Freezes 1.1–2.1 were presented in /SKB 2004, 2005, 2006a/.

2.1.1 Single-hole bedrock investigations

Figure 2-1 shows a map of completed, ongoing and planned core-drilled boreholes (KFMxxx). The map in Figure 2-2 shows the corresponding information for the percussion-drilled boreholes (HFMxx). The geological map in these two figures represents the interpretation from stage 1.2 /SKB 2005a/. Table 2-1 lists the boreholes with regard to the geological information acquired at the time of the different Data Freezes (modelling stages). Currently, there are 25 core-drilled and 38 percussion-drilled boreholes planned for the site investigations in Forsmark. Table 2-2 lists which of the cored boreholes that are or will be investigated with the Posiva Flow Log (PLF) unit and the Pipe String System (PSS) unit, respectively. All percussion-drilled boreholes are investigated with the HTHB unit (combined pumping and impeller flow logging) except those with a very low yield.

Table 2-1. List of completed and planned cored and percussion-drilled boreholes with regard to the different Data Freezes in Forsmark.

Data Freeze	No. of core drilled boreholes	KFMxxx	No. of percussion drilled boreholes	HFMxx
1.1 2003-04-30	1	KFM01A	8	HFM01–08
1.2 2004-07-31	5	KFM02A-05A KFM01B	11	HFM09–19
2.1 2005-07-29	4	KFM06A–07A KFM03B, -06B	3	HFM020–22
2.2 2006-09-30	11	KFM08A–10A KFM06B–09B KFM01C, KFM07C–08C KFM01D	10	HFM23–32
2.3 2007-03-31	4	KFM11A–12A KFM02B KFM08D	6	HFM33–38
All	25	KFM01A–12A KFM01B–03B KFM06B–09B KFM01C, KFM07C–08C KFM01D, -08D	38	HFM01–38

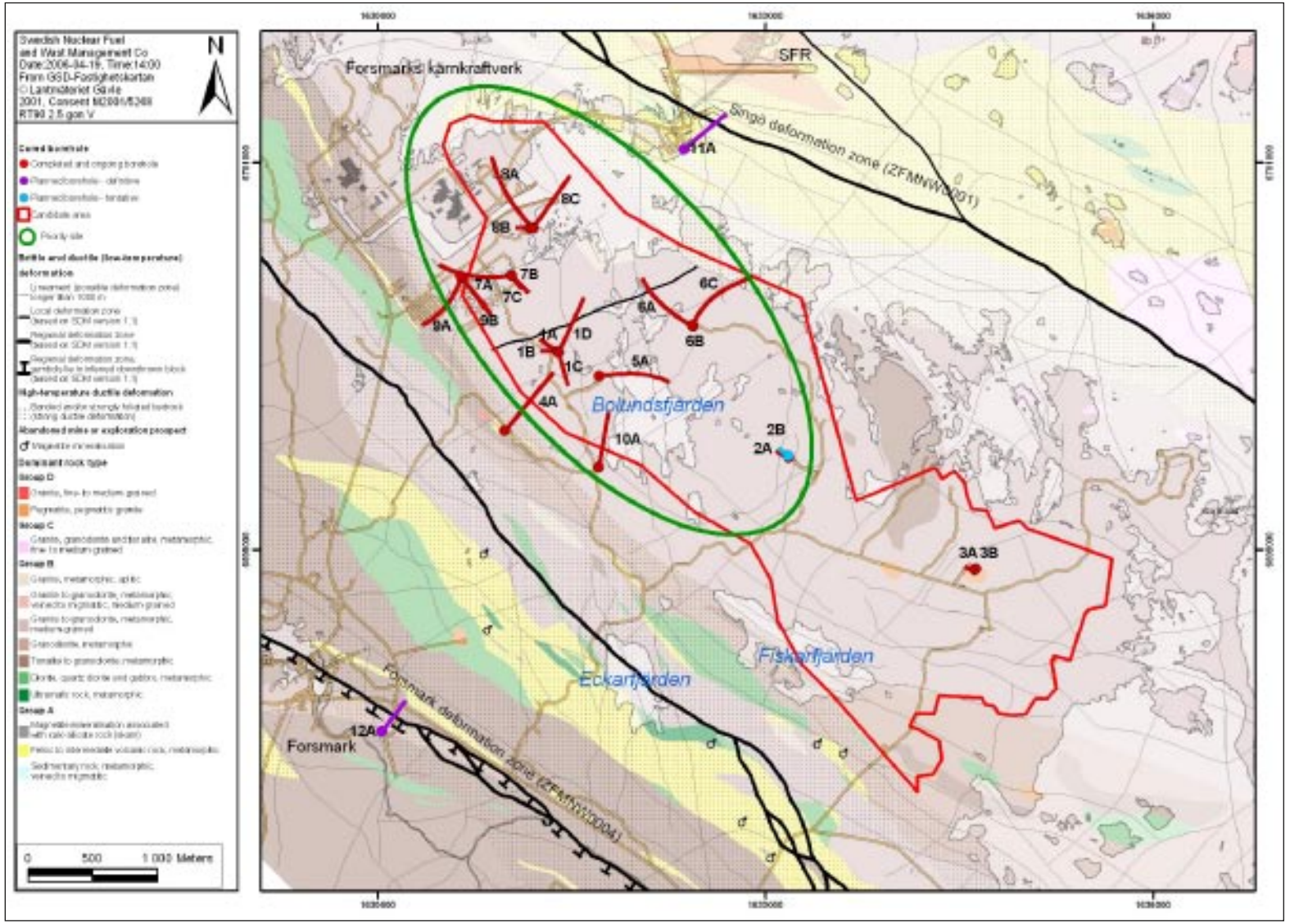

Figure 2-1. *Completed, ongoing and planned core drilled boreholes in Forsmark (2006-05-31). The underlying geological map is from stage 1.2 /SKB 2005a/. The green ellipse shows the location of the so-called target area (priority site).*

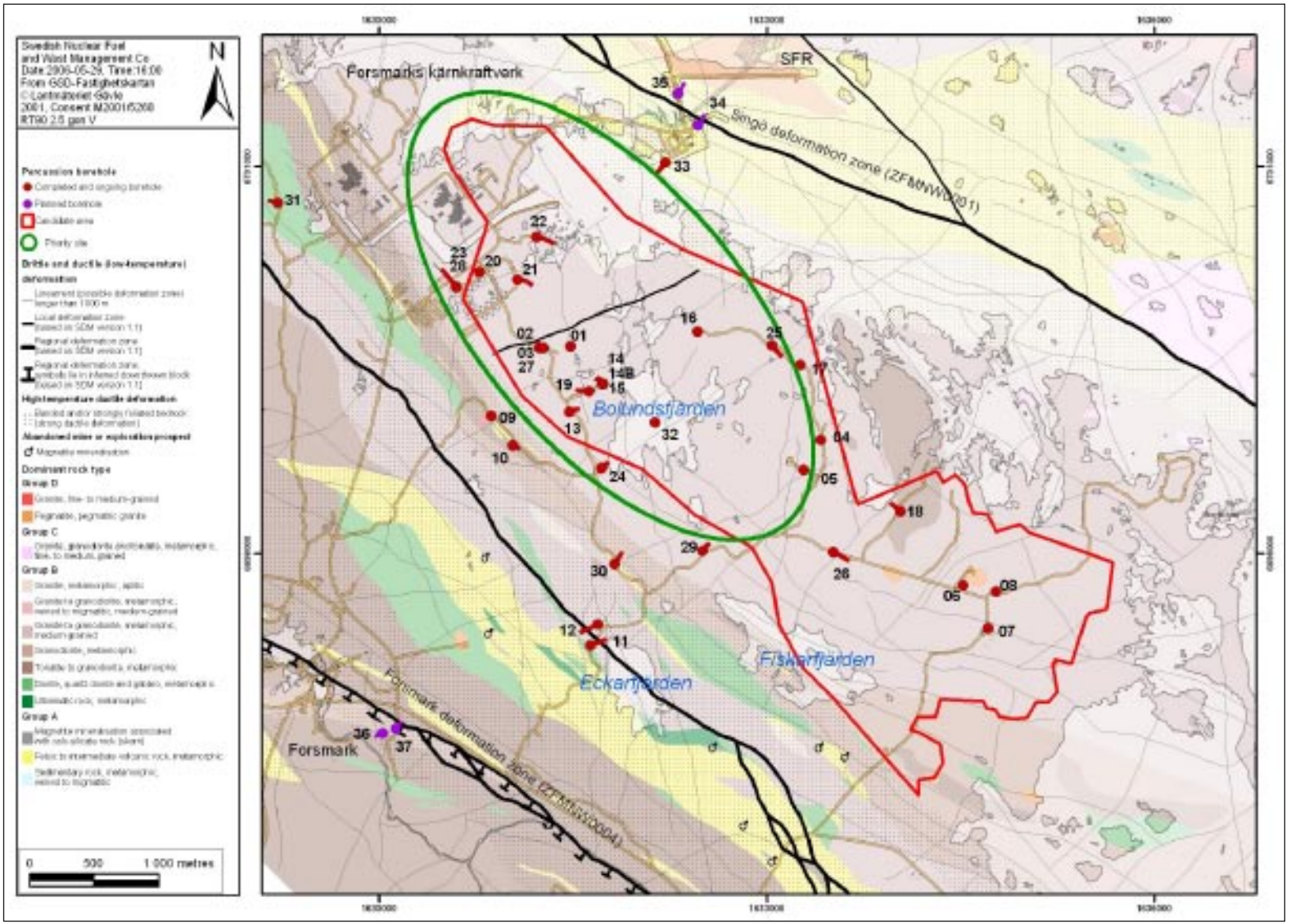

Figure 2-2. *Completed and upcoming percussion drilled boreholes in Forsmark (2006-05-31). The underlying geological map is from stage 1.2 /SKB 2005a/. The green ellipse shows the location of the so-called target area (priority site).*

Table 2-2. List of completed and planned PFL-f and PSS tests in Forsmark.

Data Freeze	No. of PFL-f tested boreholes	PFL-f tested boreholes KFMxxx	No. of PSS tested boreholes	PSS tested boreholes KFMxxx
1.1 *2003-04-30*	1	KFM01A	0	–
1.2 *2004-07-31*	4	KFM02A–05A	3	KFM01A–03A
2.1 *2005-07-29*	2	KFM06A–07A	6	KFM04A–07A KFM03B, -06B
2.2 *2006-09-30*	5	KFM08A, -10A KFM07C–08C KFM01D	8	KFM08A–09A KFM07B–09B KFM01C, -06C KFM01D
2.3 *2007-03-31*	3	KFM11A KFM02B KFM08D	5	KFM10A–12A KFM07C–08C
All	15	KFM01–08A KFM10A–11A KFM02B KFM07–08C KFM01D, -08D	22	KFM01A–12A KFM03B KFM06B–09B KFM01C KFM06C–08C KFM01D

2.1.2 Cross-hole bedrock investigations

Table 2-3 shows completed, ongoing and upcoming pumping tests with the potential to reveal hydraulic properties in the bedrock between adjacent boreholes; that is, cross-hole investigations (interference tests).

Table 2-3. List of completed and planned pumping tests in the bedrock intended to function as interference tests.

Data freeze	Pumped borehole	Duration	Target of investigation
1.1	HFM01	7 hrs	Foot-wall of ZFMNE00A2
2003-04-30	HFM02	6 hrs	Foot-wall of ZFMNE00A2
1.2 *2004-07-31*	HFM11	4 hrs	Eckarfjärden Deformation zone
2.1	HFM16	4 hrs	Foot-wall of ZFMNE00A2
2005-07-29	HFM16	1 day	Foot-wall of ZFMNE00A2
	HFM18	2 days	Hanging wall of ZFMNE00A2
	KFM04A	5 days	South-west border
	KFM02A	8 days	Hanging wall of ZFMNE00A2
2.2	HFM01	3 weeks	Foot-wall of ZFMNE00A2 (Jakob's IT)
2006-09-30	HFM14	3 weeks	ZFMNE00A2 (Peter's IT)
2.3	HFM14	Not decided yet	ZFMNE00A2
2007-03-31	KFM02B	Not decided yet	Hanging wall of ZFMNE00A2
	HFM33	Not decided yet	North-east border

2.1.3 Quaternary deposits and surface water investigations

Table 2-4 lists the different kinds of near-surface single-hole investigations carried out in Forsmark with regard to the five Data Freezes 1.1–2.3. The current plan (2006-11-30) is to drill in total 70 monitoring wells in the Quaternary deposits. Sixty of these are planned to be terrestrial and ten are marine/lacustrine; that is, drilled through the sea/lake sediments into the underlying till. BAT filter tips are use to collect hydrogeological data in low-permeable sediments such as silt, gyttja and clay. Surface water levels in the lakes and in the sea are gauged in stand pipes. Table 2-5 lists the number of slugtests conducted in the monitoring wells at the time of the different Data Freezes. The map in Figure 2-3 shows existing monitoring wells for Quaternary deposits investigations in Forsmark 2006-05-29; that is, hydraulic conductivity and groundwater levels. Figure 2-4 shows completed stand pipes for surface water level measurements in the lakes (6) and in the sea (2).

2.1.4 Use of F2.1 hydrogeological data

The primary objective of the stage 2.1 work /SKB 2006a/ was to provide feedback to the site investigations at Forsmark in order to ensure that sufficient information is gathered during the remainder of the complete site investigation (CSI) phase. A secondary objective was to evaluate the analysis and intra-discipline modelling work carried out so far and to resolve remaining modelling issues identified during previous modelling stages. In order to meet these objectives, updated stages of the geological model of rock domains (lithology) and deformation zones as well as of some aspects of the rock mechanics model, versions 2.1, were developed. However, no complete integrated site description based on data compiled in Data Freeze 2.1 was provided within the framework of modelling stage 2.1, implying, e.g. no geological and no hydrogeological DFN modelling.

Table 2-4. List of completed and planned monitoring wells, BAT filter tips and stand pipes for groundwater (GW) levels and hydraulic conductivity (K) with regard to the different Data Freezes in Forsmark.

Type of installation	Data freeze 1.1	Data freeze 1.2	Data freeze 2.1	Data freeze 2.2	Data freeze 2.3	Total
Monitoring wells for GW levels and K on land	32	13	3	10	2	60
Monitoring wells for GW levels and K below surface water	6	3	–	1	–	10
BAT filter tips for pore pressure and K	3	–	–	7	–	10
BAT filter tips for water sampling	3	–	–	7	–	10
Stand pipes for lake water levels	3	3	–	–	–	6
Stand pipes for sea water levels	2	–	–	–	–	2

Table 2-5. List of completed hydraulic tests (single-hole BAT tests, slug tests and pumping tests) in Quaternary deposits with regard to the different Data Freezes in Forsmark.

Type of installation	Data freeze 1.1	Data freeze 1.2	Data freeze 2.1	Data freeze 2.2	Data freeze 2.3	Total
BAT tests	3	–	–	7	–	10
Slug tests	36	12	–	11	–	59
Pumping tests	–	2	–	3	–	5

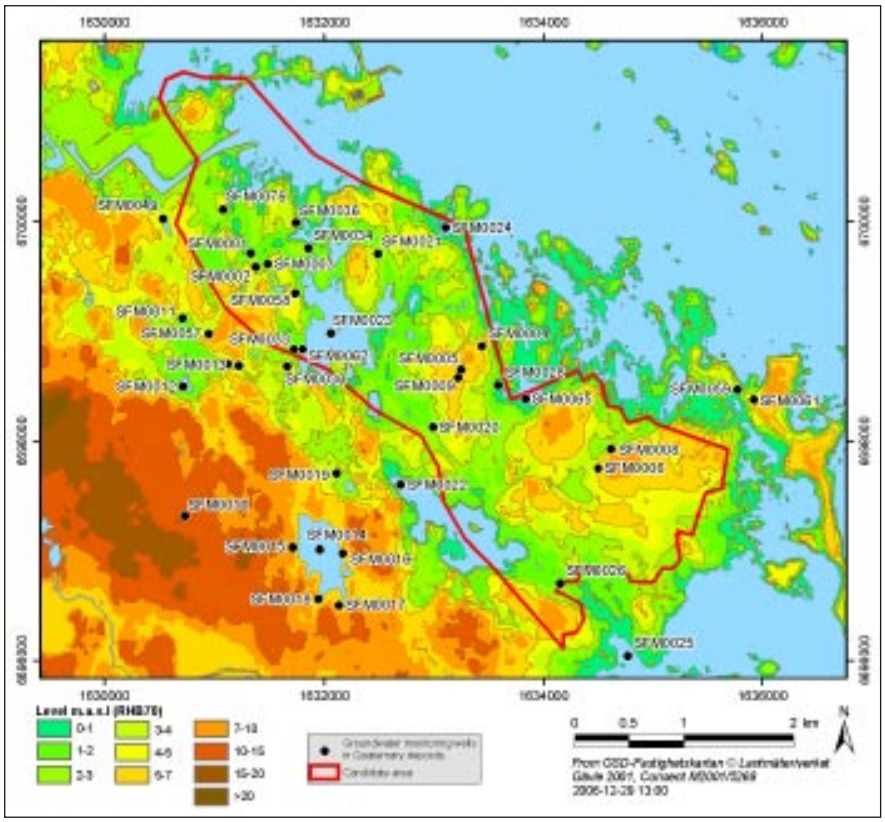

Figure 2-3. *Locations of groundwater monitoring wells in Quaternary deposits with automatic registration of groundwater levels /Juston et al. 2007/.*

Figure 2-4. *Locations of the surface water level gauges /Juston et al. 2007/.*

The development of the bedrock hydrogeology model presented here is largely based on the hydraulic information acquired up to Data Freeze 2.1 with one addition; the three-week long pumping test in borehole HFM01 /Gokall-Norman et al. 2005/. This test was executed shortly after Data Freeze 2.1 was closed (less than a month). This interference test has had a major impact on our understanding of the bedrock hydrogeology in Forsmark and, consequently, the site investigation carried out thereafter. (The three-week long pumping test in borehole HFM01 was conducted by Jakob Levén and hence is often referred to as 'Jakob's Interference Test', cf. Table 2-3.)

The interpretation of hydrological interactions in Forsmark between, on the one hand, the meteorological and surface hydrological data, and, on the other, the groundwater levels in the Quaternary deposits and in the bedrock are facilitated by an extensive hydrologic monitoring system (HMS), which is designed to monitor stream discharge rates, lake levels, sea levels and groundwater levels in open boreholes as well as between packers /Juston et al. 2007/. The present-day numbers of observation sections for groundwater levels at different depths are: 66 sections in cored boreholes, 67 sections in percussion-drilled boreholes and 44 sections in boreholes drilled in the Quaternary deposits. At the time of Data Freeze 2.1 less observation sections were completed, of course, but still a sufficient number of observation section existed to allow for a comprehensive numerical modelling using the data recorded. The data recorded by the HMS are transferred to SICADA and constitute a cornerstone in the work reported here.

Another important piece of information used in this report is the hydrogeochemical data set acquired up to Data Freeze 2.1. The hydrogeochemical information is presented in /SKB 2006a/. Of particular importance for the work reported here is pore water chemistry data acquired in the KFM06A borehole.

It is noted that the updated deformation zone model 2.1 concerned a smaller area in the north-western part of the candidate area only. For the sake of the work presented here, it was decided to use the previous deformation zone model 1.2 since this stage covers a larger area and is already well established (implemented) in the numerical code to be used, see /Hartley et al. 2005, 2006a/. The deformation zone model 1.2 came in three variants /SKB 2005a/. In this work we used the *alternative model*, see Figure 2-5, which contains the greatest number of deformation zones, many of which are associated with a low confidence, cf. /SKB 2005a/.

2.2 Inter-disciplinary data and interpretations

A key characteristic of the hydrogeological modelling in Forsmark is the notion of inter-discipline correlations between, on the one hand, structural and geophysical data observed on outcrops and in boreholes, and, on the other, hydraulic and hydrogeochemical data acquired in boreholes. Further, this notion of correlation is likely to be reinforced by the pronounced anisotropy in the current stress field. The notion of a hydrogeological model based on integration of different kinds of geoscientific data was touched upon already in the 1.1 modelling stage, but hydraulic and hydrogeochemical data to strengthen the formation of the current hydrogeological model were first gathered during the 1.2 modelling stage. The data acquired up to Data Freeze 2.1 stage reveal a greater variability in the hydraulic properties, which is natural considering the increase of the database and the increased level of detail (resolution) by which some investigations are carried out.

The reasons for inter-discipline correlations can in a broad context be explained by two important processes:

- the more than 1.7 billion years old historic tectonic evolution of the Forsmark area, which has formed characteristic patterns of deformation zones of different orientations and character, and
- the shorelevel displacement of the Fennoscandian Shield during Holocene and the associated changes of the sea water salinity in the Baltic basin.

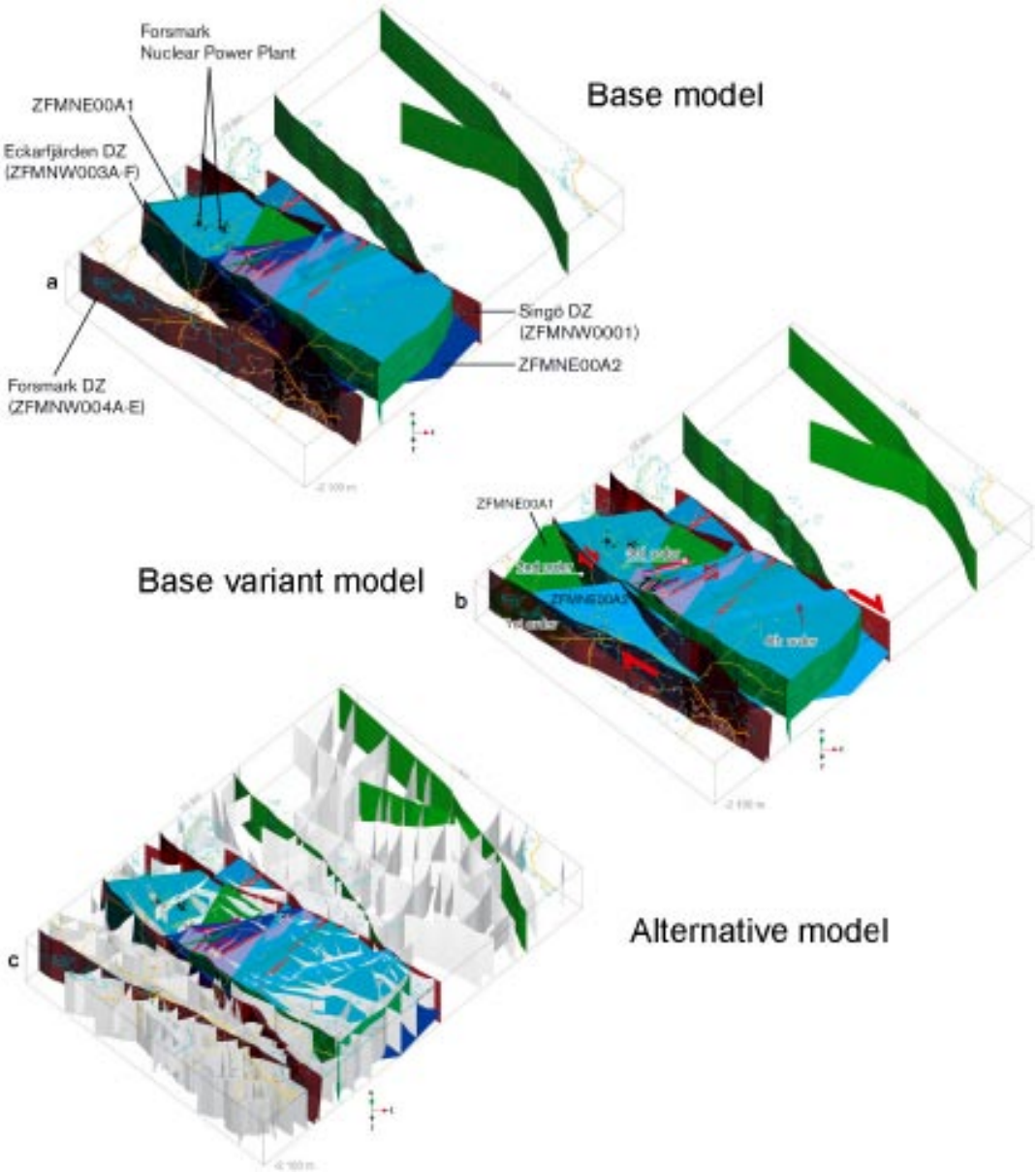

Figure 2-5. *The deformation zone model 1.2 came in three variants /SKB 2005a/. In this work we used the alternative model (lowermost inset).*

2.2.1 Tectonic evolution and present-day rock stresses

Figure 2-6 shows a NW-SE cross-section of the 1.2 three-dimensional deformation zone model. The deformation zone ZFMNE00A2 is a gently dipping major fault important to describing both the geology and hydrogeology in proximity to the candidate area. The two sides of an inclined fault are called the *hanging wall* and *foot wall*. By definition, the hanging wall occurs above the fault and the foot wall occurs below the fault. The cross-section, which passes close to drill sites 1, 2, 3, 5 and 7 (cf. Figure 2-1), demonstrates the significant difference in the deformation zone pattern with regard to the foot wall and hanging wall of ZFMNE00A2 (blueish shade); that is, the hanging wall contains a greater number of gently dipping structures.

Figure 2-7 illustrates the envisaged tectonic evolution of the Forsmark area and the mechanisms causing the difference in the deformation zone pattern. In stage 1.2 the relationships between the principal stresses at 400 m depth in the foot wall of zone ZFMNE00A2 were estimated to $\sigma_H : \sigma_h : \sigma_v = 43\pm8 : 29\pm8 : 10$ MPa, where σ_H has a northwest azimuth; that is, its direction is parallel with the Forsmark and Singö deformation zones.

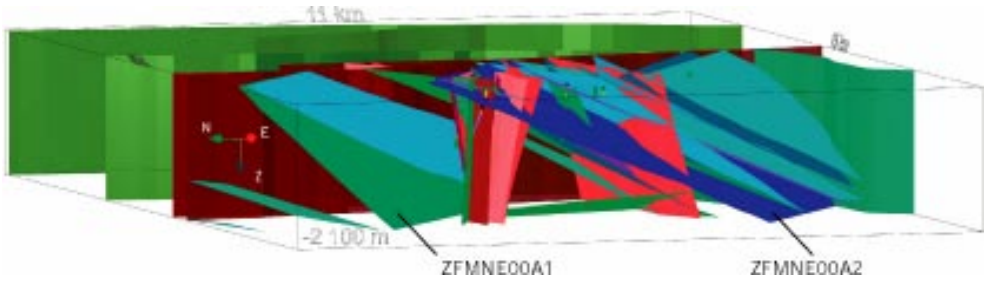

Figure 2-6. *NW-SE cross-section that passes close to drill sites 1, 2, 3, 5 and 7 inside the candidate area. This view of the deformation zone model to the north-east shows a selected number of gently and steeply dipping fracture zones that strike ENE and NE, and transect the candidate volume. The gently dipping zone ZFMNE00A2 (blueish shade) is in the centre. All these zones are sandwiched between the regionally more significant, vertical and steeply dipping deformation zones which strike WNW or NW; that is, the Forsmark, Eckarfjärden and Singö deformation zones, cf. Figure 2-5. The complex Singö deformation zone, which shows evidence of both ductile and brittle deformation, is present in the background (brownish shade) /SKB 2005a/.*

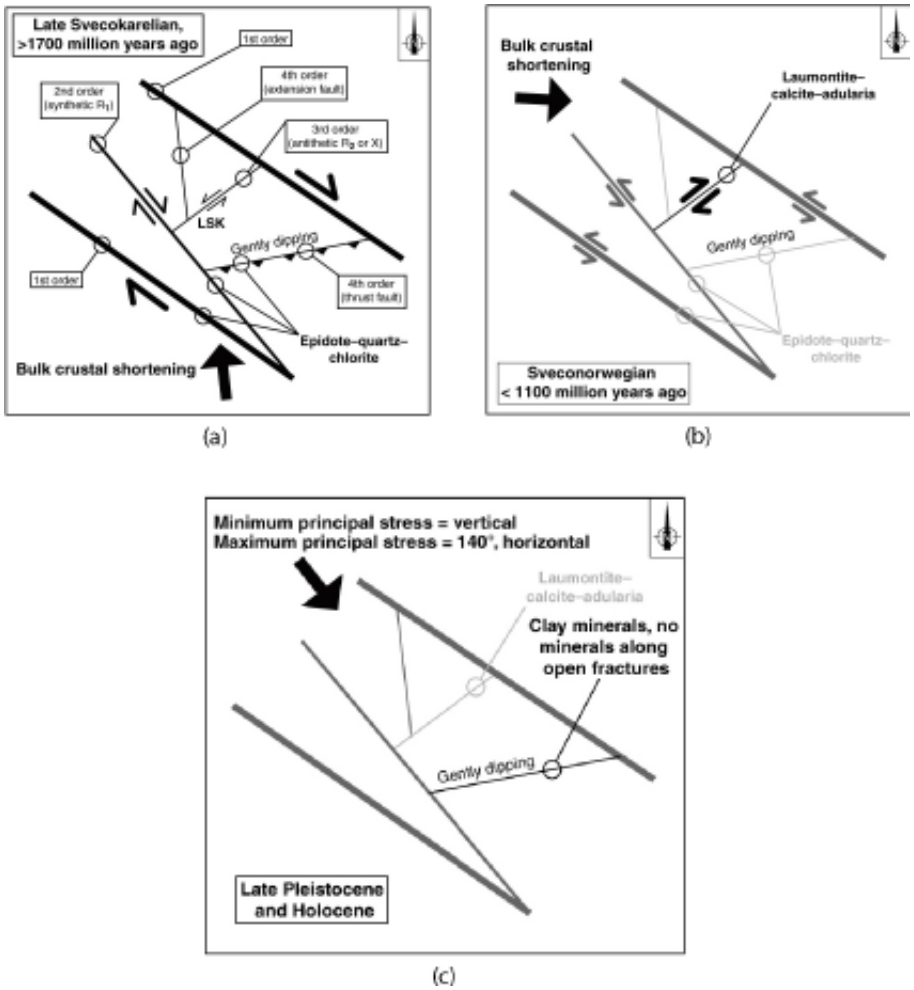

Figure 2-7. *Two-dimensional cartoons illustrating (a) the regional scale kinematics during the formation of the different sets of deformation zones at the Forsmark site. In this conceptual model, it is assumed that all structures formed in response to the same tectonic event during the later part of the Svecokarelian orogeny; (b) the regional scale kinematics in connection with possible phase of reactivation of the different sets of deformation zones at the Forsmark site during the Sweconorwegian orogeny; (c) the current conceptual model for a reactivation of the different sets of deformation zones at the Forsmark site in the current stress regime (Quaternary). The different colour shadings along the zones indicate a variable degree of response to the maximum principal stress field. The black line along the gently-dipping structures indicates a considerable change in aperture development along the fractures in these zones; the dark grey line indicates a moderate change and the pale grey line little change /SKB 2006a/.*

As a result of the high horizontal stresses the open fractures in bedrock within the tectonic lens are believed to be predominantly horizontal with a second order steeply fracture set around NE and NS, cf. inset (c) in Figure 2-7.

The notion of a structural anisotropy is supported by the hydrogeological data acquired at different elevations in the bedrock; that is, the structural-hydraulic conditions vary incredibly both in the horizontal and vertical directions, see Figure 2-8 and Figure 2-9.

Figure 2-8. *Two pictures of the near-surface bedrock in the north-western part of the tectonic lens. The leftmost picture shows a structurally dominant, but highly heterogeneous, horizontal fracture/sheet joint. The rightmost picture shows the flushing of a high yielding horizontal fracture/sheet joint encountered at c. 40 m depth in the HFM02 percussion borehole. The yield is c. 1,000 litres per minute.*

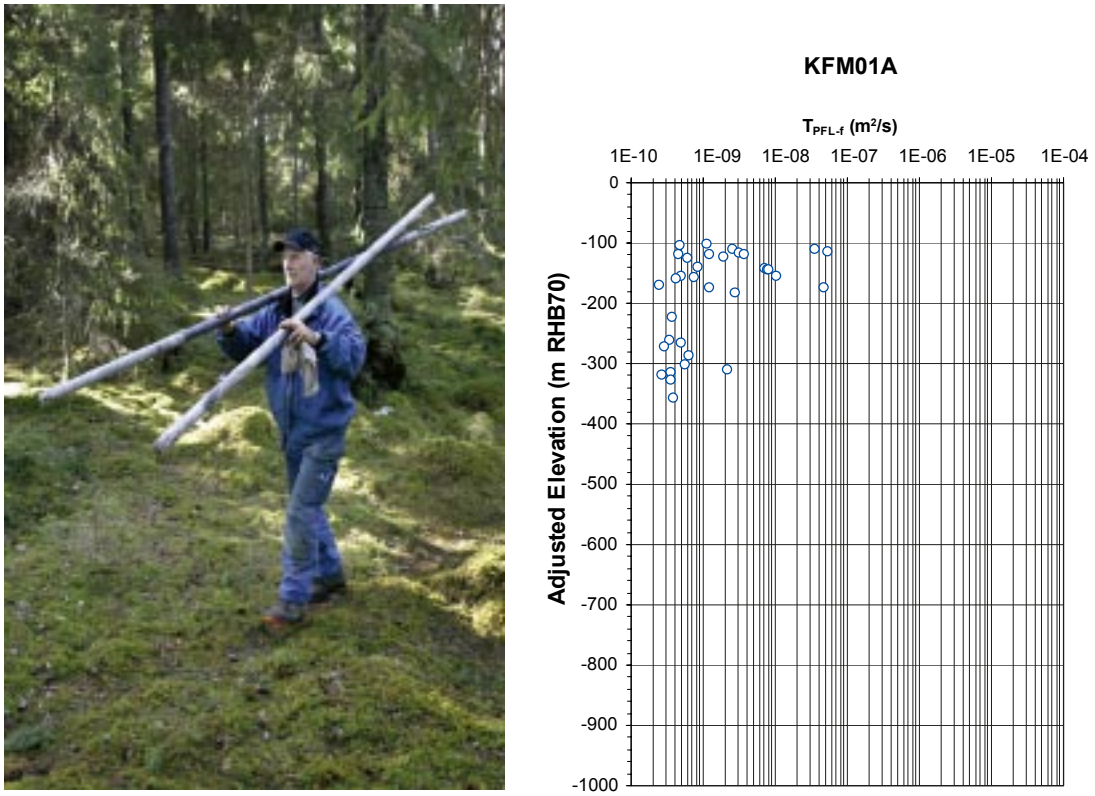

Figure 2-9. *The rock at repository depth (400–700 m depth) in the north-western part of the tectonic lens is sparsely fractured by open (naturally broken and potentially flowing) fractures. About 200 unbroken 3-m-long rock cores have been recorded during the coring drillings (c. 15 km). There are few transmissive fractures below 400 m depth.*

Figure 2-10 shows a cross-section through the centre of the tectonic lens. The illustration outlines some of the key features of the 2.1 structural model:

- the gently dipping ZFMNE00A2 deformation zone divides the bedrock inside the tectonic lens into a foot wall bedrock (target volume for a final repository in Forsmark) and a hanging wall bedrock,
- the foot wall bedrock has higher rock stresses than the hanging wall bedrock; it is divided into two different fracture domains, FFM01 and FFM02, where the latter is closer to surface and substantially more fractured than the former, and
- the hanging wall bedrock is intersected by several gently-dipping deformation zones.

2.2.2 Shore level displacement and hydrogeochemical data

The left ordinate axis in Figure 2-11 shows the shore level displacement for Forsmark during the last 10,000 years (Holocene) as modelled in stage 1.2. During this period of time the shore level at 8,000 BC has been uplifted c. 115 m as a result of glacial rebound and sea level changes. The highest ground elevations within the Forsmark candidate area became islands c. 900 AD, i.e. at the time of the Vikings.

The right ordinate axis in Figure 2-11 shows the salinity changes in Baltic basin during the same period of time. The retreating land ice of the Weichsel period crossed the Forsmark area at c. 9,000 BC. About that time the surface water in the Baltic basin was changing from marine conditions (Yoldia Sea) to lacustrine conditions (Ancylus Lake). There is no evidence reported that supports a marine signature in the sea sediments in the Forsmark area. Probably, the sea water at the margin of the retreating land ice was fairly diluted by glacial melt water even if more marine conditions still prevailed in the southern Baltic. An important event for Forsmark is the change from lacustrine to marine conditions beginning at c. 6,500 BC (Littorina Sea). For more than 8,000 years brackish water conditions have prevailed in the Baltic basin, with a maximum salinity of c. 1.2% between 4,500–3,000 BC. At that time the water depth in Forsmark was c. 50 m.

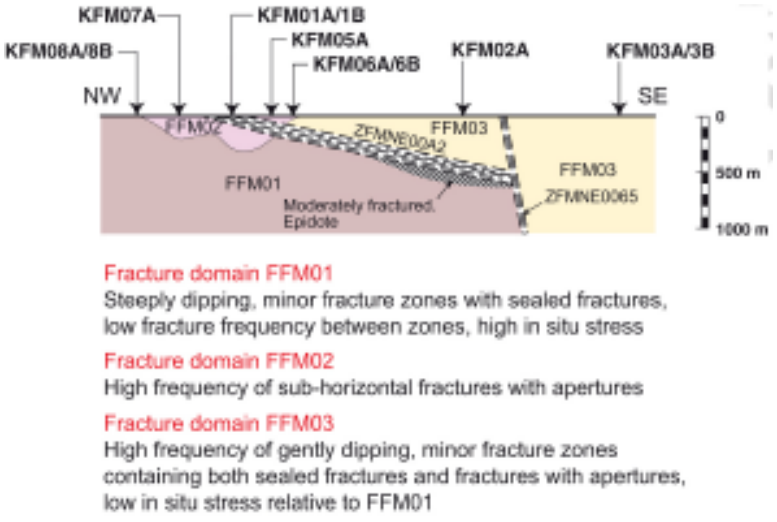

Figure 2-10. *The extensive and fairly transmissive gently dipping deformation zone ZFMNE00A2 divides the bedrock inside the tectonic lens into a foot wall bedrock (target volume for a final repository in Forsmark) and a hanging wall bedrock. FFM01–FFM03 are different fracture domains, cf. /SKB 2006a/.*

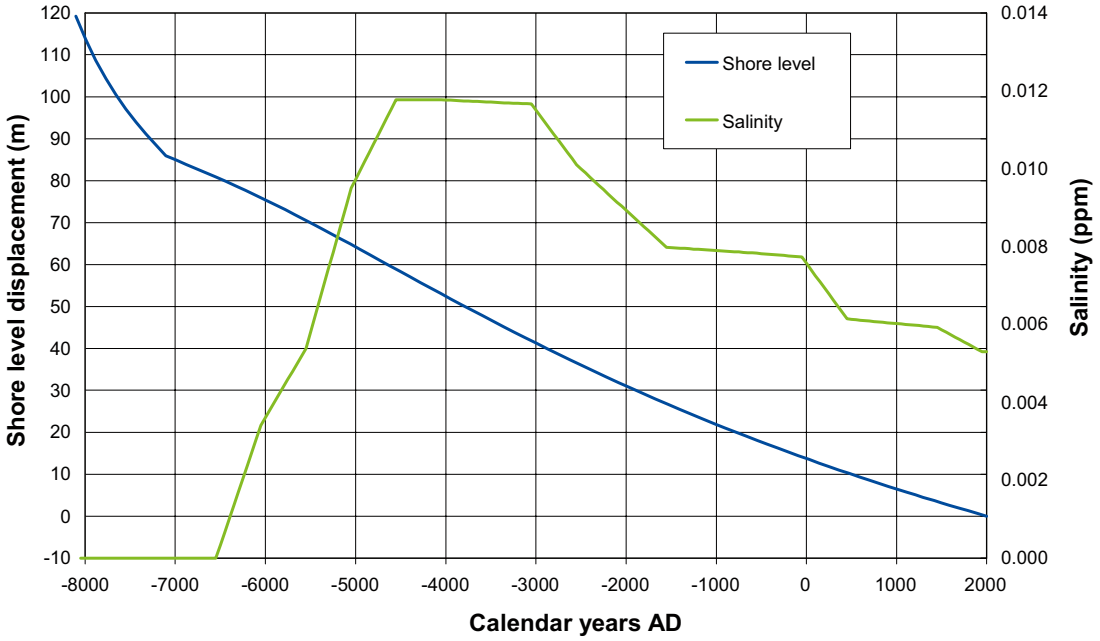

Figure 2-11. *Shore level displacement and salinity changes in the Baltic basin as modelled for Forsmark stage 1.2. The shore level graph is based on /Påsse 1997/ and the salinity graph is based on /Westman et al. 1999/.*

Figure 2-12 through Figure 2-14 show a cross section through the tectonic lens, which passes close to drill sites 1, 2, 3, 5 and 7 (cf. Figure 2-1); that is, parallel to the cross-section shown in Figure 2-10. The cross section illustrates the notion that the hydrological processes during Holocene has interplayed with the structural geology in different ways in the hanging wall bedrock and in the foot wall bedrock of ZFMNE00A2, respectively. As a consequence, the present-day groundwater composition varies within the bedrock depending on the geological structures and their hydraulic properties. The conceptual model assumed for Forsmark stage 2.1 can be summarised as follows:

1. Glacial melt water penetrated into the bedrock due to high water pressures below the retreating ice cap. The salinity of the Glacial melt water was assumed to be close to that fresh water. At great depths in the bedrock the hydrogeochemical conditions are assumed to be unaffected. The salinity of the deep groundwater was set to c. 10% TDS by weight at –2,100 m above sea level ("brine type" groundwater conditions). Data to support this assumption are sampled in the c. 1,660 m deep borehole KLX02 in Laxemar /SKB 2005c, 2006d/.
2. A density turnover occurred during the Littorina Sea period (c. 7,000–3,000 BC) due to a greater salinity at the surface than in the near-surface bedrock groundwater. Probably, the penetration of Littorina Sea water varied depending on the occurrence of geological structures and their hydraulic properties. The greatest penetration was assumed to occur in the hanging wall bedrock. A maximum salinity of c. 1.2% TDS by weight was assumed for the Littorina water.
3. The flushing of the relatively flat and moderately undulating topography within the Forsmark candidate area by Meteoric water probably began c. 900 AD as a result of the ongoing shore level displacement. (The present-day rate is 6–7 mm/year.) The shore level displacement is function of two processes – glacial rebound and global sea level changes. The salinity of the Meteoric water was assumed to be close to that of fresh water. The flushing was assumed to be short-circuited by high-transmissive horizontal fractures/sheet joints in the uppermost part of the bedrock, thus leaving some fractions of Deep Saline, Glacial water Littorina Sea water behind.

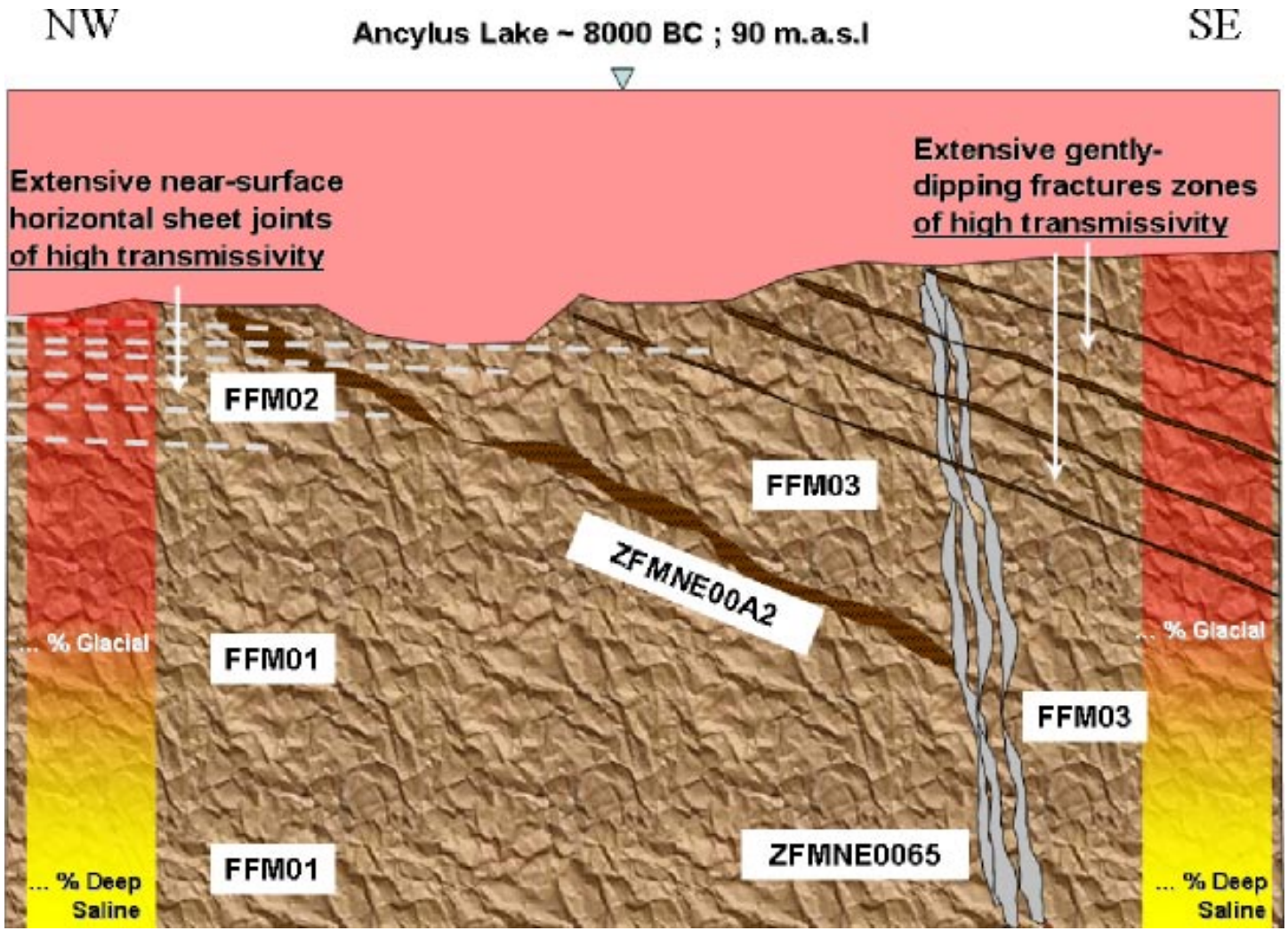

Figure 2-12. *In the conceptual model for Forsmark stage 1.2 it was assumed that Glacial melt water penetrated into the bedrock due to high water pressures below the retreating ice cap. The salinity of the Glacial melt water was assumed be close to that of fresh water. At great depths the hydrogeochemical conditions were assumed to be unaffected. The salinity of the deep groundwater was set to c. 10% TDS by weight at –2,100 m above sea level.*

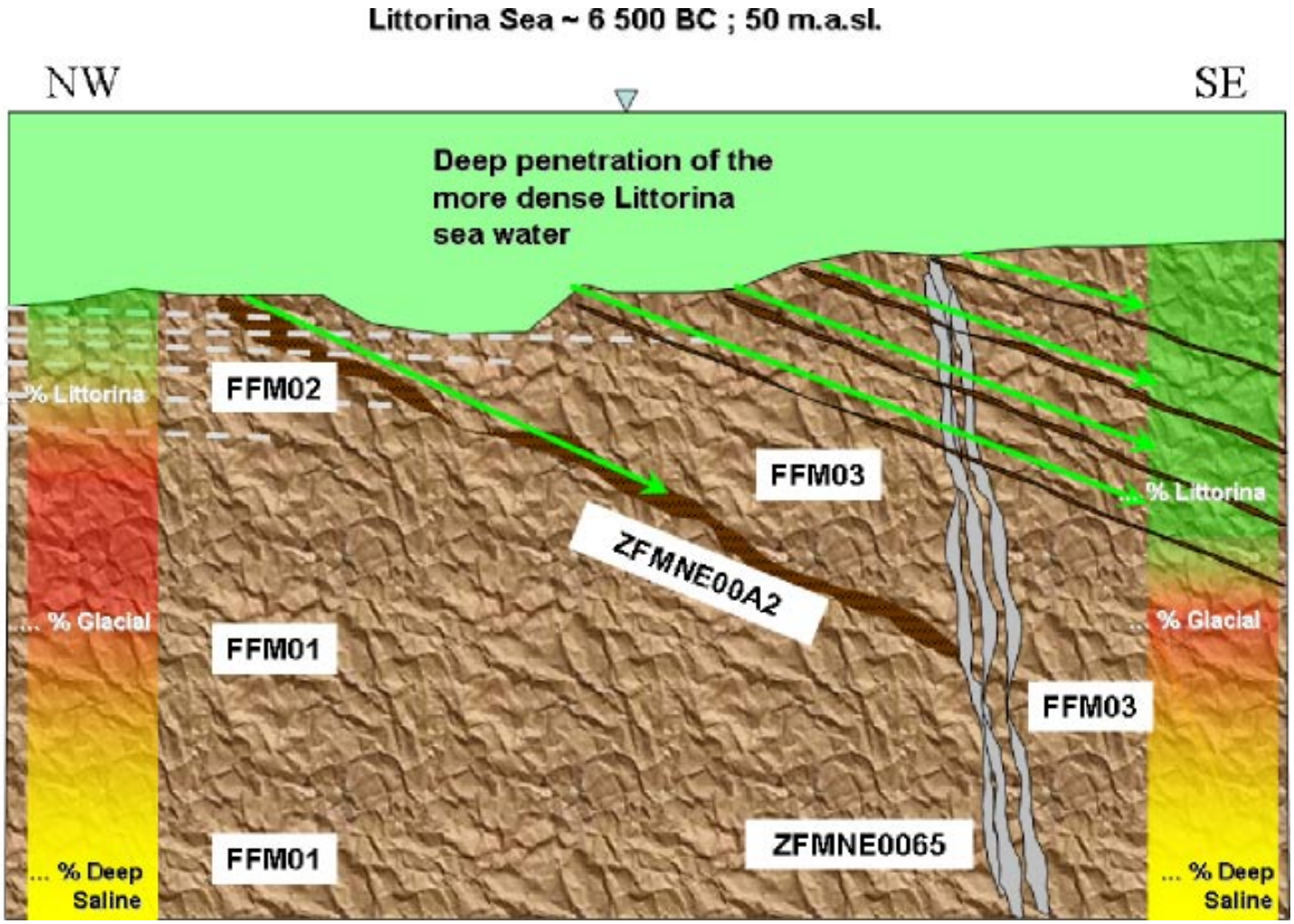

Figure 2-13. *In the conceptual model for Forsmark stage 1.2 it was assumed that a density turnover occurred during the Littorina Sea period (c. 7,000–3,000 BC) due to a greater salinity at the surface than in the near-surface bedrock groundwater. Probably, the penetration of Littorina Sea water varied depending on the occurrence of geological structures and their hydraulic properties. The greatest penetration was assumed to occur in the hanging wall bedrock. A maximum salinity of c. 1.2% TDS by weight was assumed for the Littorina water.*

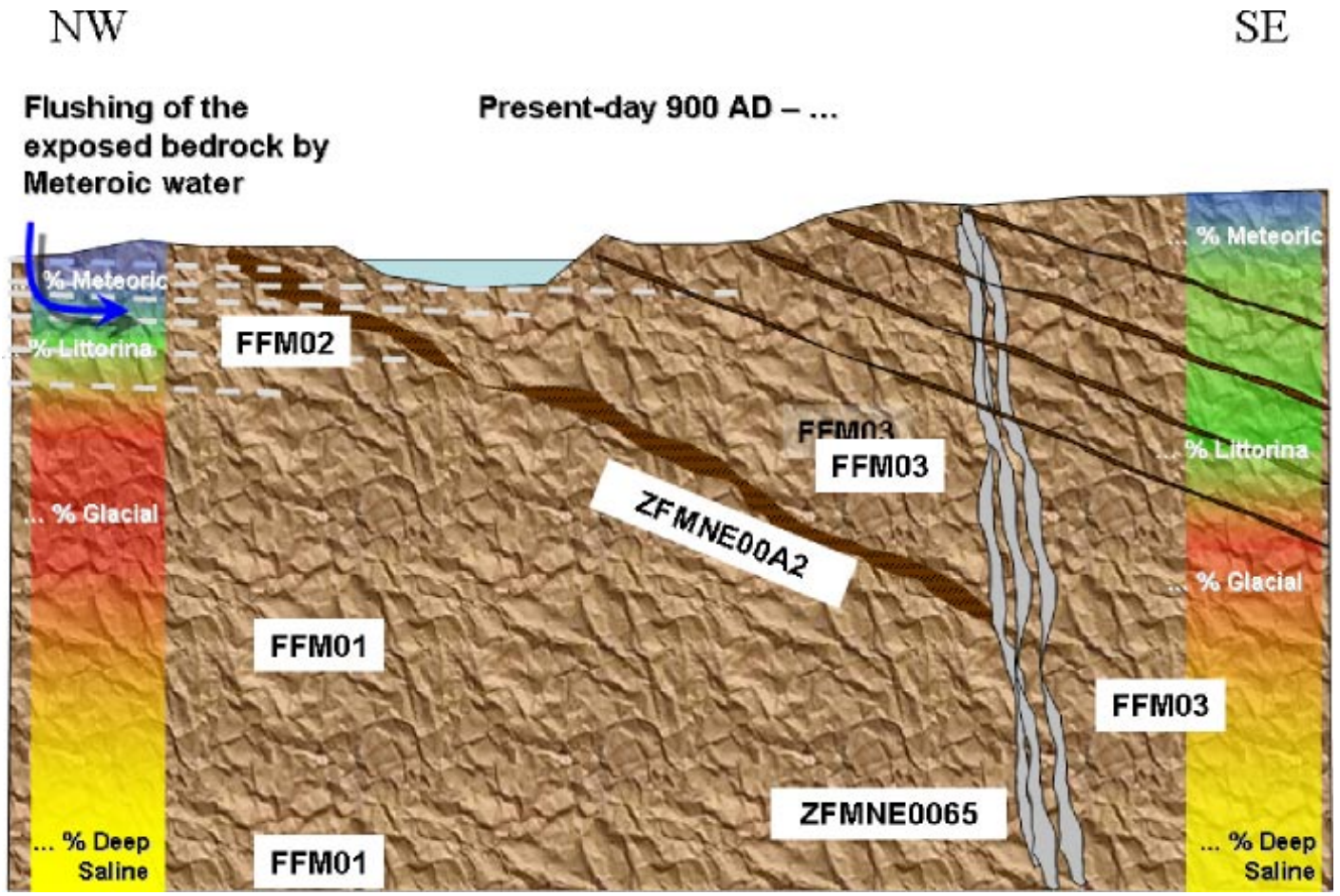

Figure 2-14. *In the conceptual model for Forsmark stage 1.2 it was assumed that the flushing of the relatively flat and moderately undulating topography within Forsmark candidate area by Meteoric water probably began c. 900 AD as a result of the ongoing shore level displacement. (The present-day rate is 6-7 mm/year.) The shore level displacement is a function of two processes – glacial rebound and global sea level changes. The salinity of the Meteoric water was assumed to be close to that of fresh water. The flushing was assumed to be short-circuited by high-transmissive horizontal fractures/sheet joints in the uppermost part of the bedrock, thus leaving some fractions of Deep Saline, Glacial water Littorina Sea water behind.*

The penetration depth of Glacial melt water envisaged in Figure 2-12 is uncertain, but there are several strands of evidence for assuming that Glacial melt water affected the groundwater in the bedrock at the margin of the retreating land ice, at least in the uppermost parts within the candidate area. Figure 2-15 shows a pertinent example from the excavations for the nuclear power reactors in the north-western part of the candidate area. The picture reveals that large amounts of fine-grained glaciofluvial sediments have been injected into the horizontal sheet joints. The thickness of the sediment infilling in Figure 2-15 is c. 0.5 m. During the site investigations, glaciofluvial sediments have been observed at various elevations down to c. 65 m depth in outcropping gently-dipping deformation zones, e.g. in KFM06A (ZFMNE00A2), KFM03A, KFM03B (ZFMNE00A5) and HFM07 (ZFMNE00A6).

Figure 2-16 shows a plot of chloride concentrations versus depth acquired in cored and percussion-drilled boreholes belonging to Data Freeze 2.1. The information shown is:

- Blue squares denote fracture data sampled in the gently-dipping deformation zone ZFMNE00A2.
- Yellow squares denote fracture data sampled in the gently-dipping deformations zones above ZFMNE00A2 encountered in the hanging wall bedrock (Block FFM03).
- Brown squares indicate fracture data sampled in steeply-dipping deformation zones encountered in the foot wall bedrock (Block FFM01+FFM02).
- Green squares denote fracture data sampled in steeply-dipping deformation zones bordering the tectonic lens.
- Red squares denote pore water data sampled from the rock cores of borehole KFM06A located in the foot wall bedrock.
- The dashed lines at 3,000 mg/L and 5,600 mg/L of chloride indicate the present-day salinity and the assumed maximum salinity of the Littorina Sea.
- Samples from percussion-drilled boreholes have pink labels, whereas samples from cored boreholes have blue labels.

Understanding Figure 2-16 is vital for the hydrogeological description, but more data are needed from the fracture groundwater in the foot wall bedrock to strengthen the conceptual modelling. The most interesting observations indicated by Figure 2-16 are:

- the relatively speaking lower chloride concentrations observed in the pore water groundwater samples as compared to the fracture groundwater samples; an important observation for the diffusion model, and
- the significantly higher concentrations at shallower depths associated with in the fracture groundwater samples gathered in the bordering deformation zones; an important observation for the assignment of initial conditions required in the palaeo-hydrogeological-hydrogeochemical modelling.

Figure 2-15. *Photograph of a sediment filled horizontal sheet joint encountered during the excavations for the nuclear power reactors in Forsmark /Carlsson 1979/.*

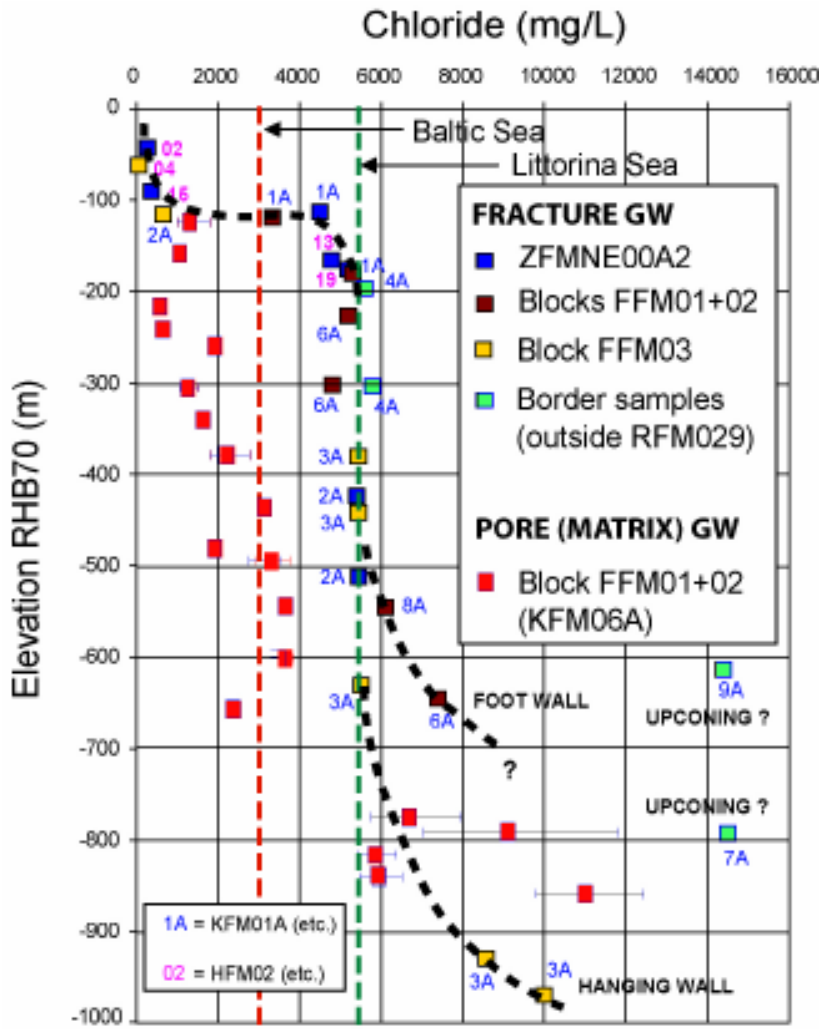

Figure 2-16. *Chloride concentrations of samples acquired in boreholes drilled in the foot wall and hanging wall of the gently-dipping deformation zone ZFMNE00A2. Note the difference between samples acquired from fractures in deformation zones "FRACTURE GW", and samples acquired from the matrix pore water "PORE (MATRIX) GW". The dashed lines are an integrated interpretation of the data presented in /SKB 2006c/ and /Waber and Smellie 2005/.*

2.3 Hydrogeological description

The description of the hydrogeological conditions in Forsmark presented in this section is based on hydrologic observations (head time series) and hydraulic properties (transmissivity, hydraulic diffusivity) acquired up to Data Freeze 2.1. To some extent results from the numerical flow modelling conducted in stage 1.2 are also included in the description.

The description of the bedrock hydrogeology focuses on the following subjects:

1. The deterministically modelled deformation zones.
2. The sparsely fractured bedrock at repository depth within the tectonic lens outside the deterministically modelled deformation zones, in particular within the target volume in the north-western part of the candidate area.
3. The intensely fractured superficial bedrock within the tectonic lens, in particular within the target volume in the north-western part of the candidate area.
4. The intensely fractured bedrock (zones) bordering the tectonic lens.

The description of the near-surface hydrogeology focuses on the following subjects:

1. The spatial distribution of different types of Quaternary deposits and their hydraulic properties, especially the hydraulic contact between the Quaternary
2. Interaction between the groundwater heads in the Quaternary deposits and the groundwater heads in the superficial bedrock.
3. Interaction between surface water heads and groundwater heads.

2.3.1 The deterministically modelled deformation zones

The deterministically modelled deformation zones were defined in model stage 1.2 /SKB 2005a/, which treated, among other things, the need for far field realism in terms of three regional structural models; the *base model*, the *base variant model*, and the *alternative model*, cf. Figure 2-5. It was concluded by means of numerical modelling that detailed geometrical and hydraulic information about the deformation zones within the tectonic lens are much more important for the bedrock hydrogeological description within the target volume than the positions and hydraulic properties of deformation zones outside the tectonic lens /Follin et al. 2005/.

The assignment of hydraulic properties to the different deformation zones in stage 1.2 was based on depth trend regression analyses of single-hole transmissivity data acquired at a reasonable number of borehole intercepts (44 borehole intercepts with 28 deformation zones) /Follin et al. 2005/. Although the difference in the inferred transmissivity trends between steeply-dipping and gently-dipping deformation zones was found to be considerable at repository depth (c. two orders of magnitude), it was also noted that use of regression models had a significant impact on the local matching of simulated versus measured hydrogeochemical data; that is, it was noted that a simplified description of the deformation zone heterogeneity within the tectonic lens undoubtedly affected the flushing of bedrock and hence the matching against hydrogeochemical data /Hartley et al. 2005/.

The data gathered in Data Freeze 2.1 confirm the deformation zone heterogeneity envisaged in stage 1.2. Most deformation zones in Forsmark are of ductile nature from the onset. The ones that reveal brittle deformations today, e.g. flowing fractures, are often partly (heterogeneously) reactivated only. That is, at some locations they show up in the boreholes drilled with no measurable flow, whereas at other locations (boreholes) they have one to several flowing fractures over a short interval ranging from a metre to tens of metres. It should be noted that the number of open fractures in the deformation zones is much larger than the number of open fractures with a sustainable measurable flow. The assignment of hydraulic properties will be revisited in stage 2.2, when the final deformation zone model is developed.

2.3.2 The sparsely fractured bedrock at repository depth

Two different conceptual models were used in stage 1.2; a multi-component continuous porous medium /Follin et al. 2005/ and a statistically homogeneous discrete fracture network /Hartley et al. 2005/. The numerical modelling conducted revealed that neither of these two approaches could capture the spatially varying hydrogeological conditions observed very well. In particular, it was concluded that the hydrogeology of the sparsely fractured bedrock at and below repository depth was difficult to model. This conclusion led to the working hypothesis that the fractures outside the deterministically modelled deformation zones should be divided into subvolumes with the intension to homogenise, locally, the spatial variability in the fracture statistics. This notion was fed back to the site geologists who addressed the issue in stage 2.1. Based on available geological information a division of the bedrock into so called ‘Fracture Domains’ was suggested, see Figure 2-10.

In preparation for stage 2.2 all mechanical, hydrogeological and hydrogeochemical data collected in core-drilled and percussion-drilled boreholes will be compiled according to the "Fracture Domain" concept. The objectives are:

- to collate and present bedrock data acquired by rock mechanics, hydrogeology and hydrogeochemistry up to Data Freeze 2.2 for the benefit of other (future) modellers, and
- to provide a means for integrated modelling between the different disciplines.

Figure 2-19 through Figure 2-18 present the PFL-f[1] results from the boreholes belonging to the 2.1 Data Freeze, i.e. KFM01A–KFM07A. The data are plotted with regard to the 'Fracture Domain Concept'. (It is noted that the majority of the fractures observed in these boreholes are sealed, both inside and outside the intervals with deformation zone type properties.)

Figure 2-17 and Figure 2-18 suggest that there are almost no flowing fractures at and below repository depth. This interpretation is supported by the many unbroken 3-m-long rock cores recorded during the coring drillings, cf. Figure 2-9, as well as the double-packer injection tests run /SKB 2006a/. Figure 2-19 suggests that the flowing fractures above and below repository depth in the target volume are predominantly gently dipping.

In summary, the low frequencies of flowing fractures ($P_{10,PFL}$) in the boreholes penetrating the target volume at repository depth, i.e. KFM01A, -02A, -4A, -05A, -06A and –07A, suggest a low value of the connected open fracture surface area per unit volume of rock ($P_{32,cof}$). If this notion is correct, the modelling of groundwater flow at and below repository depth can be envisaged in different ways:

(i) flow occurs predominantly in a few, extensive, gently-dipping open fractures,

(ii) flow occurs predominantly in networks of predominantly gently-dipping open fractures of moderate sizes (radii), or

(iii) flow occurs in a sparsely interconnected lattice consisting of a few steeply-dipping open fractures and, gently dipping open fractures of the first or second category.

The three notions are illustrated in Figure 2-20, which shows a deposition drift with canister holes.

2.3.3 The intensely fractured superficial bedrock within the tectonic lens

The intensely fractured superficial bedrock within the tectonic lens is predominantly investigated in the north-western part of the candidate area, see Figure 2-1 and Figure 2-2. Each of the seven cored boreholes KFM01A–07A is percussion-drilled in its upper part and has a casing installed to c. 100 m depth. The casings prohibit a detailed hydraulic characterisation of the superficial bedrock. Instead the current hydrogeological conceptualisation is based on impeller flow logging data from altogether 22 percussion-drilled boreholes, HFM01–22, see Figure 2-21. The penetration depths of the percussion boreholes vary, but the median depth is c. 140 m. The borehole lengths vary between 26 and 301 m and the borehole inclinations vary between 49° and 88°.

Figure 2-21 shows the inferred flow logging transmissivities in depth intervals of 50 m for the uppermost 200 m of bedrock. The pattern of high transmissivities in the uppermost parts of the bedrock is quite heterogeneous, i.e. high values can occur at any depth and location. This is interpreted to be due to structural/hydraulic discontinuities in a lattice of interconnected fractures consisting of outcropping deformation zones and horizontal fractures/sheet joints. Figure 2-22 shows a pertinent evidence for the existence of horizontal fractures/sheet joints in the superficial bedrock in the foot wall of ZFMNE00A2. The picture shows the excavation of the more than one kilometre long and 13 m deep canal between the Baltic Sea and the nuclear reactors.

[1] The spatial resolution of the PFL-f method is 0.1 m, which means that the transmissivity of individual fractures can be mapped. In combination with Boremap data and tele-viewer (BIPS) data the orientations of the flowing fractures can be assessed as well. The practical transmissivity threshold is c. $1 \cdot 10^{-9}$ m^2/s.

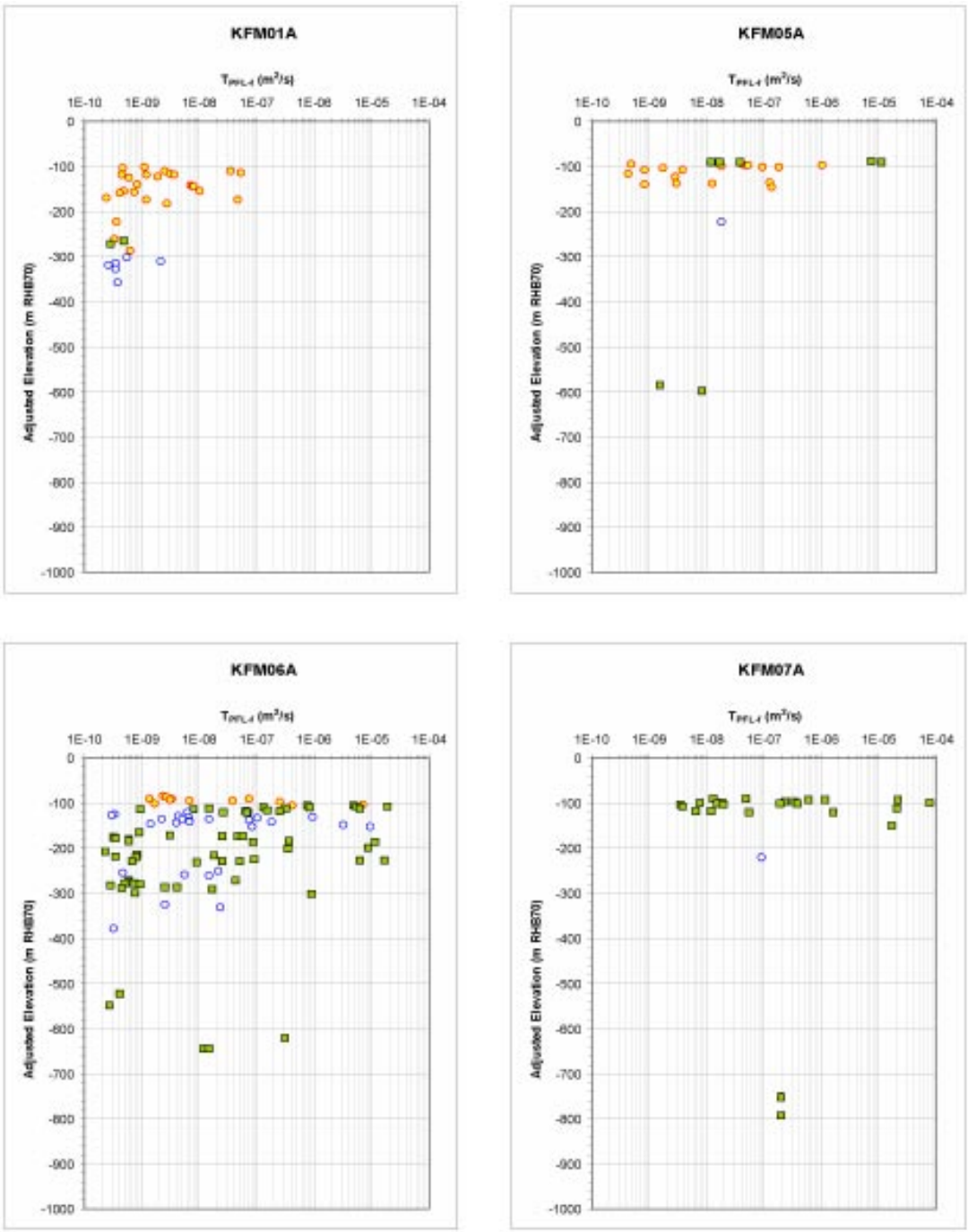

Figure 2-17. *PFL-f transmissivity data acquired in four of the seven boreholes belonging to Data Freeze 2.1. The data are coloured according to the fracture domain concept illustrated in Figure 2-10; blue/white dots for flow anomalies in fracture domain FFM01, red/yellow dots for flow anomalies in fracture domain FFM02 and, finally, black/green squares for flow anomalies in intervals with deformation zone type properties. Boreholes KFM01A, -05A, -06A, and -07A are all located in the foot wall of ZFMNE00A2.*

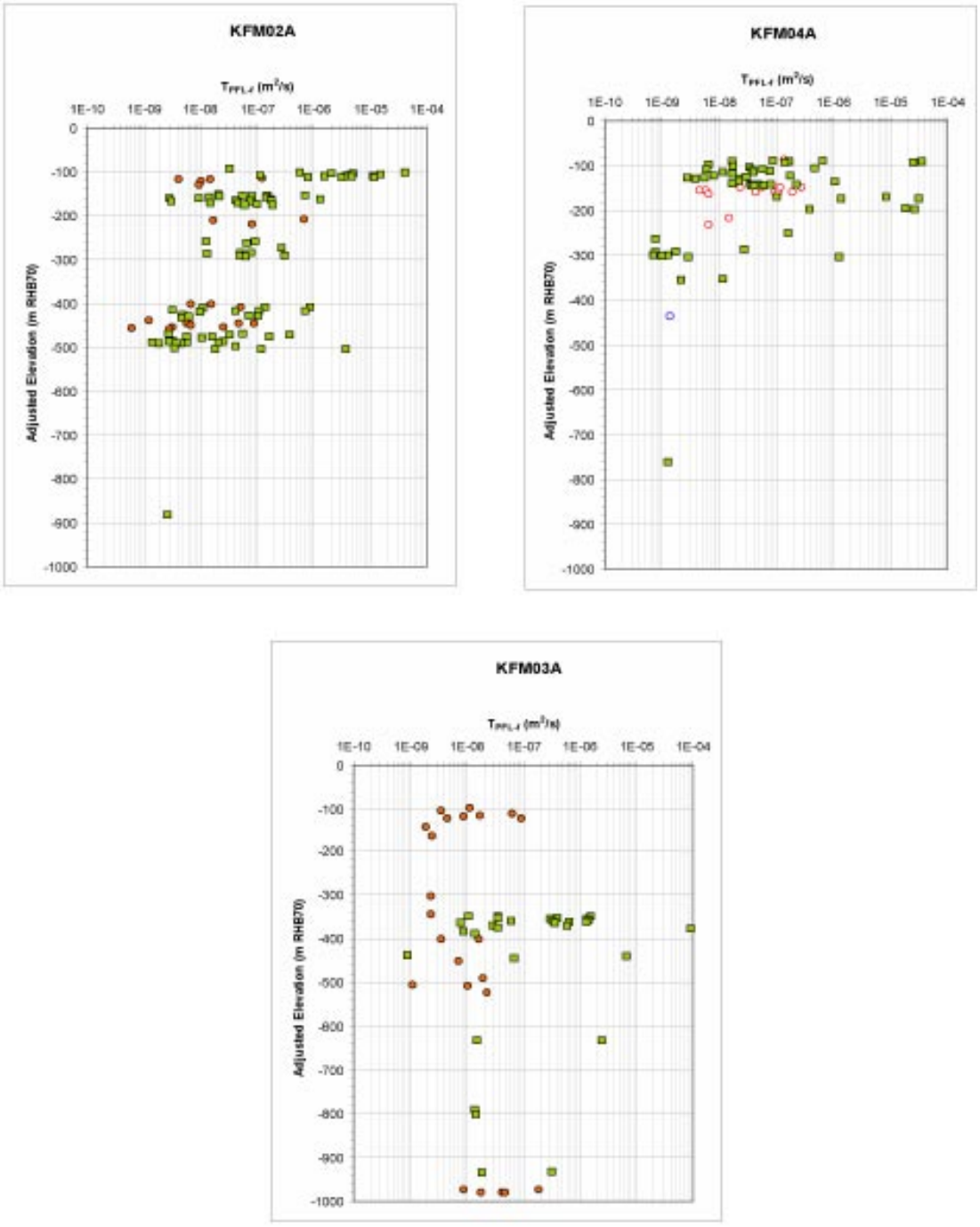

Figure 2-18. *PFL-f transmissivity data acquired in three of the boreholes belonging to the 2.1 Data Freeze. The data are coloured according to the fracture domain concept illustrated in Figure 2-10; blue/white dots for flow anomalies in fracture domain FFM01, red/white dots for flow anomalies in fracture domain in FFM04, black/orange dots for flow anomalies in fracture domain FFM03 and, finally, black/green squares for an interval with deformation zone type properties. The whole of KFM03A and the upper half of KFM02A intersect the hanging wall of ZFMNE00A2. The upper half of KFM04A intersects the bedrock bordering the tectonic lens southwest of the target volume.*

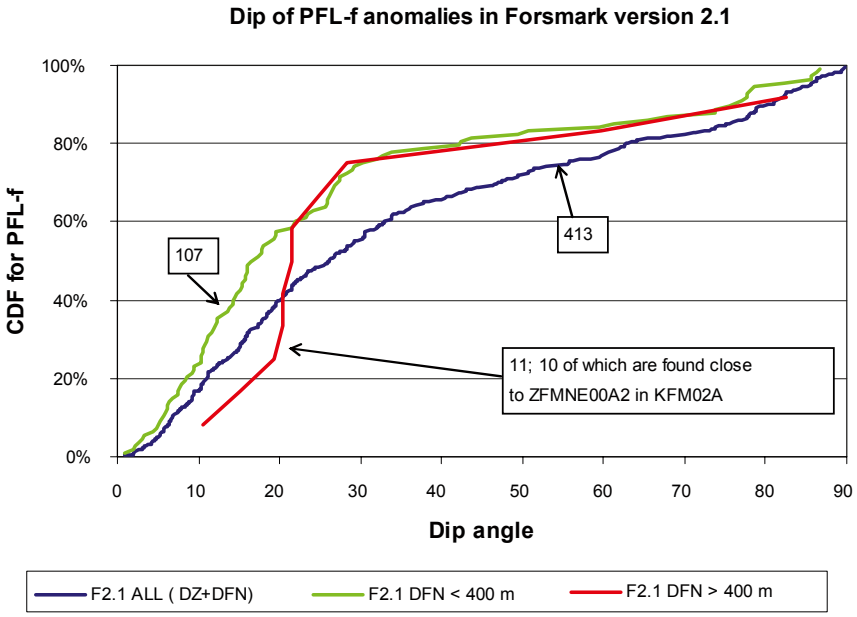

Figure 2-19. *Dips of fractures associated with PFL-f flow anomalies acquired in Data Freeze 2.1, boreholes KFM01A–KFM07A. The blue graph encompasses all PFL-f flow anomalies in these boreholes, i.e. including data inside the deterministically modelled deformation zones. Among the seven boreholes the whole of KFM03A and the upper halves of KFM02A and KFM04A are outside the target volume located in the north-western part of the tectonic lens. The green and red graphs represent data above and below 400 m depth within the target volume, respectively, excluding data coinciding with the deterministically modelled deformation zones.*

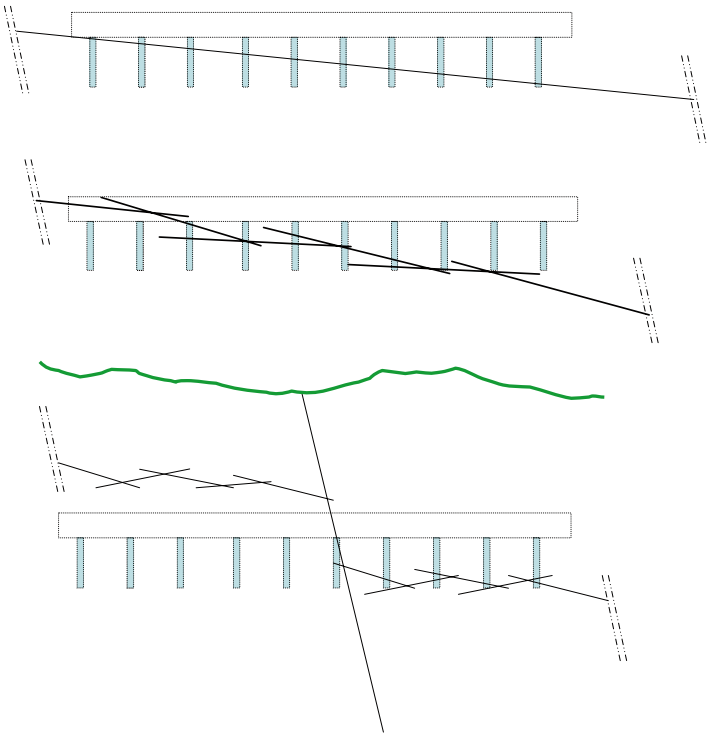

Figure 2-20. *Cross-section cartoons illustrating a deposition drift with a sequence of canister holes together with three tentative DFN models of the large-scale open fracture connectivity in the target bedrock at repository depth in Forsmark. Top: The large-scale connectivity is due to a few single, but large, gently-dipping fractures, some of which have been mapped. Middle: The large-scale connectivity is due to extensive, stochastic networks of gently-dipping open fractures of shorter size (radius). Bottom: The large-scale connectivity is due to intersections between a few steeply-dipping open fractures, of deterministic or stochastic nature, and, more or less isolated stochastic compartments of clustered fractures of shorter, gently-dipping open fractures. In each case flow is likely to be channelised.*

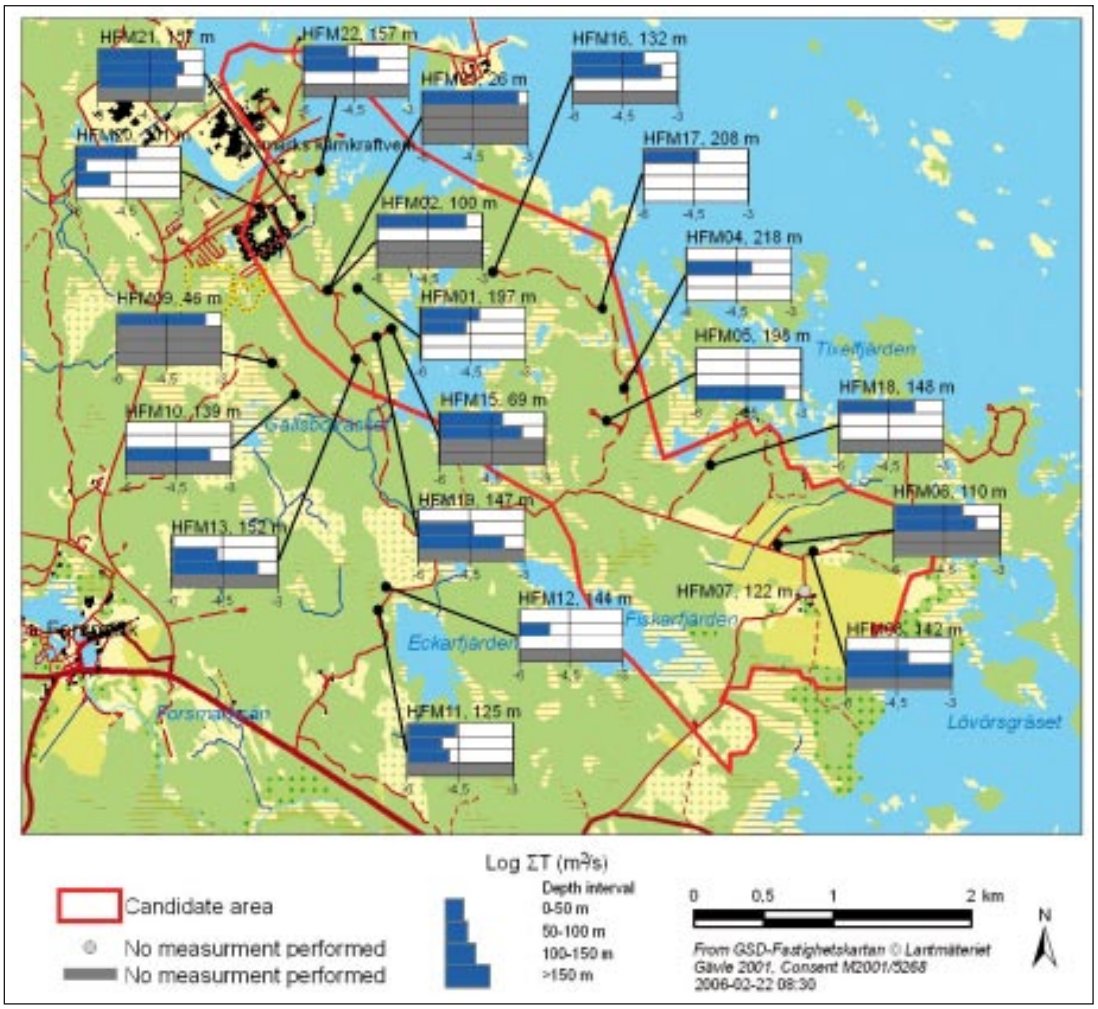

Figure 2-21. *Inferred transmissivities in depth intervals of 50 m in the uppermost 200 m of rock. The figure after the borehole number is the vertical penetration depth. Note that many boreholes do not reach 200 m depth. Modified after /Gentzschein el al. 2006/.*

In stage 2.1 it was suggested that there can be a “hydraulic cage” phenomenon within the target volume in the north-western part of the tectonic lens. The hypothesis implies that horizontal fractures/sheet joints in the uppermost part (e.g. 100 m of rock) short circuit the recharge of meteoric water and also constitute the main discharge zone/elevation for potential deeper groundwater flow, e.g. from outcropping steeply and gently-dipping deformations zones. The cartoon shown in Figure 2-23 visualises the hypothesis. The size and orientation of the different arrows indicate the relative magnitudes and directions of the generalised flow pattern.

Figure 2-22. *Picture from the construction of the 13 m deep and more than one kilometre long canal between the Baltic Sea and the nuclear reactors. The horizontal fractures/sheet joints are encountered along the entire excavation. There are several "beds" of more or less extensive sheet joints on top of each other. The picture is taken from the southern side of the canal where the bridge crosses the canal between drill sites 7 and 8, see Figure 2-1.*

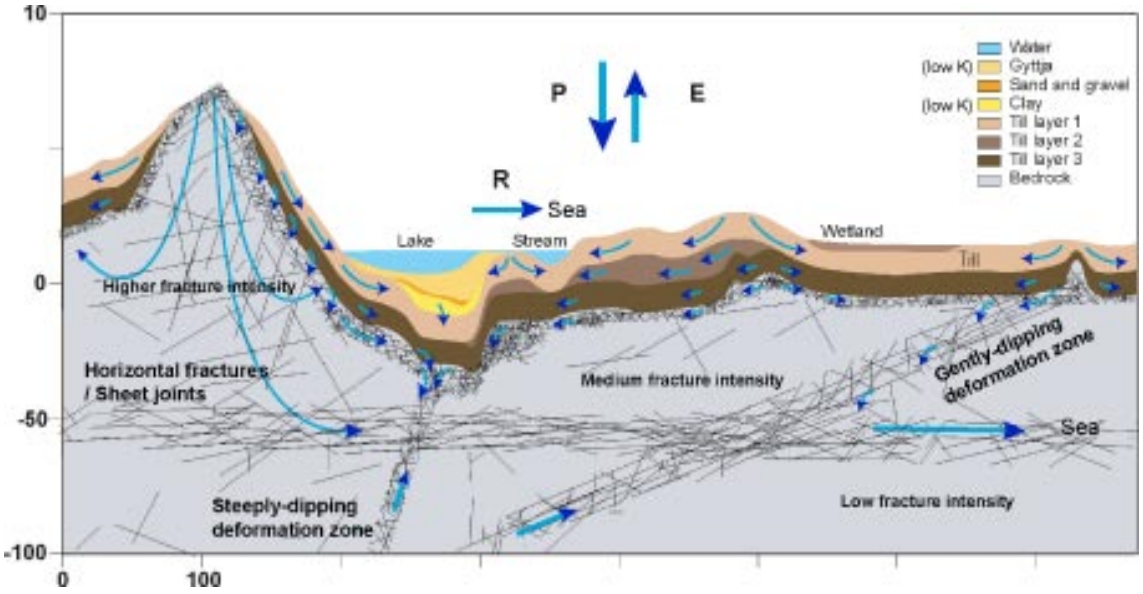

Figure 2-23. *Cross-section cartoon visualising the "hydraulic cage" hypothesis and its impact on the groundwater flow system (P = precipitation, E = evapotranspiration, R = runoff). Strands of evidence that support the envisaged hydraulic interplay between the groundwater in the superficial bedrock and in the Quaternary deposits and between surface water and the groundwater in the Quaternary deposits are presented in Section 2.3.5 and Section 2.3.6, respectively.*

Besides the structural evidence shown in Figure 2-22 there are also four strands of hydrogeological evidence that support the hypothesis of a "hydraulic cage" phenomenon:

Exceptionally high well yields for the percussion boreholes drilled inside the candidate area, see

1. Exceptionally high well yields for the percussion boreholes drilled inside the candidate area, see Figure 2-24. The median yield of the percussion drilled boreholes (wells) within the candidate area is c. 12,000 L/h, which is c. twenty (20) times higher than the median yield in the nearby domestic water wells, which is no different than the median yield of all bedrock water wells in Sweden (c. 200,000 wells) /Berggren 1998/. A representative example of a high yielding percussion borehole in the candidate area is shown in Figure 2-8 (HFM02).
2. The near uniform groundwater point-water heads inside the tectonic lens, see Figure 2-25. In particular, the point-water heads in the target area suggest a well connected network of superficial fractures of high transmissivity in the uppermost c. 150 m of bedrock, cf. Figure 2-21.
3. Fairly fresh groundwater at shallow depths of 100–200 m on top of relatively saline waters consistent with present-day marine (Baltic Sea) and older marine (Littorina Sea) water, see Figure 2-16.
4. The rapid, "large-range", transmission of pressure signals induced during a large-scale interference tests conducted in the target area /Gokall-Norman et al. 2005/, see Figure 2-26 and Figure 2-27.

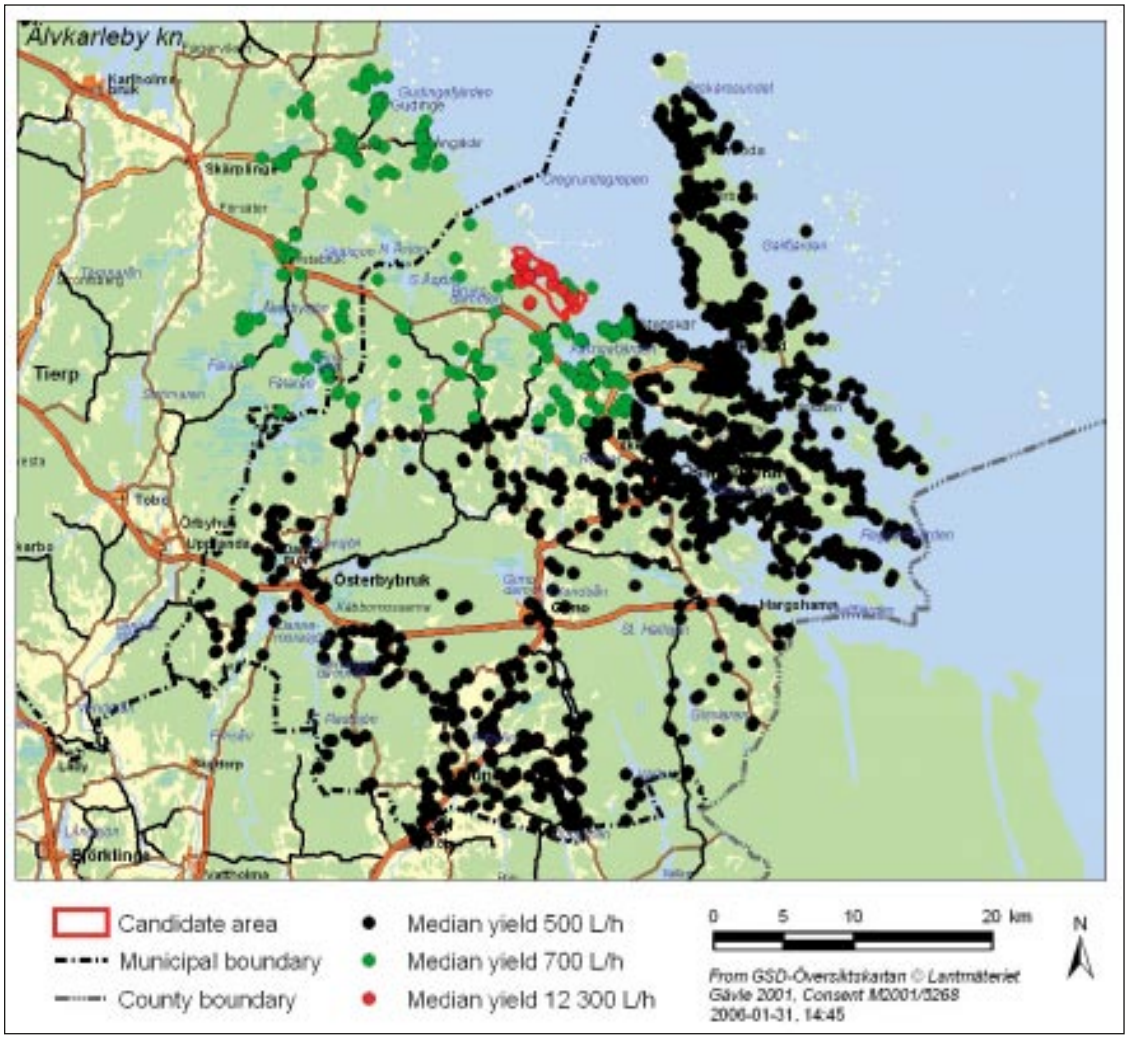

Figure 2-24. *Map showing the percussion boreholes in the candidate area (red dots) and the nearby domestic bedrock water wells (black and green dots). The median well yield of the HFM01–HFM22 boreholes is c. 20 times higher than the median well yield of the nearby domestic wells /Gentzschein et al. 2006/.*

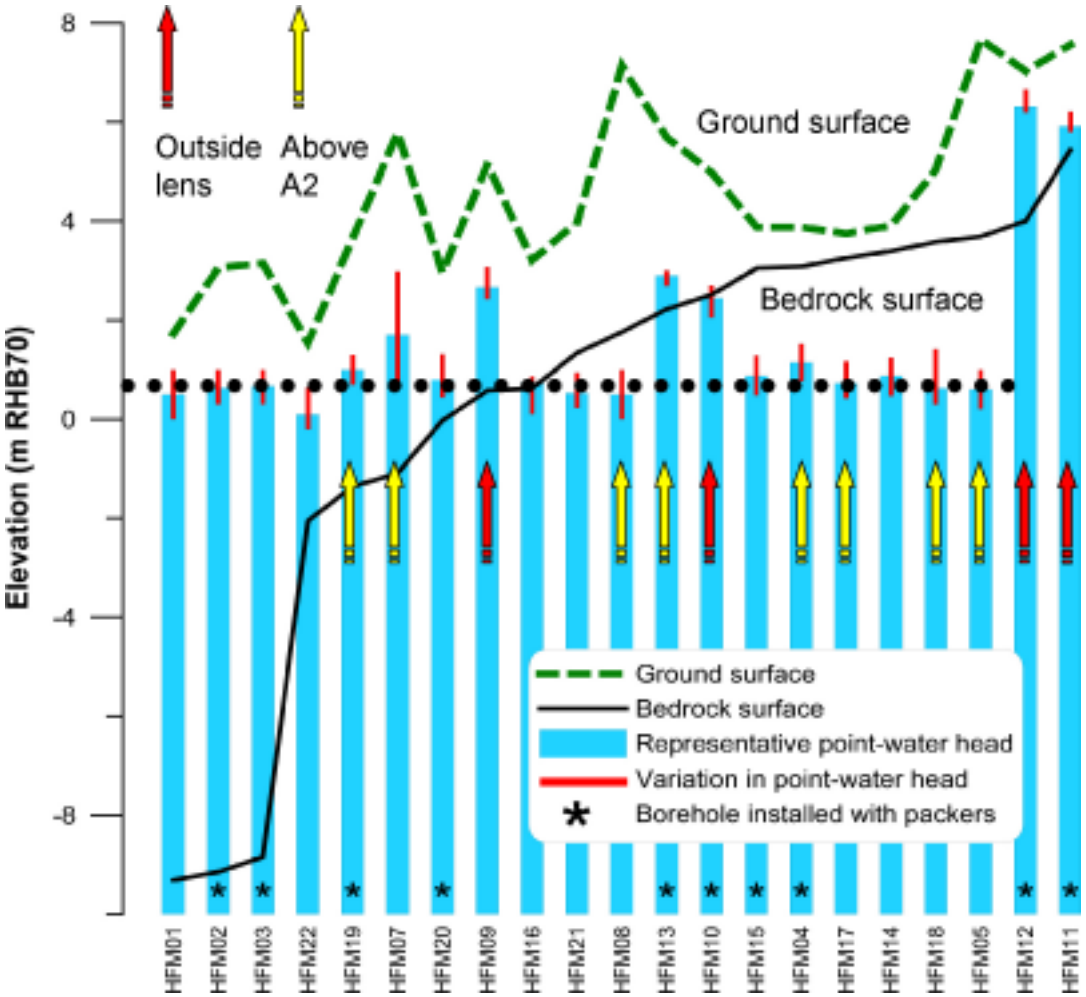

Figure 2-25. *Mean point-water heads in the superficial bedrock in the north-western part of the tectonic lens. The boreholes are ordered with regard to bedrock elevation. The plot shows that many mean point-water heads in the superficial bedrock are insensitive to the surface elevation as well as to the bedrock elevation, which indicate a well connected lattice of fractures of high transmissivities. Red arrows indicate boreholes drilled outside the tectonic lens, yellow arrows indicate boreholes drilled within the tectonic lens. Stars indicate that the point-water head shown is monitored in a borehole with multiple packers. The values shown here represent the uppermost, open, intervals. The monitored borehole intervals in HFM07 and HFM13 have low transmissivities. Modified after /Gentzschein et al. 2006/.*

Understanding the lateral extent and properties of the horizontal fractures/sheet joints is an important component of the hydrogeological site description. There are several observations that the "hydraulic cage" phenomenon is more pronounced in the superficial bedrock in the foot wall of the gently-dipping ZFMNE00A2 than in the hanging wall of this zone. In the hanging wall, the groundwater flow appears to be governed by a sequence of gently dipping deformation zones (ZFMNE00A2–A7 and -B1) rather. These zones were first predicted by the reflection seismics and later confirmed by the drilling and the hydraulic testing of KFM02A and KFM03A. Two hydraulic interference tests have been conducted in the hanging wall, see Table 2-3. The working hypothesis is that the horizontal fractures/sheet joints encountered in the target volume continue under Lake Bolundsfjärden to the southeast, however, with a decreasing intensity as schematically outlined in Figure 2-14.

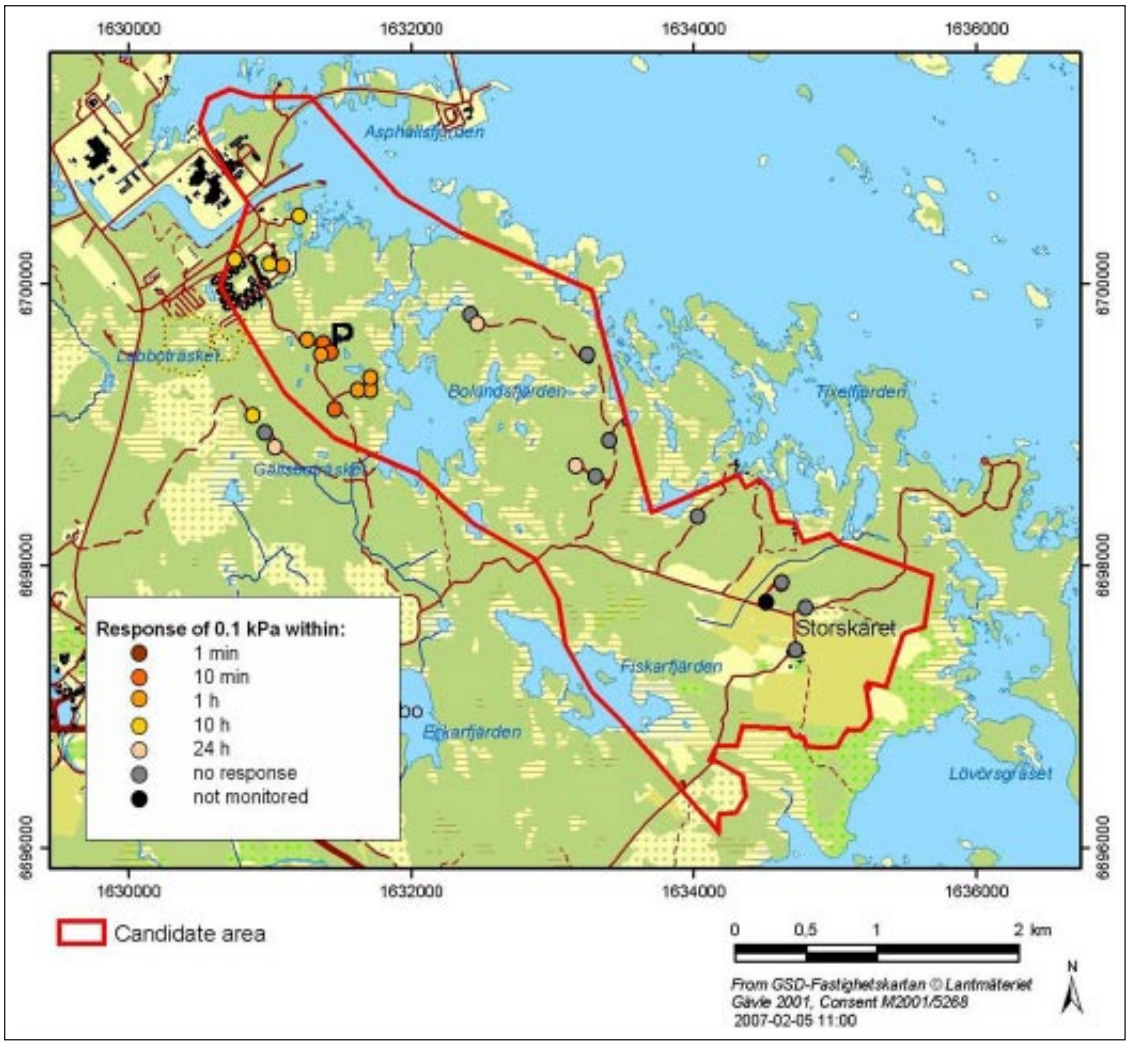

Figure 2-26. *Map showing response times in hours in the bedrock to 'Jakob's Interference Test' (JIT). The pumping was conducted in HFM01 (P) and the interference test responses were monitored at 37 "observation points", see /Gokall-Norman et al. 2005/, using the Hydrologic Monitoring System (HMS). The location of the pumping well is indicated with a* **P**.

Figure 2-24 suggests that the "hydraulic cage" phenomenon does not extend far beyond the tectonic lens, possibly ending somewhere adjacent to the regional deformation zones the bordering the candidate area, cf. Figure 2-5. The true conditions are unknown, of course, but the observed 'anomaly in well yield' for percussion boreholes within the candidate area compared with the water supply wells outside the lens is striking. One of several working hypotheses at this stage is that the horizontal fractures/sheet joints in the north-western part of the candidate area follow the bedrock surface as this dips under the Baltic Sea towards north-east. Possible, the horizontal fractures/sheet joints within the candidate area connect to the Singö deformation zone. The structural and hydraulic properties of the Singö deformation zone will be investigated by borehole KFM11A, see Figure 2-1. However, this information will not be available until after Data Freeze 2.3, see Table 2-2.

A hydraulic note on Jakob's Interference Test

The pumping well, HFM01, and the nearby observation well, HFM02, are both located at drill site 1. The distance from drill site 1 to drill site 2, where the cored borehole KFM02A is interpreted to intersect ZFMNE00A2 at c. 411–519 m depth is 1.9 km, see Figure 2-1. HFM01 and HFM02 intersect a horizontal fracture/sheet joint in close connection to ZFMNE00A2 at c. 42.8 m and 43.5 m depth, respectively, see Figure 2-28. The distance between HFM01 and HFM02 is c. 220 m and the cross-hole transmissivity at drill site 1 is c. $(1.5–4)\cdot10^{-4}$ m^2/s /Ludvigson and Jönsson 2003, Gokall-Norman et al. 2005/. Figure 2-8 shows the high yield acquired in HFM02 when the horizontal fracture/sheet joint (or ZFMNE00A2) was intersected during the drilling.

During 'Jakob's Interference Test' c. 15 mm of rain was observed, see Figure 2-29. The precipitation caused a total head response of c. 0.2 m in HFM02:2 (38–48 m) at drill site 1 between the 22nd and 26th of July 2005, see Figure 2-30. (HFM02 is located close to the pumping well HFM01.) In KFM02A:5 (411–442 m), c. 1.9 km away from drill site 1, the head response was c. 0.10–0.15 m, see Figure 2-31.

The head response in ZFMNE00A2 to the precipitation event is striking. A tentative guess of the "pressure break-through" is c. 12–24 hours, cf. Figure 2-29 and Figure 2-31. The hydraulic diffusivity of ZFMNE00A2 may be estimated by computing the ration of r^2/dt /Streltsova 1998/. Inserting r = 1,900 m and dt = 18 hours renders a hydraulic diffusivity of 56 m^2/s. The hydraulic diffusivity of ZFMNE00A2 evaluated from 'Jakob's Interference Test' is in the range 50–60 m^2/s, see Figure 2-27.

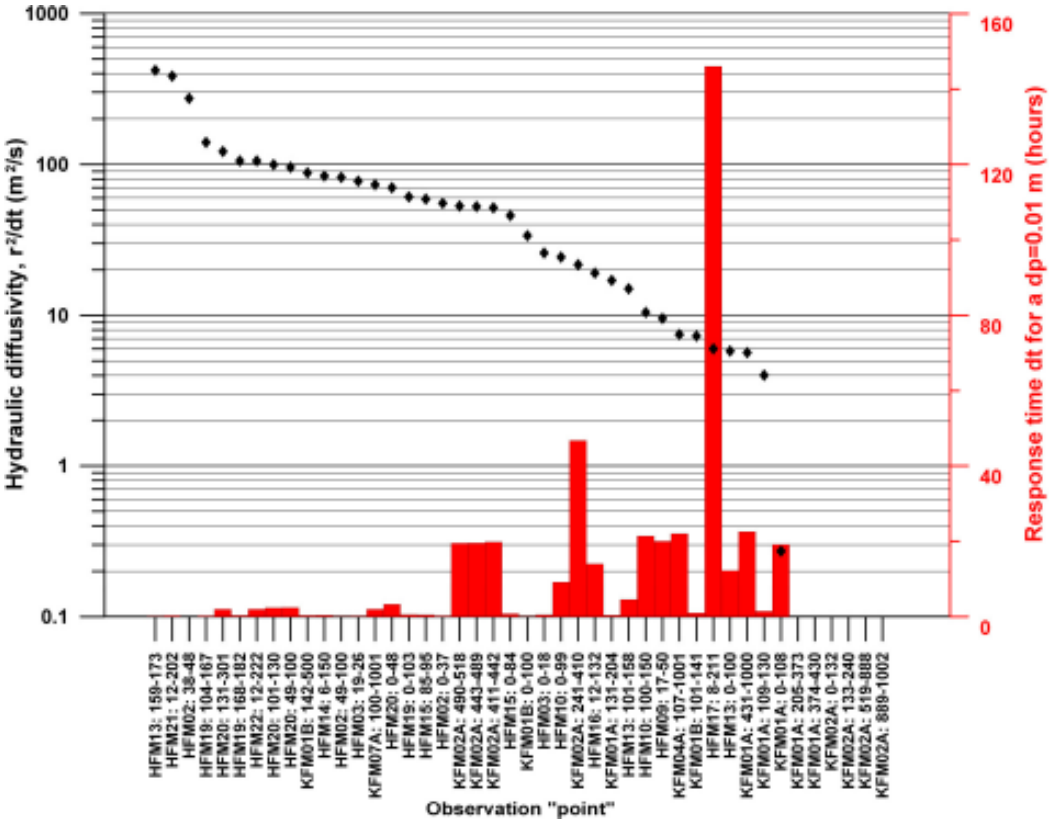

Figure 2-27. *Hydraulic diffusivities (evaluated as r^2/dt, /Streltsova 1998/) at the 37 "observation points" monitored during 'Jakob's Interference Test', cf. Figure 2-26. The body of the interpreted values range between 4–500 m^2/s, which implies a quite transmissive network of little or no storativity. In comparison, the reported correlation between storativity and transmissivity from the investigations at the Äspö HRL /Rhén et al. 1997/ suggests a much smaller range in the hydraulic diffusivity, 2–40 m^2/s.*

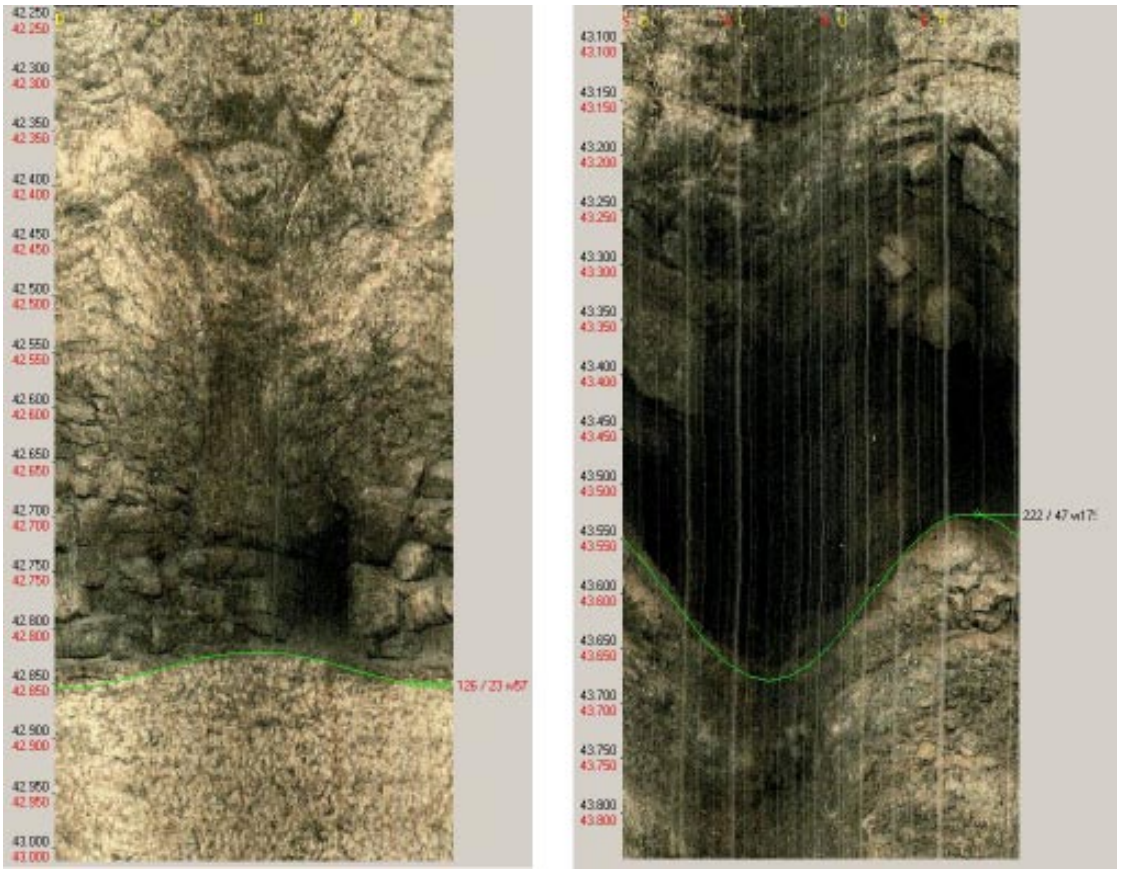

Figure 2-28. *Two BIPS pictures showing the intersections with the horizontal fracture/sheet joint in close connection to ZFMNE00A2 at drill site 1. Left: HFM01; z=42.8 m, strike/dip = 126/23, $T=4.5\cdot10^{-5}$ m^2/s. Right: HFM02; z=43.5 m, strike/dip=222/45, $T=5.9\cdot10^{-4}$ m^2/s. The apertures in the pictures are 1–3 dm wide and show evidence of being channelised.*

Figure 2-32 shows a cartoon of the observed precipitation phenomenon. The geometry is based on the cross-section shown in Figure 2-10. In Figure 2-32 we also display a one-dimensional mathematical model of the phenomenon. A solution to the diffusivity equation for a linearly increasing head at x = 0 is provided by /Edelman 1947/.

Figure 2-33 shows the match between the one-dimensional model and field data for three values of the hydraulic diffusivity. The source term is the linear increasing head change at drill site 1, i.e. in HFM02:2. The transient responses at drill site 2, i.e. in KFM02A:5, is matched with a hydraulic diffusivity of 60 m^2/s. The solutions for T/S = 30 m^2/s and T/S = 90 m^2/s are inserted to demonstrate the sensitivity of the model to the value of the hydraulic diffusivity as well as to the uncertainty in the interpreted head response in KFM02:5.

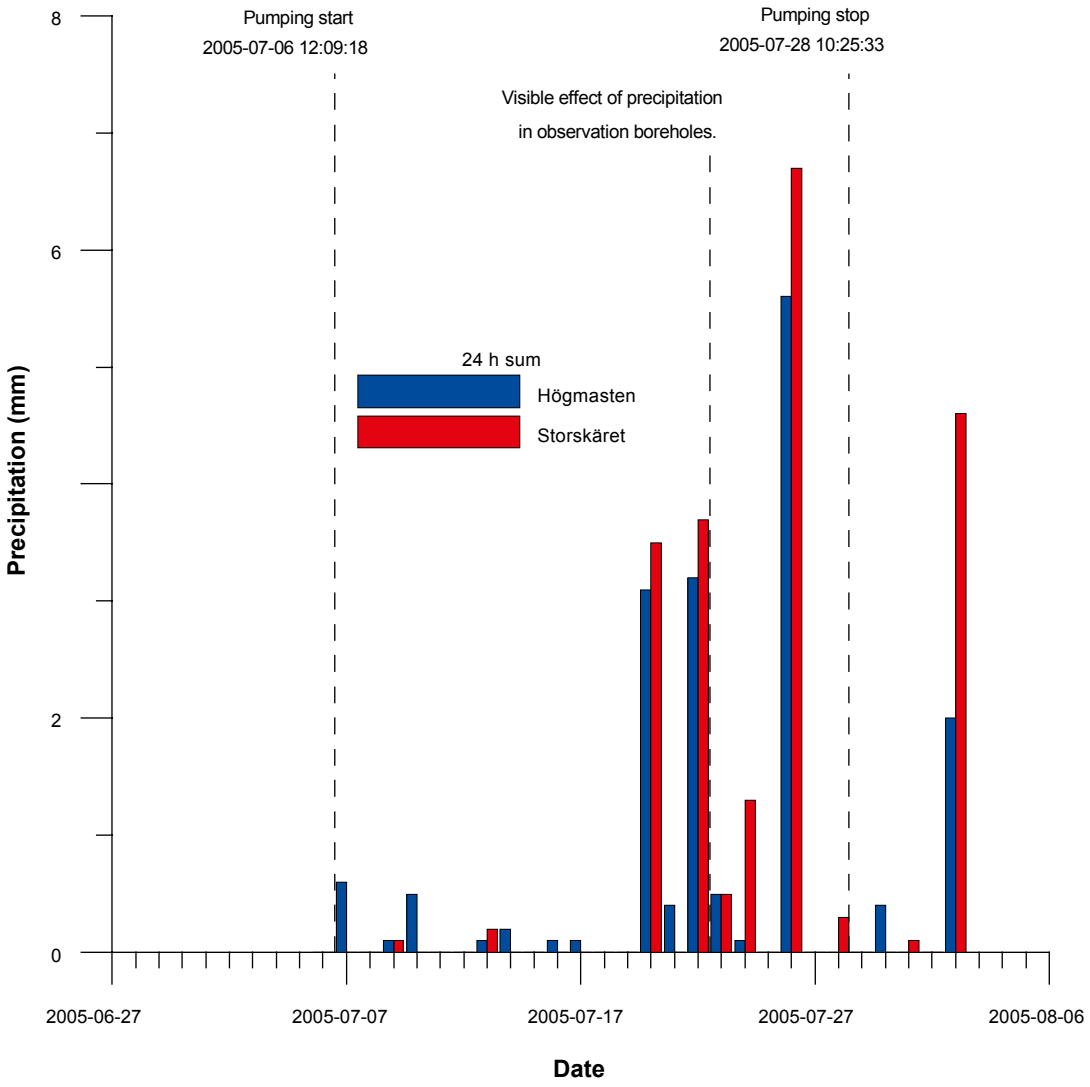

Figure 2-29. *Precipitation observations during 'Jacob's Interference Test' summed up to 24 hours rates. The station Storskäret is close to KFM03A in the south-eastern part of the candidate area whereas station Högmasten is located in the vicinity of the power plant northwest of the candidate area. Modified after /Gokall-Norman et al. 2005/.*

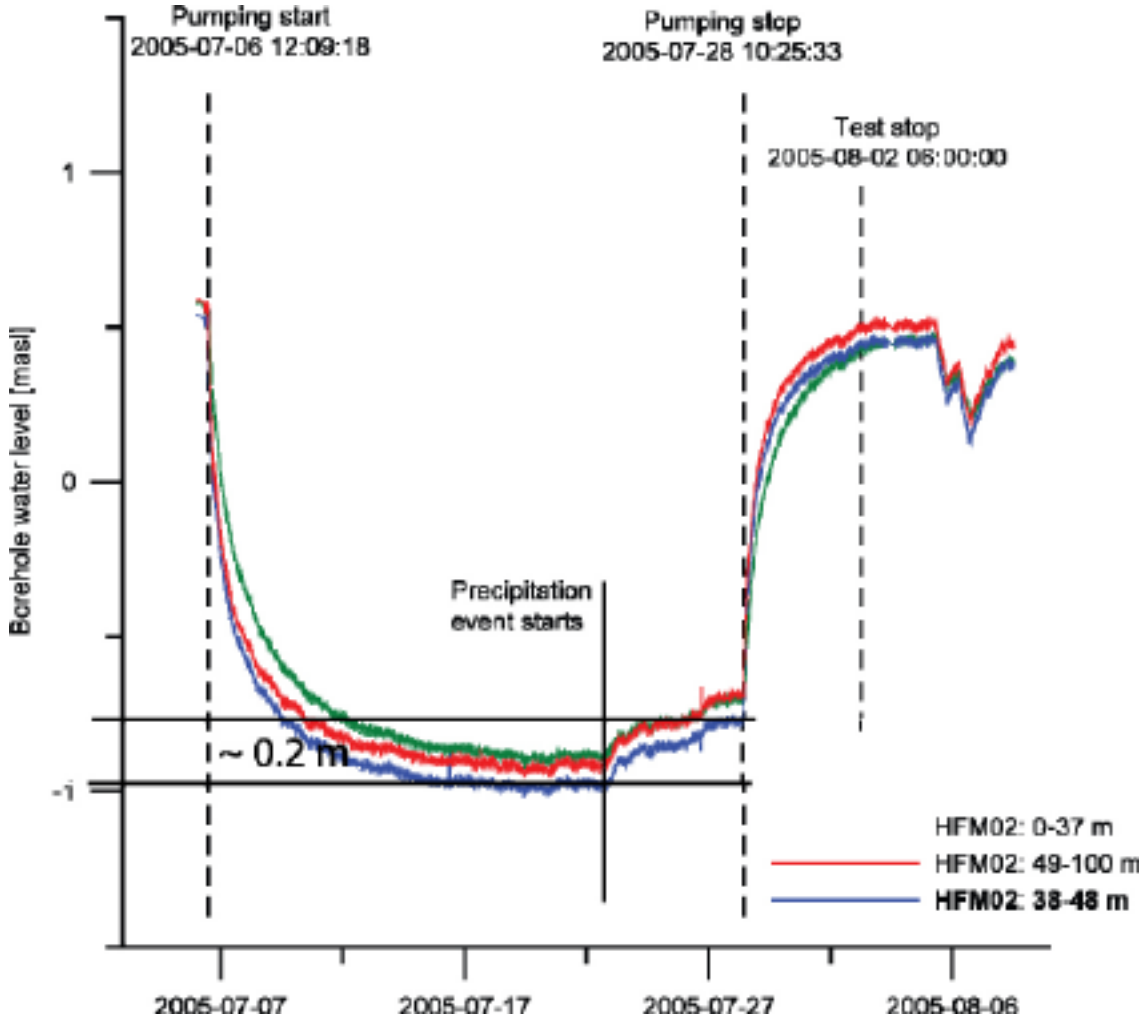

Figure 2-30. *Point-water head responses in HFM02 adjacent to the pumping well HFM01. Deformation zone ZFMNE00A2 intersects HFM02 at c. 40 m depth. The solid line in centre indicates when the effects of the precipitation event in Figure 2-29 show up in the head observations in HFM02. Modified after /Gokall-Norman et al. 2005/.*

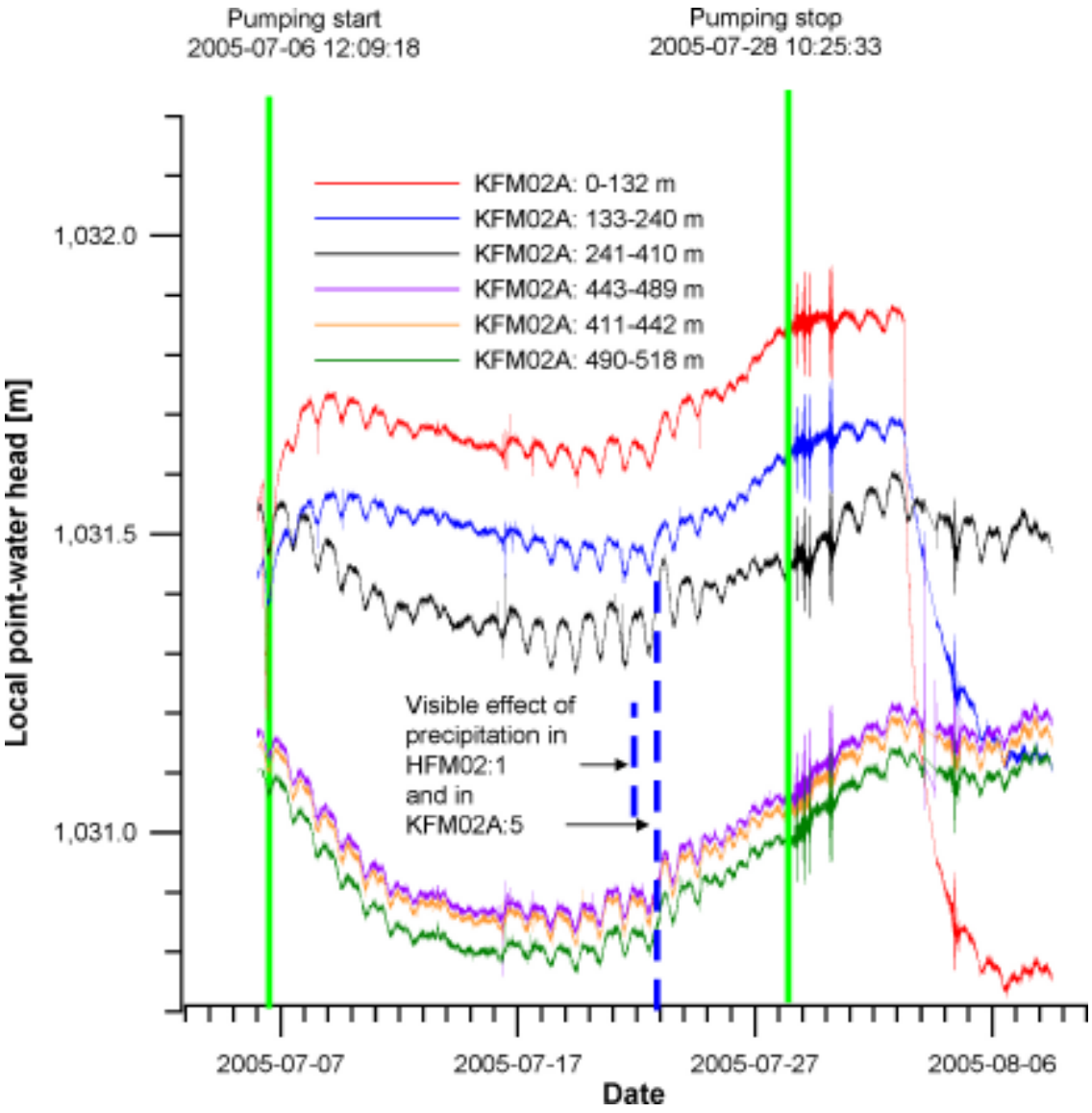

Figure 2-31. *Local point-water head responses in KFM02A, i.e not recalculated with regard to the datum plane RHB70. ZFMNE00A2 intercepts KFM02A between 411–518 m borehole length according to the deformation zone model for Forsmark stage 1.2. Modified after /Gokall-Norman et al. 2005/. The dashed blue lines indicate when the effects of the precipitation event in Figure 2-29 show up in the head observations in HFM02 and KFM02A:5, respectively.*

The key conclusion drawn here is that the heads in the gently-dipping deformation zones follow closely the variations in precipitation, sea level changes, barometric changes and tidal effects. Indeed, this has previously been demonstrated for ZFMNE00A4 /SKB 2005a/. This deformation zone is intersected by KFM03A at drill site 3 at c. 390 m depth. ZFMNE00A4 outcrops in the Baltic Sea some 800–1,000 m away from drill site 3. Sea level changes are observed in KFM03A with a delay of 4 hours, which suggests a hydraulic diffusivity of 40–70 m^2/s.

The hydraulic responses obtained during ‘Jakob’s Interference Test’ have been cross-checked by a second interference test, ‘Peter’s Interference Test’, during the summer of 2006 using percussion borehole HFM14 as a sink (pumping well) instead of HFM01 (the two boreholes are c. 350 m apart). HFM14 probably penetrates ZFMNE00A2 in its upper part, see Figure 2-32. Results from ‘Peter’s Interference Test’ belong to Data Freeze 2.2 and will be analysed and modelled in stage 2.2, cf. Table 2-3.

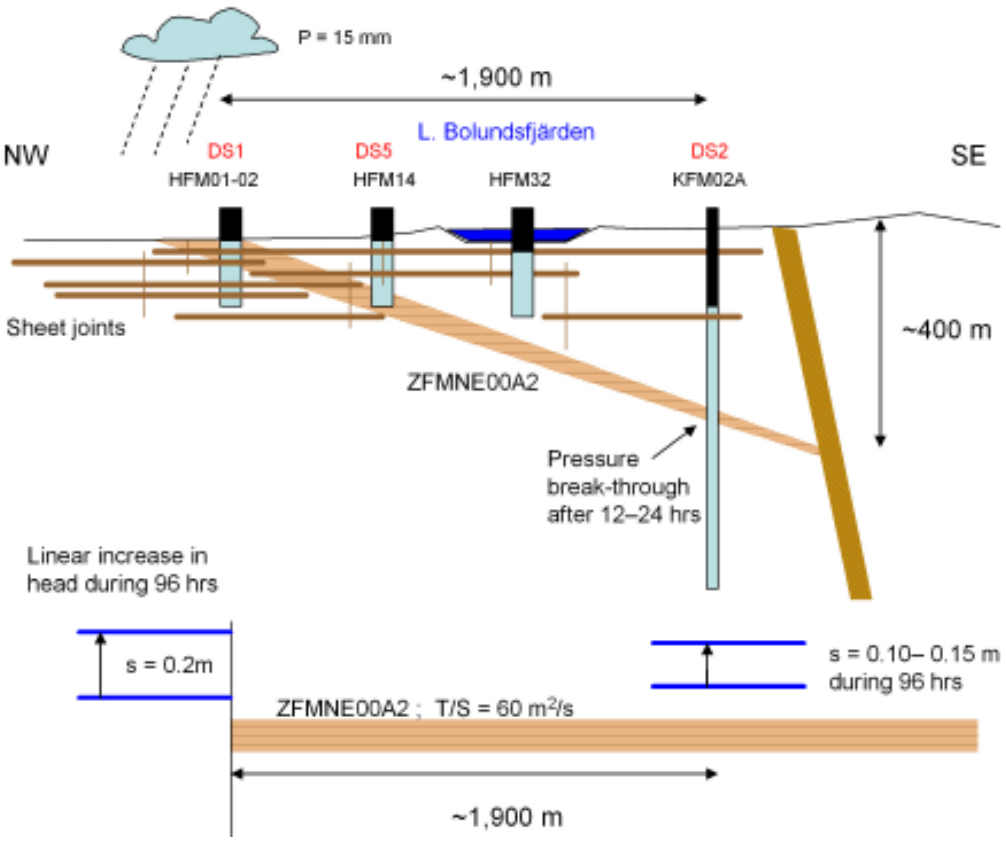

Figure 2-32. *Cartoon of the observed precipitation phenomenon. The geometry is based on the cross-section shown in Figure 2-10. The solution to the one-dimensional model shown in the bottom part of the cartoon is displayed in Figure 2-33.*

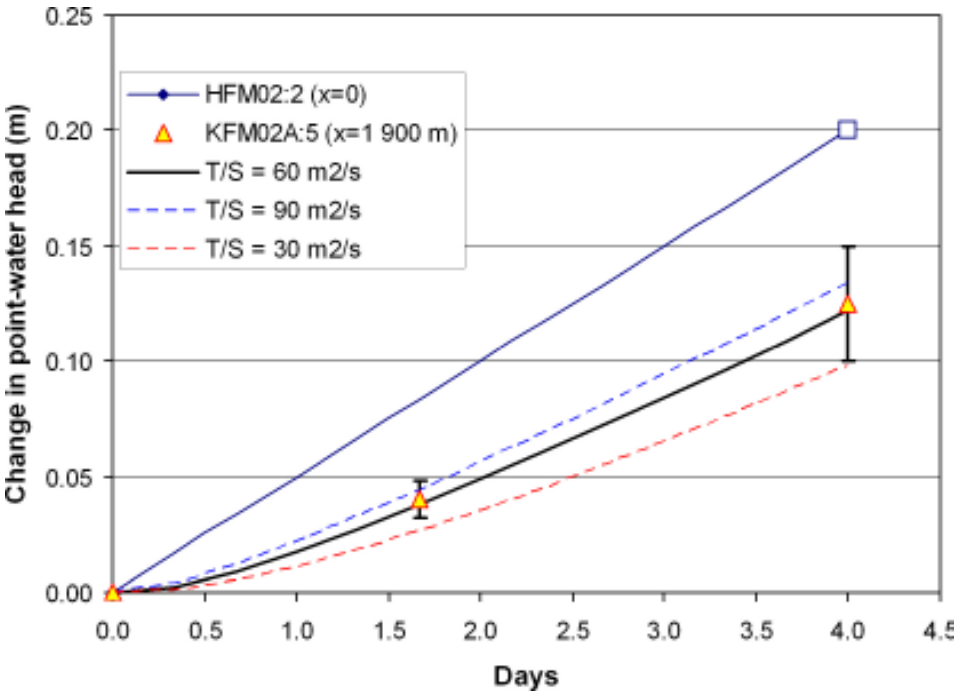

Figure 2-33. *Measured head responses in KFM02A:5 (triangles with uncertainty range) for a linearly increasing head at drill site 1 using data from HFM02:2 and the mathematical model envisaged in Figure 2-32. The tested models (dashed blue, solid black and dashed red) have different hydraulic diffusivities.*

2.3.4 The intensely fractured bedrock bordering the tectonic lens

The intensely fractured bedrock bordering the tectonic lens to the southwest of the target volume is investigated by two boreholes, KFM04A and KFM09A. Unlike KFM04A, KFM09A is not investigated by the PFL tool. Double-packer test data from KFM09A will not be available until Data Freeze 2.2, see Table 2-2. However, hydrogeochemistry data are available form KFM09A already in Data Freeze 2.1, cf. Figure 2-16.

KFM04A starts outside the target volume and enters the target volume at –400 m above sea level, see Figure 2-1 and Figure 2-18. The body of the flowing fractures in the upper half of KFM04A is predominantly associated with the deformation zones bordering the tectonic lens in this part of the candidate area. Hence, it is not possible to draw any particular conclusion on the properties of the background fracturing outside the tectonic lens from KFM04A.

Borehole KFM07A is not as close the south-western boundary as KFM04A and KFM09A, but it approaches this boundary at depth. That is, KFM07A starts inside the target volume and approaches the more intensely fractured bedrock at the very end, see Figure 2-1. Both KFM04A and KFM07A are very sparsely intersected by flowing fractures as long as they are intersecting the repository depth inside the tectonic lens, see Figure 2-17 and Figure 2-18.

As indicated in Figure 2-17, KFM07A intercepts a fairly high-transmissive deformation zone at depth. According to Figure 2-16 the chloride concentrations in KFM07A and KFM09A are fairly high at depth. In fact, the highest chloride concentrations recorded during the site investigations up to Data Freeze 2.1 come from KFM07A and KFM09A. Compared to KFM07A, KFM09A is intersecting more of the more intensely fractured bedrock bordering the tectonic lens to the southwest of the target volume, see Figure 2-1. The reason for the high chloride concentrations is not known. Possibly, they are a result of upconing during drilling/pumping. If natural, the observations indicate that the deeper salinity interface encountered in the gently-dipping deformation zones in the hanging wall, see Figure 2-16, is probably due to glacial flushing.

As mentioned above, the fractured bedrock bordering the tectonic lens to the northeast of the target volume will be partly investigated by borehole KFM11A, see Figure 2-1. The working hypothesis is that the fracture intensity in the sparsely fractured rock at depth within the tectonic lens increases adjacent to the Singö deformation zone similar to the observations to the southwest of the target volume in KFM04A.

2.3.5 Interaction between the groundwater in superficial bedrock and the groundwater in Quaternary deposits

The point-water heads in the superficial bedrock inside the tectonic lens are generally low and the hydraulic gradient between adjacent boreholes relatively flat, see Figure 2-25. The average point water head range between 0.0 and 1.14 m RHB70 in all percussion-drilled boreholes with exception of two sections with very little water, see Figure 2-35 and Figure 2-34.

The point-water heads in the Quaternary deposits are quite different. In contrast to the mean point-water heads in bedrock, the mean point-water heads in the Quaternary deposits are strongly correlated to the ground surface elevation, see Figure 2-36 and Figure 2-37.

At locations where point-water heads are measured both in Quaternary deposits and in the bedrock, the mean heads in the bedrock are generally considerably lower than in the Quaternary deposits. This feature is most pronounced within the tectonic lens. There are no examples within the tectonic lens of a situation where the point-water head in Quaternary deposits is constantly below the point water head in bedrock in nearby wells. However, such conditions can prevail during dry summer periods when the evapotranspiration is large and if the precipitation is low, see Figure 2-38 for an example from drill site 6.

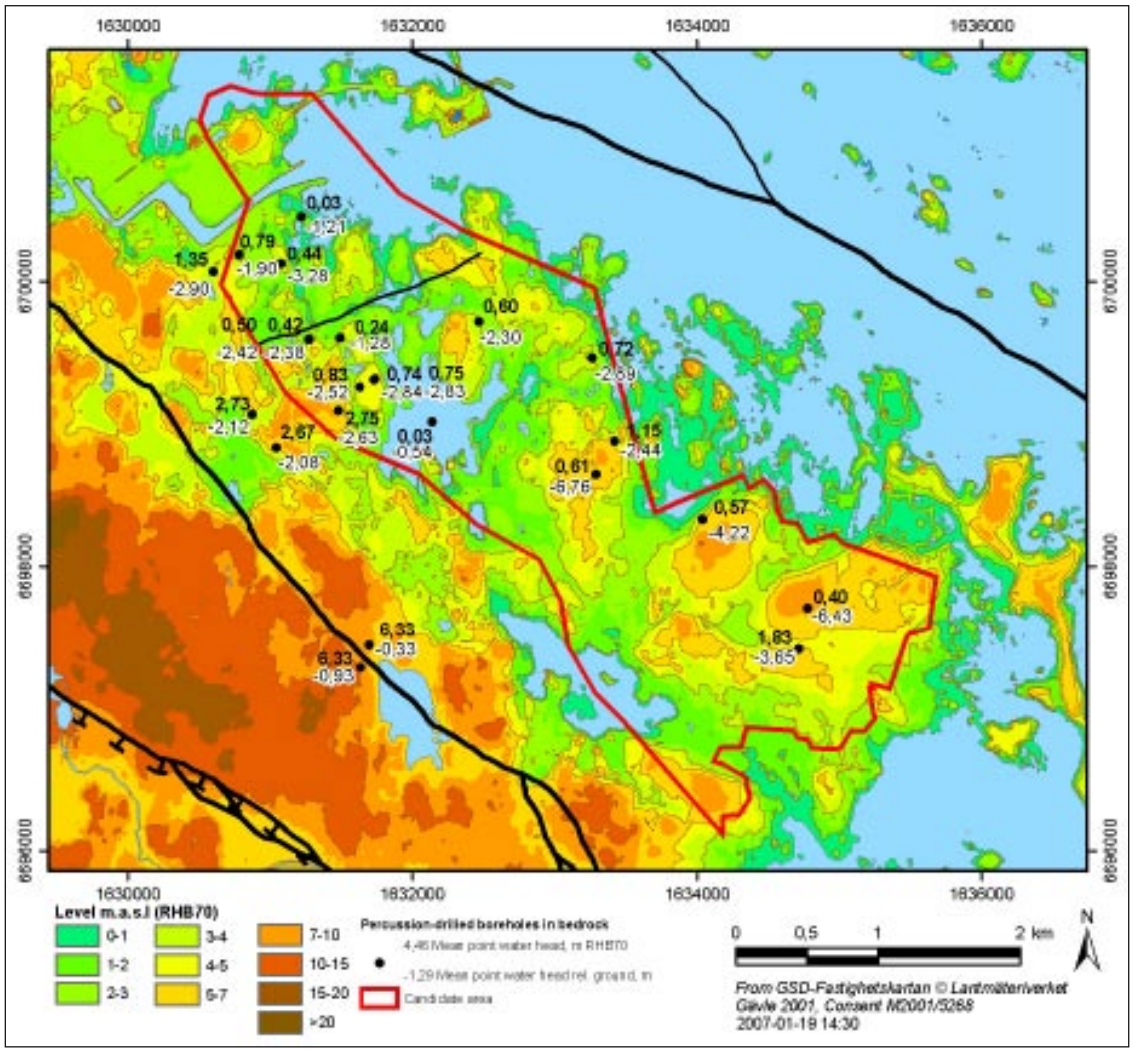

Figure 2-34. *Mean point-water heads in the percussion-drilled boreholes in the uppermost part of the bedrock expressed as elevation in RHB70 (black) and depth relative to ground surface (white) /Werner et al. 2007/.*

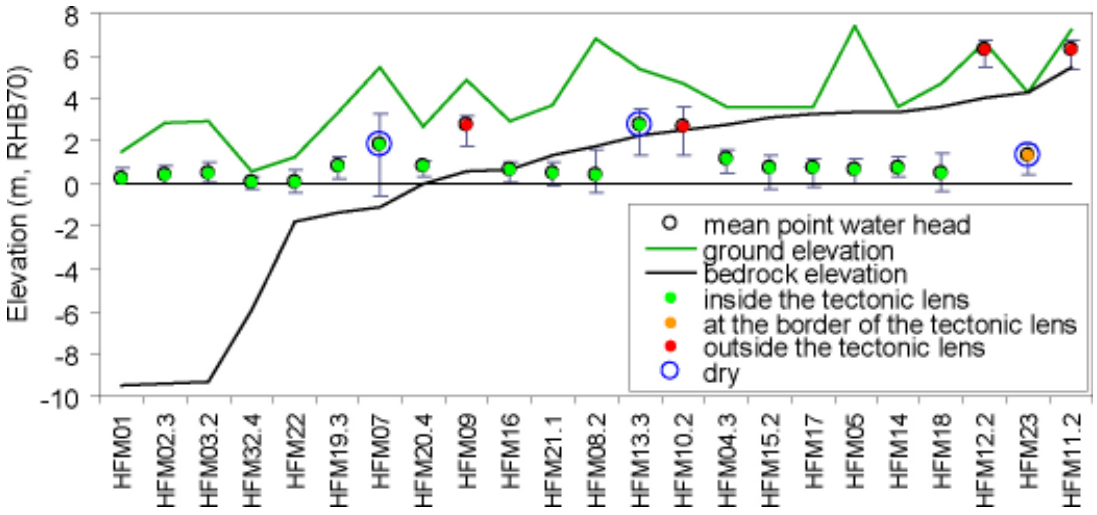

Figure 2-35. *Mean point water heads in percussion-drilled boreholes. Except for two "dry" sections in HFM07 (open hole) and HFM13:3, the point-water heads within the tectonic lens vary very little, from 0.0 to 1.14 m RHB70 (only wells with more than 150 days of level data are included). Modified after /Werner et al. 2007/.*

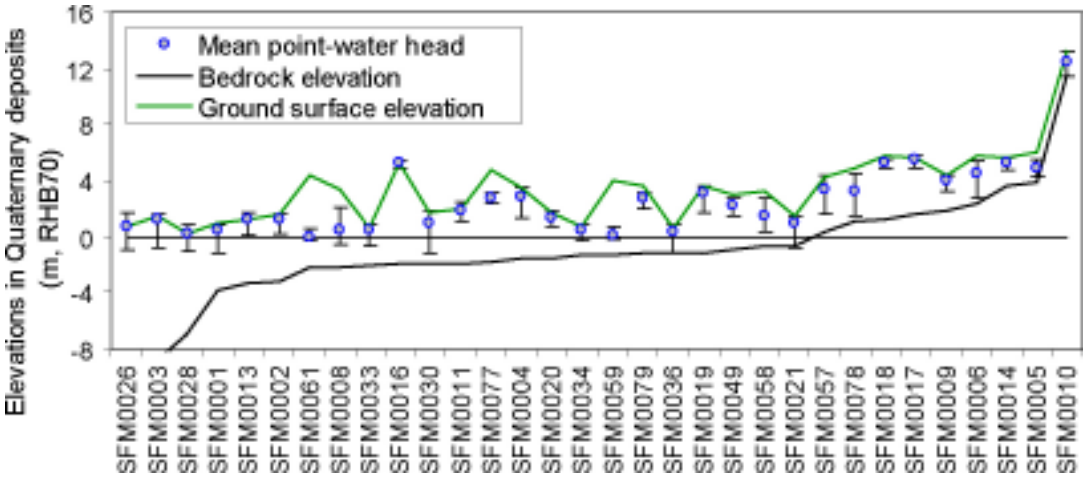

Figure 2-36. *Mean groundwater levels in Quaternary deposits (only wells with more than 150 days of level data are included). The close correlation of groundwater levels and ground levels is clear. Exceptions are SFM0059 and SFM0061, which are located in a glaciofluvial deposit, the Börstil esker, and SFM0008 and SFM0058, which are located in locally elevated till areas. Modified after /Werner et al. 2007/.*

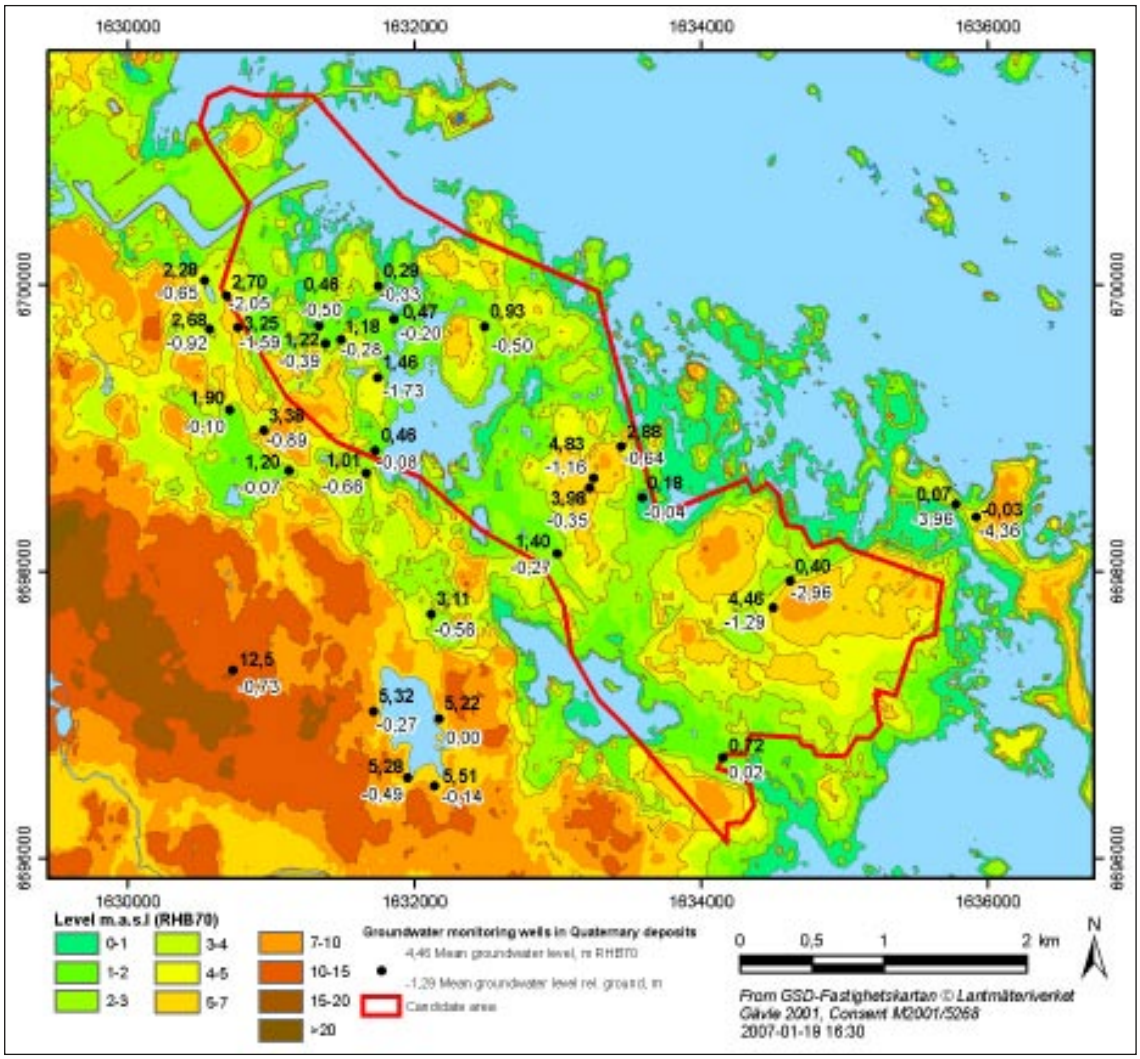

Figure 2-37. *Mean point-water heads in the monitoring wells in the Quaternary deposits expressed as elevation in RHB70 (black) and depth relative to ground surface (white). /Werner et al. 2007/.*

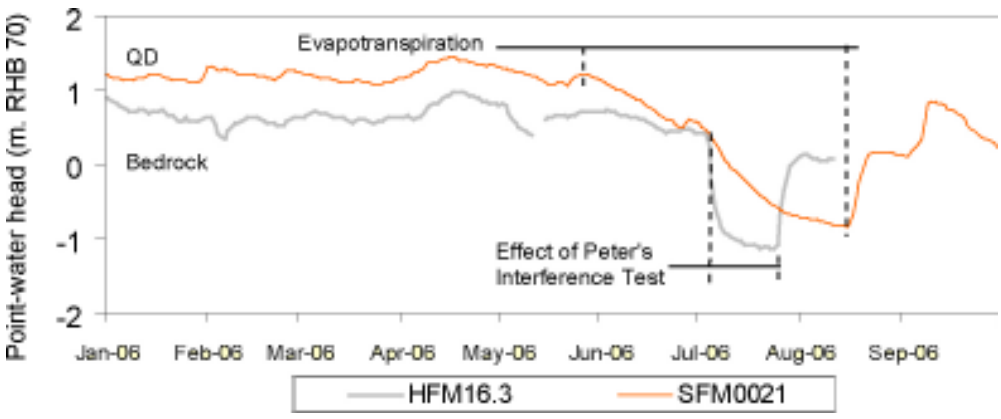

Figure 2-38. *Point-water heads in bedrock (HFM16:3) and in Quaternary deposits (SFM0021) close proximity to drill site 6. The head in the Quaternary deposit is generally greater than in the bedrock except during dry summer periods when the evapotranspiration is large and if the precipitation is low. Modified after /Werner et al. 2007/.*

2.3.6 Interaction between surface water and groundwater

During dry summers higher lake surface elevations compared with local groundwater elevations in Quaternary deposits have been observed in Forsmark area /Juston et al. 2007/. This observation suggests that the lakes act as sources of groundwater recharge to the local aquifers in the Quaternary deposits during periods when the evapotranspiration is high and if the precipitation is low. During other circumstances (seasons), higher groundwater levels suggest the lakes act as discharge areas for the surrounding aquifers in the Quaternary deposits.

A particular situation with frequently higher lake surface elevations compared with the point-water heads in the Quaternary deposits as well as the point-water heads in the bedrock has been observed below the middle of Lake Bolundsfjärden; that is in SFM0040, SFM0023 and HFM32:1–4, see Figure 2-39. Lake Bolundsfjärden is located in the centre of the target area close to the Baltic Sea and HFM32 is drilled into the bedrock in the middle of the lake, see Figure 2-32. The mean lake surface elevation is only a few decimetres above the datum plane (RHB70). The sea level, on the other hand, varies a lot. Variations in the sea level between +0.8 and –0.8 m RHB70 are not uncommon, which means that transgressions occur now and then, see Figure 2-39 for an example. Higher lake surface elevations in Lake Bolundsfjärden than point-water heads in the Quaternary deposits in the till underlying the lake as well as in the superficial bedrock means that Lake Bolundsfjärden cannot be assumed to be the ultimate discharge elevation for the groundwater at repository depth; that is, the head gradient from the lake surface, through the underlying Quaternary deposits and into the uppermost part of the bedrock is pointing downwards.

A low vertical hydraulic conductivity in the till (as well as in the gyttja/clay sediments where such sediments occur on top of till) constrains the magnitude of the recharge rate from the surface to the bedrock, however. Figure 2-23 visualises the notion. The surface runoff term in the water balance equation is fairly tentative at this point as it is based on too short a time series. /Juston et al. 2007/ report 136 mm/y for the period of August 2004 through July 2005. A very preliminary analysis including data for 2006 suggests a specific discharge of about 160 mm/y. In comparison, the Swedish Meteorological and Hydrological Institute has estimated the 30 year runoff value in the Östhammar and Tierp municipalities to 233–252 mm/y /Larsson-McCann et al. 2002/. High hydraulic conductivities in the very uppermost part of the Quaternary deposits probably contribute to the seasonal runoff process, because a pronounced overland flow has not been observed.

The heads in the deeper rock vary in a more complex fashion. Since flow in fractured rocks is governed by the geometry of the structures, it is difficult to generalise the interpretation of the point-water heads observed in Figure 2-39; that is, a classic porous medium approach can be quite misleading. Notwithstanding, the head gradient between the lake and the upper parts of the bedrock below the lake is always downwards in Figure 2-39.

The blue arrows in Figure 2-39 indicate the start and the end of two interference tests with HFM14 as a pumping well ('Peter's Interference test, Part 1 and 2). Note the moderate effect of the interference tests on the heads in the uppermost, transmissive, part of the bedrock (HFM32:3, 26–31 m; HFM32:4, 6–25 m), the pronounced effect on the heads in the deeper rock (HFM32:1, 98–203 m; HFM32:2, 32–97 m), and the hydraulic contact with the till (suggests little leakage through the gyttja/clay sediments). The red arrows indicate the start and the end of water sampling for till groundwater chemistry. From the beginning of June the sea surface elevation is higher than the point-water heads in the bedrock.

In Figure 2-40, the point-water head data from HFM32:1–4 is accompanied by point-water head data from KFM02A:5 (411–442 m), which intersects ZFMNE00A2. Despite the large lateral distance (KFM02A:5 and HFM32:1 are c. 1,000 m apart) the time series for the two borehole sections are very similar, at least up the beginning of June when the dry summer of 2006 starts. (The main drought is during July and the first part of August.). A plausible interpretation of this similarity is that head data in HFM32:1 (98–203 m) are affected by the closeness of ZFMNE00A2, cf. Figure 2-32. The time series suggest that the uppermost, transmissive, part of the bedrock constitutes the discharge zone for the deeper groundwater flow. Why the heads in the bedrock are lower than the sea level during the dry summer period is currently being investigated.

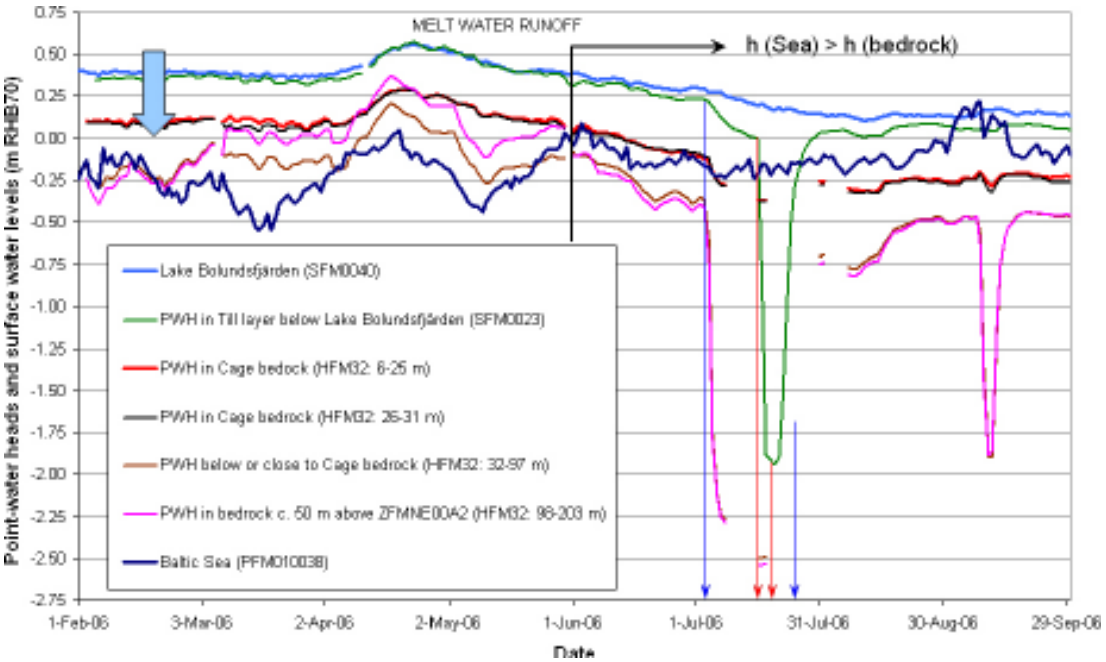

Figure 2-39. *Time series of surface water levels (SFM0040) and point-water heads in the till (SFM0023) and the bedrock (HFM32:1 (98–203 m), HFM32:2 (32–97 m), HFM32:3 (26–31 m); and HFM32:4 (6–25 m)) below Lake Bolundssfjärden. The head gradient between the lake and the upper parts of the bedrock below the lake is always downwards (fat blue arrow). The thin blue arrows indicate the start and the end of two interference tests with HFM14 as a pumping well ('Peter's Interference test, Part 1 and 2). Note the moderate effect of the interference tests on the heads in the uppermost, transmissive, part of the bedrock (HFM32:3 (26–31 m) and HFM32:4 (6–25 m)) and more the pronounced effect on the heads in the deeper rock (HFM32:1 (98–203 m) and HFM:2 (32–97 m)). The effect on the head in the till (SFM0023) suggests little leakage through the gyttja/clay sediments. The thin red arrows indicate the start and the end of water sampling for till groundwater chemistry. From the beginning of June the sea level is greater than the point-water heads in the bedrock.*

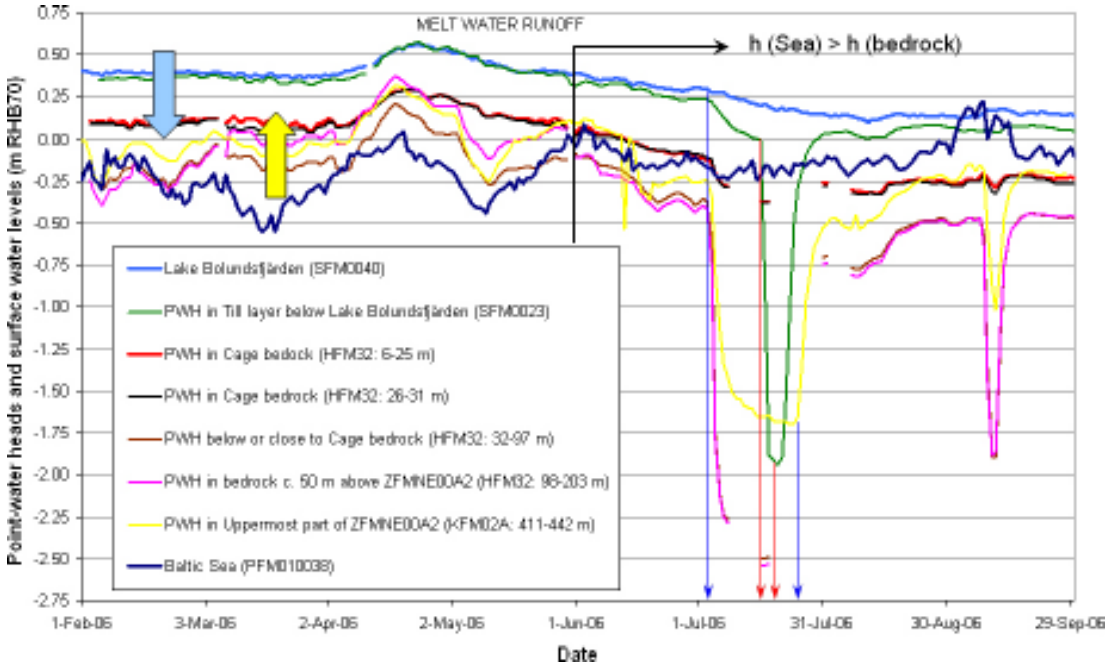

Figure 2-40. *The point-water head data from HFM32:1 (98–203 m), HFM32:2 (32–97 m), HFM32:3 (26–31 m); and HFM32:4 (6–25 m) in Figure 2-39 are here accompanied by point-water head data from KFM02A:5 (411–442 m). Despite the distance (KFM02A:5 and HFM32:1 are c. 1,000 m apart) the time series for the two borehole sections are very similar, at least up the beginning of June when the dry summer of 2006 starts. (The main drought is during July and the first part of August.). A plausible interpretation is that head data in HFM32:1 (98–203 m) are affected by the closeness of ZFMNE00A2, cf. Figure 2-32. The time series suggest that the uppermost, transmissive, part of the bedrock constitutes the discharge zone for the deeper groundwater flow (fat yellow arrow).*

It should be noted that the groundwater in the till and in the uppermost part of the bedrock (HFM32:1–3) have similar fluid densities, c. 1,002.0–1,002.5 kg/m^3. Likewise, the groundwater at depth have similar fluid densities; in HFM32:1 the density is 1,003.4 kg/m^3 and in KFM02A:5 it is 1,004.0 kg/m^3. The small differences in fluid density within each type of groundwater suggest that the moderate differences in depth within each group of data have little or no practical implication for the qualitative gradient interpretations envisaged; that is, the uppermost, transmissive, part of the bedrock constitutes the final discharge zone for all groundwater flows, from surface as well as from depth. Finally, the salinity in Lake Bolundsfjärden varies and the density range between 998–1,000 kg/m^3. The Baltic Sea, finally, has a fairly constant density of c. 1,001.5 kg/m^3.

Figure 2-41 shows the flow directions in KFM02A with depth (green for inflow and red for outflow) as acquired by the Posiva Flow Log after the drilling was completed. Note the upward flow direction and the location of the main discharge zone below the casing shoe. That is, the borehole short-circuits the fracture system penetrated and groundwater is flowing into the borehole at depth and out of the borehole in the uppermost, transmissive, part, thus indicating an upward flow direction in the borehole. Hence, the data shown in Figure 2-41 supports the conceptual model envisaged in Figure 2-40.

An interesting observation presented and discussed in /Juston et al. 2007/ is the lack of a good correlation between the variations in the seawater level variations and the point-water head variations in the Quaternary deposits as well as in the uppermost, transmissive, part of bedrock. This observation supports the aforementioned working hypotheses that the horizontal fractures/sheet joints in the north-western part of the candidate area follow the bedrock surface as this dips under the Baltic Sea towards north-east.

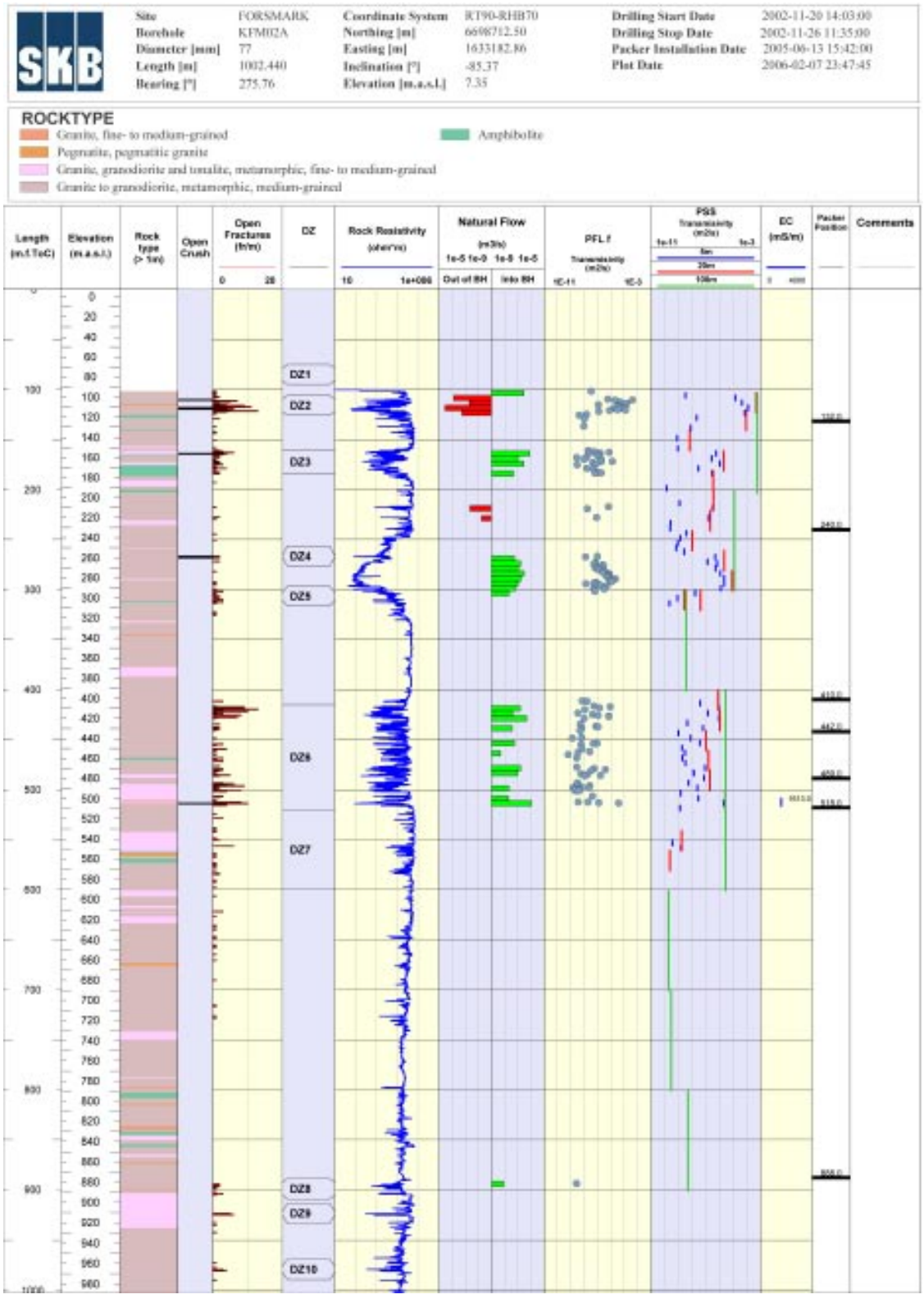

Figure 2-41. *Flow directions in KFM02A with depth (green for inflow and red for outflow) as acquired by the Posiva Flow Log after the drilling was completed. Section KFM02A:5 is located between 410–442 m. Reproduced from /Levén et al. 2006/.*

3 Hydraulic cage modelling

In this chapter the hypothesis of a hydraulic cage proposed in Section 2.3.3 is illustrated by numerical modelling starting with its effect on point-water heads in the near-surface. As described in Section 2.3.3, point-water heads are observed to be almost uniform within the tectonic lens, and do not correlate to either the topographic or bedrock surfaces. Hence, modelling is used here to demonstrate how such an observation is consistent with the concept of a hydraulic cage resulting from shallow horizontal sheet joints, and to inform on the possible extent and properties of such features. A simplified representation of the sheet joints is considered here by representing their effect by a single tabular feature with homogeneous properties. A basis for this study, an existing numerical model was adapted from the representative case equivalent continuum porous medium (ECPM) model from SR-Can F1.2 /Hartley et al. 2006a/.

3.1 Model set-up

For simplicity, the sheet joints were represented by a single homogeneous high transmissivity cage feature in the top 50 m of the candidate area. Two alternatives for the horizontal extent of cage feature were considered. The first was that it corresponds to the full extent of rock domain RFM029, and the second was to restrict this to only the foot wall of ZFMNE00A2. Both alternatives result in a cage feature overlies the candidate volume. To improve the spatial resolution of variations of groundwater flow, the SR-Can F1.2 ECPM model was modified to use higher refinement, 25 m, in the local-scale embedded grid around the site area. Since the future shorelevel evolution was not important for this study, the model was also trimmed out under the sea beyond the major "medium confidence" ZFMNE0486 north of Singö DZ. For the purposes of numerical simulations, the cage feature was assumed to be horizontal, centre on an elevation of –25 m, and 20 m thick. In reality, the cage is thought to consist of several parallel features ranging from just below the bedrock surface to about –150 m elevation.

As well as illustrating the difference to groundwater heads when the cage feature is introduced, the model was used to explore what are appropriate boundary conditions for flow in the near-surface, essentially considering a specified infiltration of water from the top surface, an appropriate effective transmissivity for the cage feature, and whether the horizontal extent of the cage feature could be determined based on point-water head data. Therefore, the main calibration targets for this study are transmissivities measured in the percussion drilled boreholes at Forsmark (HFM), and the heads measured in the HFM boreholes. The boreholes are open holes, and so for the purposes of comparisons with the model the average modelled head within the HFM holes is compared to the measured head. Also, heads were measured in July 2004, October 2004 and January 2005, and so the measured head was calculating as the mean of these 3 values.

Figure 3-1 shows the model domain adapted for this study. The F1.2 deformation zone model and locations of core drilled boreholes are superimposed. Note: the ECPM approach of deriving hydraulic properties equivalent to underlying DFN model is applied in only within rock domain RFM029. Outside of that, homogeneous properties are used apart where there is a deformation zone. Only a single realisation of the underlying DFN model was considered in this preliminary study. It is not expected that effect of the cage feature will be sensitive to stochastic variations in properties in the background rock, since it has much higher effective conductivity compared with the background. The finite-element grid is shown in Figure 3-2. The regional-scale model is based on a 100 m grid size, but an embedded region of higher refinement of 25 m is used around the site area surrounding the boreholes to give greater resolution of hydrogeological structures. The conceptual model is that a highly transmissive horizontal feature connects with the mapped deformation zones to form a hydraulic cage inside of which there is reduced advective flow within the

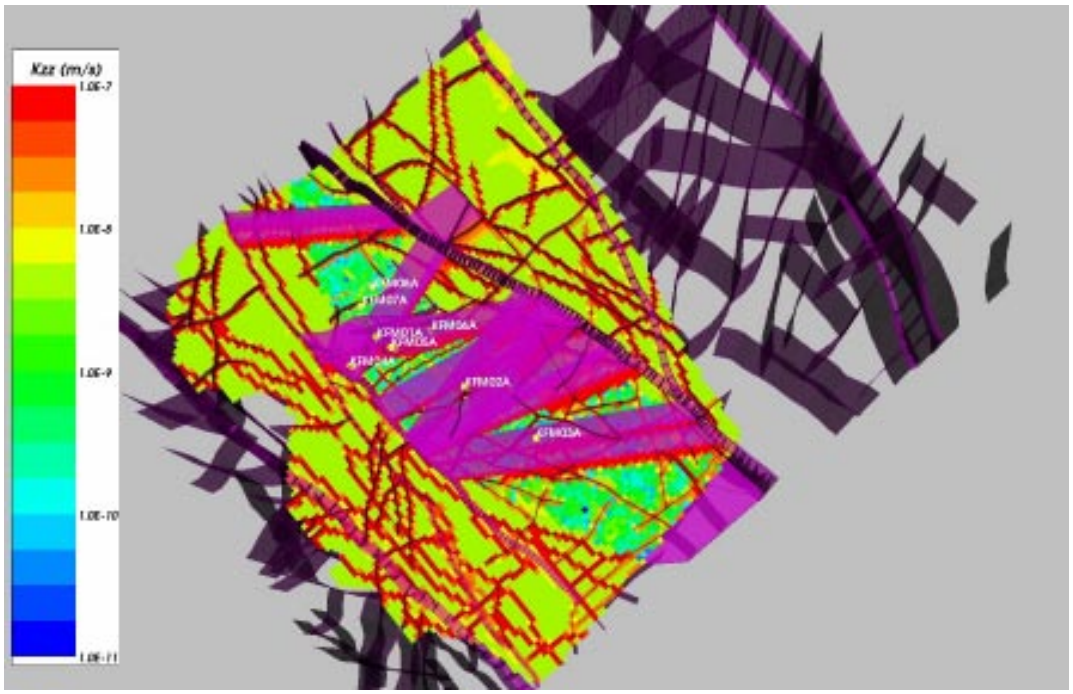

Figure 3-1. *ECPM model used for hydraulic cage simulations based on SR-Can F1.2 model /Hartley et al. 2006a/, but trimmed to north of zone ZFMNE0486 and using 25 m embedded grid in site-scale area. The alternative case (AC) DZ model was used (as shown in purple) and cored drilled boreholes.*

candidate area. The two alternative horizontal extents for cage feature are illustrated in Figure 3-3 and Figure 3-4. Figure 3-3 shows the case based on the extent of rock domain RFM029, while Figure 3-4 shows the case with the cage feature truncated on ZFMNE00A2.

The F1.2 ECPM model used in SR-Can specified head to be equal to the height of the topographic surface on the top boundary. However, in view of the lack of correlation between point-water heads and ground surface demonstrated by Figure 2-25, then this assumption will over-predict the head gradients within the candidate area. For this reason, the boundary condition on the top surface was changed to one based on a specified flux onshore.

Specifying an appropriate flux type boundary condition is not necessarily straightforward because in reality, the flux through the top surface will vary spatially, both in magnitude and direction since in some areas groundwater is recharging and in others it is discharging. This distribution of flux varies according to the amount of potential groundwater recharge and the hydraulic properties. The approach taken in CONNECTFLOW is to define the recharge flux, R, into or out of the model as a function of the current head, h, in the model, the topographic surface height, z, and the potential groundwater recharge, R_p. The maximum potential groundwater recharge is equal to the precipitation minus evapo-transpiration (P-E) and surface run-off. Surface run-off is subtracted because we are only interested in the potential recharge to the sub-surface. The Appropriate functions for the flux, R, must have certain characteristics. For recharge areas, the head, h, or watertable, is below ground surface and so the recharge must be equal to the full recharge, R_p. In discharge areas, the watertable is just above ground surface and so head is just above ground surface, which can be achieved by taking a suitably large flux out of the model, i.e. a negative value of R, whenever the head goes above ground surface. The standard function used in CONNECTFLOW is:

$$R = \begin{cases} R_p & h \le z - \varepsilon \\ -R_p(h - z)/\varepsilon & h > z - \varepsilon' \end{cases}$$

where ε is a small number. This function implies that if the watertable is more than ε below the topographic surface then recharge equals the full potential groundwater recharge.

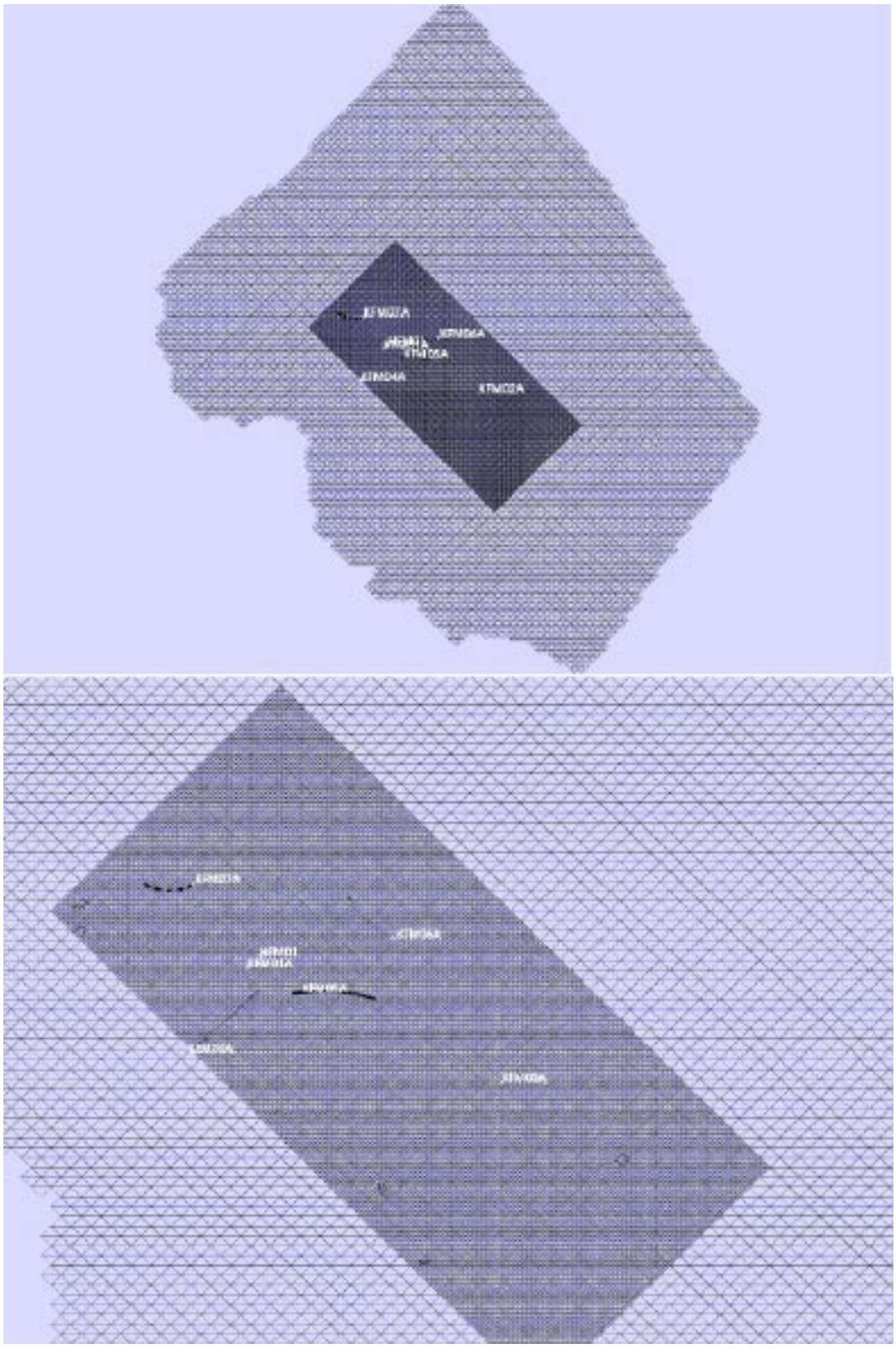

Figure 3-2. *A horizontal slice through the finite-element grid used in simulations with a 25 m resolution within the local area around the boreholes embedded within a 100 m regional-scale grid. Elements are hexahedra, but on a slice they are visualised here as 2 triangles. Top: whole model; Bottom: close-up around the core drilled boreholes.*

Above that, the recharge reduces until the watertable is at the surface. If the watertable is above the topographic surface, then recharge becomes negative, i.e. discharge, and an appropriate flux of groundwater is taken from the model to reduce the head until the watertable is restored to the topographic height. Hence, this boundary condition is a non-linear equation (the flux depends on the free-variable head) that ensures a specified flux if the watertable is low and a specified head where the watertable is at or above ground surface. The non-linearity requires that multiple iterations of the groundwater flow equations be performed at each time-step to reach convergence, which implies longer run times for this boundary condition. Newton-Raphson iteration was used to achieve convergence of the non-linear equations at each time-step. This technique works best for systems with smooth gradients. The standard function given above for flux has a discontinuous derivative at $h = z$-ε and this can lead to a slow rate of convergence. Hence, an alternative smooth function for recharge was tried:

$$R = R_p \times \left(\exp\left(\frac{h - z}{0.5} \right) - 1 \right).$$

This has similar characteristics to the standard function, but has smooth derivatives around $h = z$. This typically leads to convergence in only 2 Newton-Raphson iterations, and hence gave quicker and more robust solutions. There are other candidates for this function, such as a modification to the standard function but using a hyperbola to give a smooth transition around $h = z$.

Based on this definition of the top surface boundary condition, modelling heads in the top surface becomes a calibration exercise for the maximum infiltration rate into the bedrock and the hydraulic conductivity of the near-surface bedrock and soil. As an estimate of the maximum infiltration into the sub-surface, the maximum infiltration was set to the estimated P-E for the area, 180 mm/year.

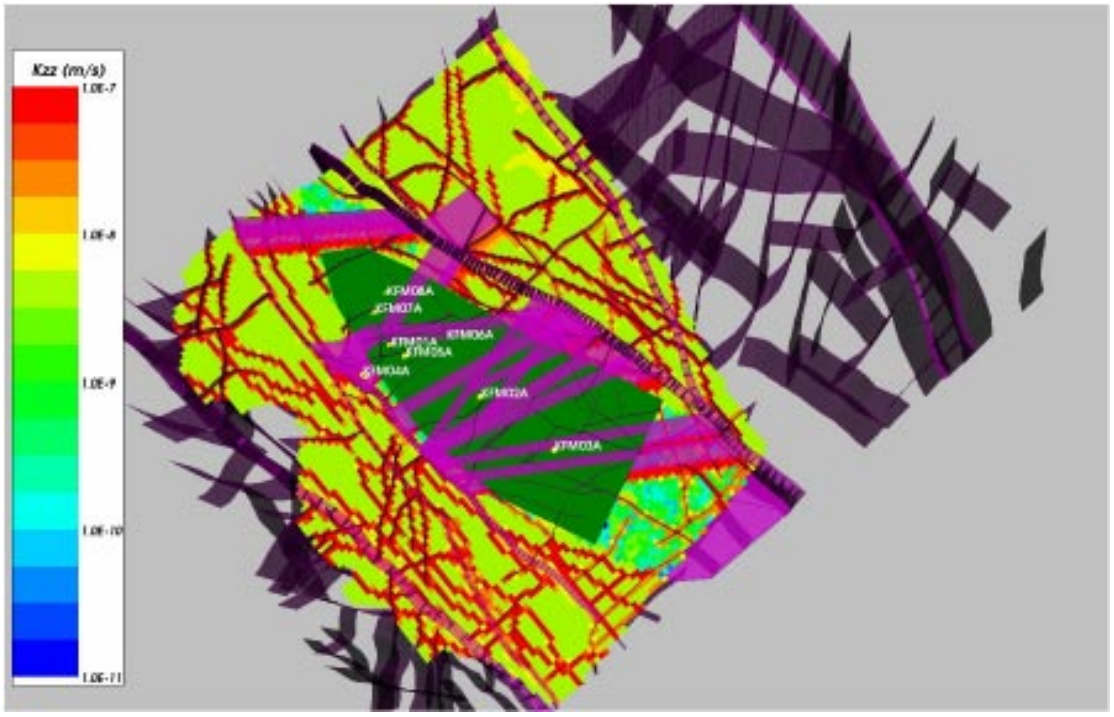

Figure 3-3. *ECPM model used for hydraulic cage simulations based on SR-Can F1.2 model /Hartley et al. 2006a/ with a high T horizontal feature throughout rock domain RFM029 shown in dark green. The alternative case (AC) DZ model was used (as shown in purple) and cored drilled boreholes.*

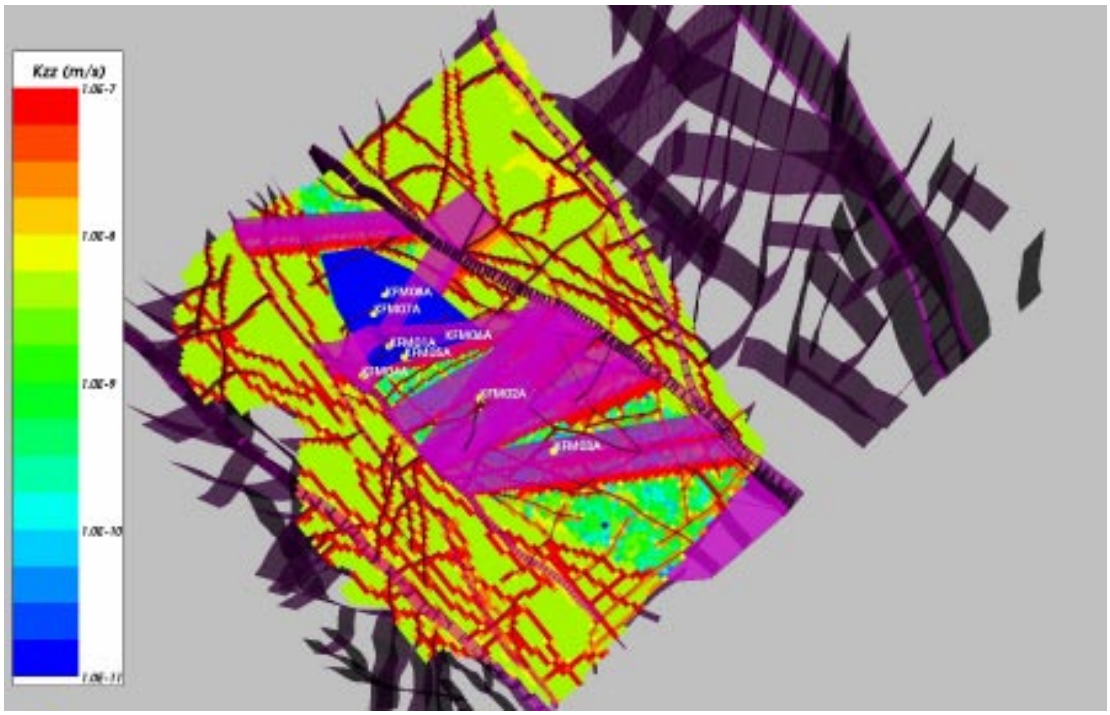

Figure 3-4. *ECPM model used for hydraulic cage simulations based on SR-Can F1.2 model /Hartley et al. 2006a/ with a high T horizontal feature in RFM029 and the foot wall of ZFMNE00A2 shown in dark blue. The alternative case (AC) DZ model was used (as shown in purple) and cored drilled boreholes.*

The real figure may be lower due to run-off. In a sense this modelling exercise is really one of consistency checking, because we have an estimate of the infiltration rate, and we have measurements of the hydraulic conductivity of the near-surface from hydraulic test in the HFM boreholes, and hence we have good estimates for the model input parameters to predict the heads.

A number of variant calculations were performed both to produce a calibration of the transmissivity of the high transmissivity feature, and illustrate some sensitivities of the model. The list of cases considered is given in Table 3-1. The names are made up of several parts corresponding to the specification of different facets of the models. HCD corresponds to the hydraulic conductor domain part, HRD is a description of the hydraulic rock domains, HSD is a description of the hydraulic soil domains, and BC is the type of boundary conditions used. As can be seen by the names, only the description of the HCD, which includes the cage feature, and the HSD were varied here.

Groundwater flow was calculated under steady-state flow conditions, so as to represent average annual balance between recharge and discharge of the hydrogeological system. Having calculated the head distribution throughout 3D model, the heads at the positions corresponding to the HFM boreholes were extracted 1 m below the topographic surface to give an estimate of the head in the Quaternary Deposits (QD) and averaged over the remaining length of borehole for comparison with the measured point-water heads. These predicted values of head in the QD and underlying bedrock were calculated to indicate the direction of vertical flow in the vicinity of the borehole. In the F1.2 model the HSD are modelled as four 1 m thick layers of finite-elements.

Table 3-1. List of cases and simulation names considered in the calibration on near-surface head distribution.

Case	Simulation case name
ECPM model (Base case based on SR-Can with flux BC 180 mm/year)	CAGE_SS_HCD3_AC_HRD3A2_T_HSD1_BC2
Horizontal feature T=1·10^{-3} m^2/s throughout RFM029	CAGE_SS_HCD3_AC_HRD3A2_T5_HSD1_BC2
Horizontal feature T=2·10^{-3} m^2/s throughout RFM029	CAGE_SS_HCD3_AC_HRD3A2_T4_HSD1_BC2
High K top 1 m soil layer T=1·10^{-3} m^2/s	CAGE_SS_HCD3_AC_HRD3A2_HSD1a_BC2
Soil T=1·10^{-3} m^2/s, horizontal feature T=1·10^{-3} m^2/s throughout RFM029	CAGE_SS_HCD3_AC_HRD3A2_T5_HSD1a_BC2
Horizontal feature T=1·10^{-3} m^2/s in foot wall of ZFMNE00A2	CAGE_SS_HCD3_AC_HRD3A2_T5foot_HSD1_BC2
Soil T=1·1 10^{-3} m^2/s, horiz. feature T=1·10^{-3} m^2/s foot wall of ZFMNE00A2	CAGE_SS_HCD3_AC_HRD3A2_T5foot_HSD1a_BC2

3.2 Simulation results

Figure 3-5 to Figure 3-11 show comparisons of measured heads in HFM boreholes and those predicted by numerical simulations of steady-state flow based on a maximum potential infiltration of 180 mm/year for the sequence of cases described in Table 3-1. The plots are in a format to compare the modelled head in the QD, bedrock, with the measured heads, topographic surface and bedrock surface. Boreholes are ordered according to the elevation of bedrock in accordance with Figure 2-25.

Figure 3-5 is intended as a benchmark to show the simulated heads for the SR-Can F1.2 representative case modified only to use a flux boundary condition rather than one of topographic head (i.e. no cage feature included). This gives heads that follows the ground surface elevation quite closely, which is generally not the case in the site data apart from a few boreholes such as HFM11 and HFM12 outside the tectonic lens. Hence, this demonstrates that a model with hydraulic conductivity based on the F1.2 Hydro-DFN model is not sufficiently conductive in the near-surface (Note the Hydro-DFN was based on Posiva flow-log measurements for core

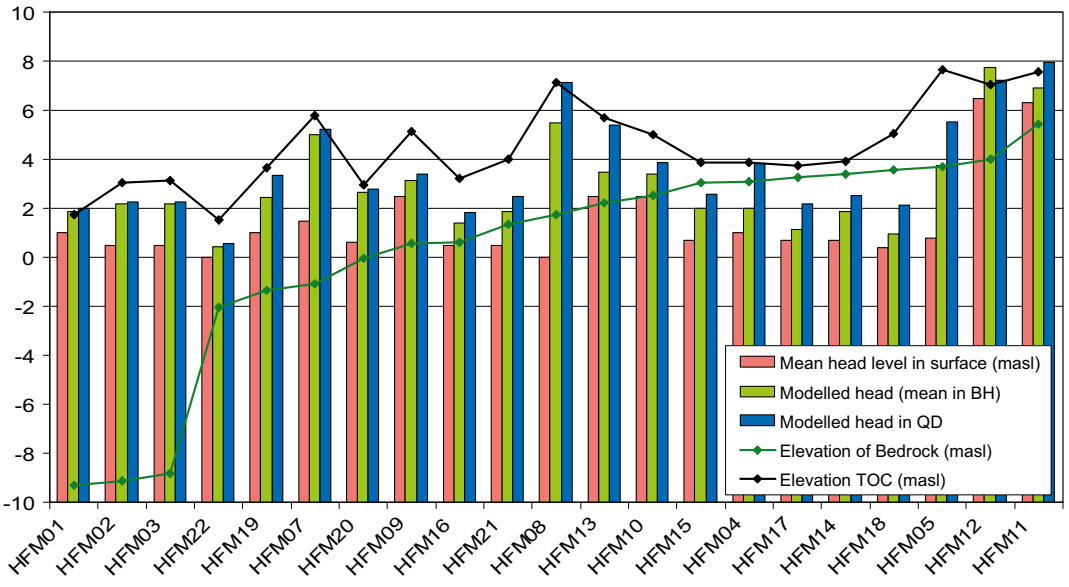

Figure 3-5. *Comparison of measured heads in percussion drilled boreholes with the ECPM model based on upscaled SR-Can DFN /Hartley et al. 2006a/ with a flux boundary condition (CAGE_SS_HCD3_AC_HRD3A2_T_HSD1_BC2).*

drilled boreholes which are cased in approximately the top 100 m). The remaining simulations all include high transmissivity near the surface as this is essential to flatten the head distribution in the candidate area.

Figure 3-6 shows the effect of introducing a cage feature that extends through rock domain RFM029 in both the hanging wall and foot wall of ZFMNE00A2 and has a transmissivity of 10^{-3} m^2/s. Clearly, this gives a dramatic improvement in the match to heads though the model still slightly over-predicts heads. Heads are unaffected in HFM11 and HFM12 as these are outside RFM029 and the cage feature. Figure 3-7 shows the effect of doubling the transmissivity of the cage feature. This now gives a very good agreement with the measured heads. Therefore, the effective transmissivity of the near-surface needs to be about $2 \cdot 10^{-3}$ m^2/s for a maximum infiltration of

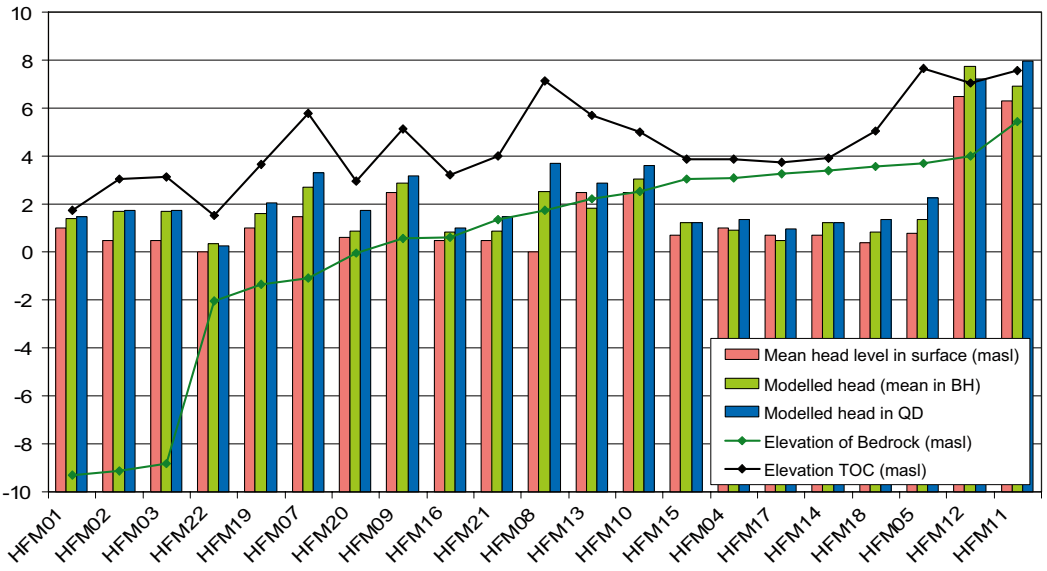

Figure 3-6. *Comparison of measured heads in percussion drilled boreholes with the ECPM model based on upscaled SR-Can DFN /Hartley et al. 2006a/ with flux boundary condition and a horizontal feature $T=1 \cdot 10^{-3}$ m^2/s throughout tectonic lens RFM029 (CAGE_SS_HCD3_AC_HRD3A2_T5_HSD1_BC2).*

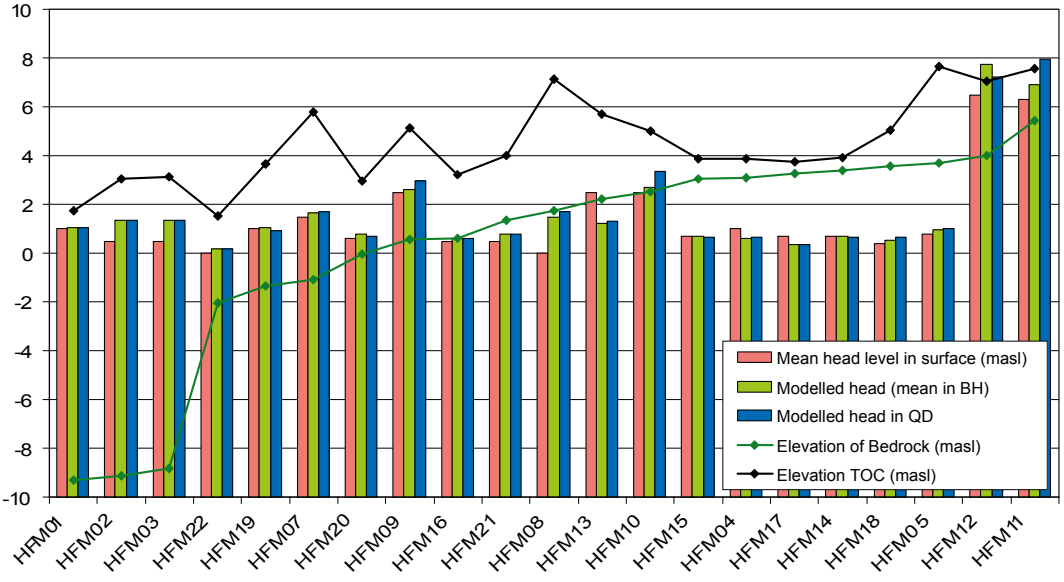

Figure 3-7. *Comparison of measured heads in percussion drilled boreholes with the ECPM model based on upscaled SR-Can DFN /Hartley et al. 2006a/ with flux boundary condition and a horizontal feature $T=2 \cdot 10^{-3}$ m^2/s throughout tectonic lens RFM029 (CAGE_SS_HCD3_AC_HRD3A2_T4_HSD1_BC2).*

180 mm/year. As will be seen in Table 3-3, the measured transmissivity in the HFM boreholes for intervals associated with cage features is only about $8 \cdot 10^{-4}$ m^2/s, which suggests that actual infiltration rate might be about half of that used, i.e. circa. 100 mm/year. One way one of illustrating the effects of a reduced infiltration rate to the bedrock without changing the specified infiltration to the top surface is increase the transmissivity of the top 1 m of soil to represent an enhanced surface run-off. Figure 3-8 shows a case with a 1 m soil layer of hydraulic conductivity 10^{-3} m/s to show the effect of enhanced run-off. The results are reasonable and similar to Figure 3-7. Figure 3-9 shows the results of a case with a cage transmissivity of 10^{-3} m^2/s and a transmissivity in the soil of 10^{-3} m^2/s. Not surprisingly, the results are similar to those in Figure 3-7 as they are essentially slightly different interpretations of the same hydraulic system.

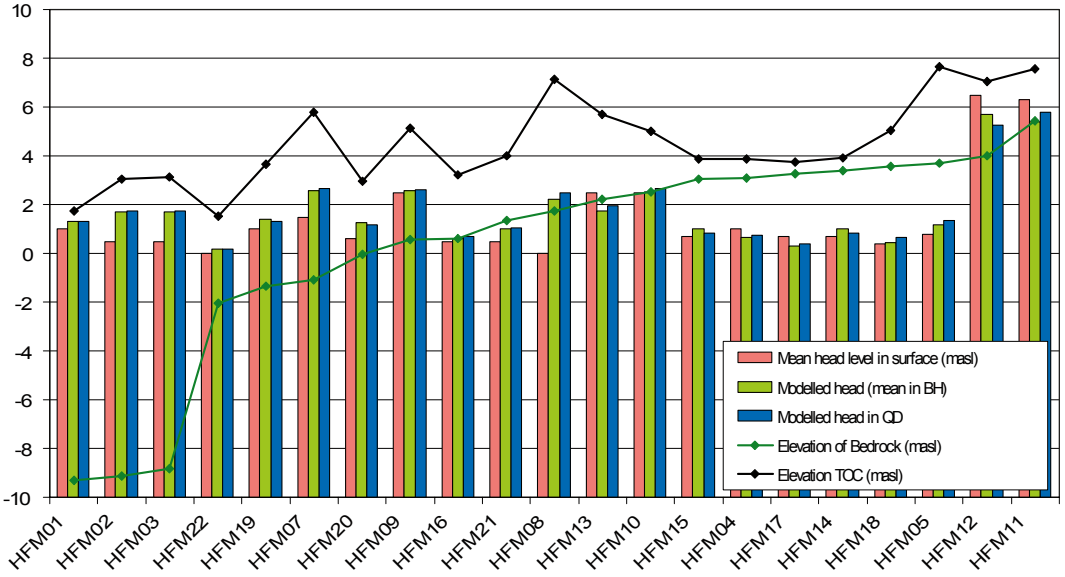

Figure 3-8. *Comparison of measured heads in percussion drilled boreholes with the ECPM model based on upscaled SR-Can DFN /Hartley et al. 2006a/ with flux boundary condition and a high $T=1 \cdot 10^{-3}$ m^2/s top 1 m soil layer (CAGE_SS_HCD3_AC_HRD3A2 _HSD1a_BC2).*

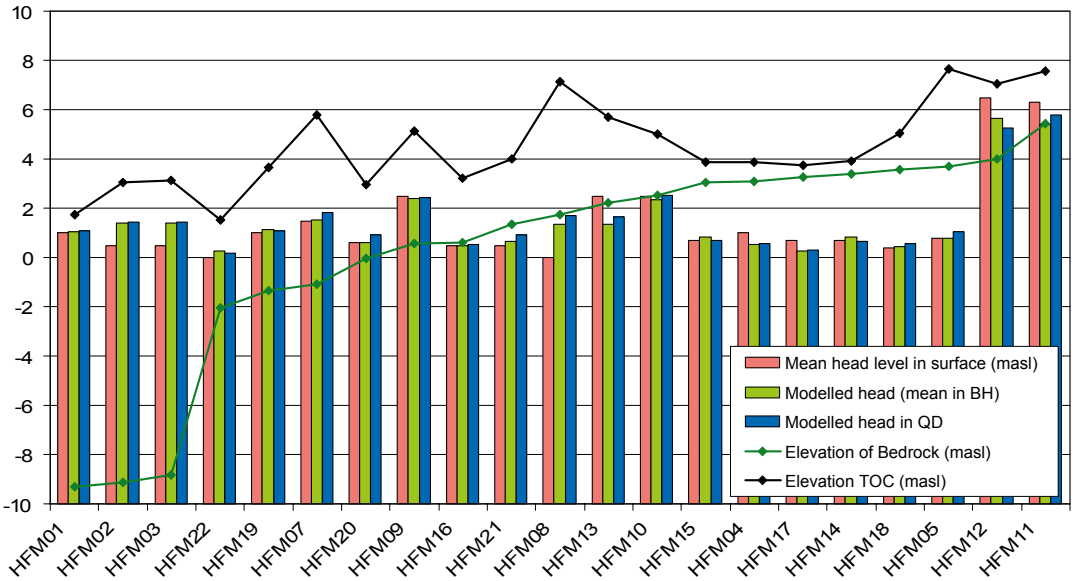

Figure 3-9. *Comparison of measured heads in percussion drilled boreholes with the ECPM model based on upscaled SR-Can DFN /Hartley et al. 2006a/ with flux boundary condition, a horizontal feature $T=1 \cdot 10^{-3}$ m^2/s throughout tectonic lens RFM029 and a high $T=1 \cdot 10^{-3}$ m^2/s top 1 m soil layer (CAGE_SS_HCD3_AC_HRD3A2_T5_HSD1a_BC2).*

The above simulations were all based on a cage feature extending over the whole of RFM029. Two more cases were considered with the cage restricted just to the foot wall of ZFMNE00A2. Figure 3-10 is equivalent to Figure 3-7 with the restricted cage feature. The heads are over-predicted in HFM07 and HFM08 which lie in the south east part of RFM029 in the hanging wall of ZFMNE00A2. By adding the high conductivity soil layer in equivalent to the case shown in Figure 3-8, the heads are reduced as shown in Figure 3-11.

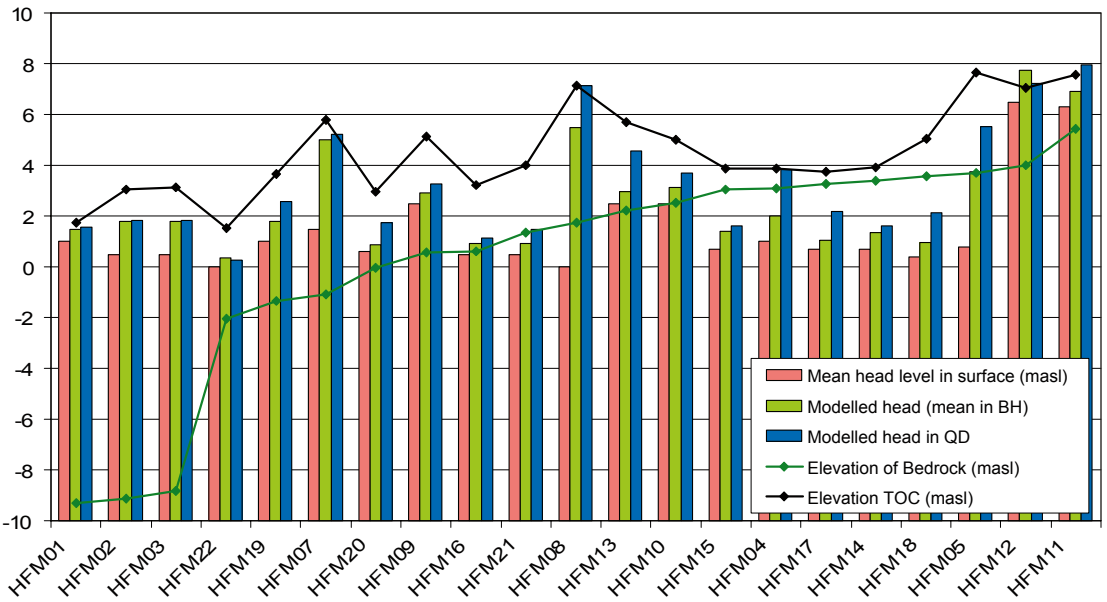

Figure 3-10. *Comparison of measured heads in percussion drilled boreholes with the ECPM model based on upscaled SR-Can DFN /Hartley et al. 2006a/ with flux boundary condition and a horizontal feature $T=1\cdot10^{-3}$ m²/s only in foot wall of ZFMNE00A2 (CAGE_SS_HCD3_AC_HRD3A2_T5foot_HSD1_BC2).*

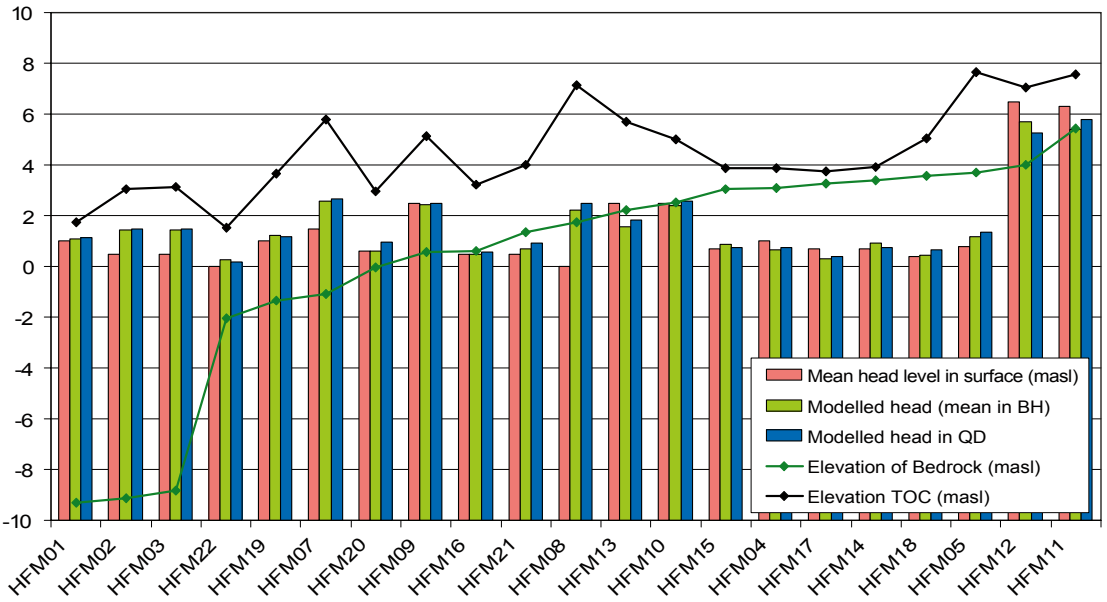

Figure 3-11. *Comparison of measured heads in percussion drilled boreholes with the ECPM model based on upscaled SR-Can DFN /Hartley et al. 2006a/ with flux boundary condition, a horizontal feature $T=1\cdot10^{-3}$ m²/s in foot wall of ZFMNE00A2 and a high $T=1\cdot10^{-3}$ m²/s top 1 m soil layer (CAGE_SS_HCD3_AC_HRD3A2_T5foot_HSD1a_BC2).*

A summary of the average difference between the measured head and the modelled head (averaged over borehole length) is given in Table 3-2. The measured data is taken as an average of three sets of measurements taken in different seasons July 2004–January 2005. The cases with a high transmissivity for the top 1 m of soil are used to illustrate the potential effect of surface run-off or very near-surface groundwater flow in the soil. Looking at Figure 3-5 to Figure 3-11, the measured head is around the elevation of the bedrock for many boreholes where the soil is more than a metre thick.

The value $T=1\cdot10^{-3}$ m^2/s for the cage feature was chosen to be of the order magnitude of the transmissivity measured in the top 50–200 m of rock in the percussion drilled boreholes. A summary of the average hydraulic conductivities measured in the percussion drilled boreholes is given in Table 3-3. The penetration of these boreholes varies from 26 m to 301 m, but mostly they are around 200 m. The geometric mean for boreholes located within the tectonic lens is about $4\cdot10^{-6}$ m/s, equating to a transmissivity of around $8\cdot10^{-4}$ m^2/s for a 200 m layer. Table 3-3 also demonstrates significant heterogeneity in the near-surface rock, and that hydraulic conductivities outside the tectonic lens are typically an order of magnitude, or more, lower in the top 200 m of rock.

Table 3-2. Comparison of modelled and measured head data.

Case	Average head difference model – data (model based on mean in borehole section)
ECPM model (Base case based on SR-Can with flux BC 180 mm/year)	1.48 m
Horizontal feature $T=1\cdot10^{-3}$ m^2/s throughout RFM29	0.58 m
Horizontal feature $T=2\cdot10^{-3}$ m^2/s throughout RFN29	0.22 m
High K top 1 m soil layer $T=1\cdot10^{-3}$ m^2/s	0.28 m
Soil $T=1\cdot10^{-3}$ m^2/s, horizontal feature $T=1\cdot10^{-3}$ m^2/s throughout RFM29	0.00 m
Horizontal feature $T=1\cdot10^{-3}$ m^2/s in foot wall of ZFMNE00A2	1.13 m
Soil $T=1\cdot10^{-3}$ m^2/s, horiz. feature $T=1\cdot10^{-3}$ m^2/s foot wall of ZFMNE00A2	0.15 m

Table 3-3. Summary of average hydraulic conductivity in percussion drilled boreholes (ones inside RFM29 in yellow). The geometric mean inside RFM29 is $4.1\cdot10^{-6}$ m/s.

Borehole	Average K(m/s)
HFM01	$4.2\cdot10^{-7}$
HFM02	$2.9\cdot10^{-5}$
HFM03	$6.0\cdot10^{-5}$
HFM22	$1.6\cdot10^{-6}$
HFM19	$3.2\cdot10^{-6}$
HFM07	$1.0\cdot10^{-8}$
HFM20	$1.4\cdot10^{-5}$
HFM09	$1.1\cdot10^{-5}$
HFM16	$4.9\cdot10^{-6}$
HFM21	$1.8\cdot10^{-6}$
HFM08	$7.5\cdot10^{-6}$
HFM13	$2.8\cdot10^{-6}$
HFM10	$2.3\cdot10^{-6}$
HFM15	$1.3\cdot10^{-5}$
HFM04	$5.2\cdot10^{-7}$
HFM17	$3.7\cdot10^{-6}$
HFM14	$1.0\cdot10^{-5}$
HFM18	$9.5\cdot10^{-7}$
HFM05	$1.6\cdot10^{-6}$
HFM12	$8.1\cdot10^{-8}$
HFM11	$4.5\cdot10^{-7}$

The cases which match the head distribution best have a high transmissivity near-surface feature and a flux boundary condition. This leads to rapid drainage of groundwater in the near-surface and hence a head distribution below the topographic surface. To illustrate this effect, Figure 3-12 shows the distribution of total pressure for a case with a high transmissivity cage feature and soil and a flux boundary condition with 180 mm/year maximum infiltration. Total pressure is shown to indicate the head level relative to ground surface. Dividing the total pressure by 10^4 gives the height of the water head above ground surface, i.e. sea and discharge areas are positive (cyan-blue), recharge areas are negative (yellow-red). The range shown here is equivalent to 5 m above ground surface to 5 m below. This plot shows that groundwater flow pattern is much localised with many small recharge and discharge areas within the modelled region. Some of the discharge areas correspond with lakes.

3.3 Conclusions

- Calibrating the model on point water head data requires the use of a flux type boundary condition. Then, based on the measured point-water heads in the HFM boreholes and calibrating against these head data suggest consistency is achieved with an equivalent transmissivity of the hydraulic cage feature around $5 \cdot 10^{-4}$–$1 \cdot 10^{-3}$ m^2/s.
- If the infiltration to the sub-surface (P-E) is about 180 mm/year, then run-off or very near-surface flows in the quaternary deposits seem to reduce the infiltration to the bedrock to about 80–100 mm/year.
- In order to calibrate the conceptual model for the upper bedrock and Quaternary deposits further it would be necessary to consider more hydrological data such as stream flow-rates and transient fluctuations in heads due to rainfall. This requires a closer integration with the SurfaceNet Team.

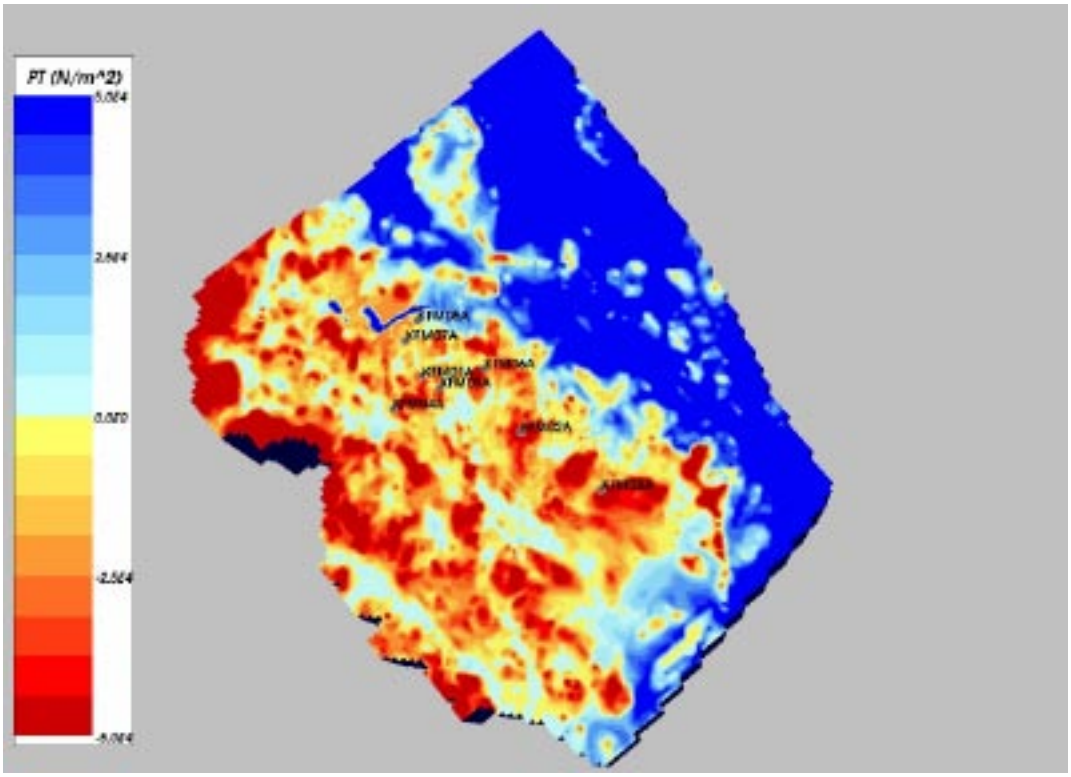

Figure 3-12. *Total pressure at surface for ECPM model based on upscaled SR-Can DFN /Hartley et al. 2006a/ with flux boundary condition, a horizontal feature $T=1 \cdot 10^{-3}$ m^2/s throughout the tectonic lens RFM029 and a high $T=1 \cdot 10^{-3}$ m^2/s top 1 m soil layer (CAGE_SS_HCD3_AC_HRD3A2_T5_HSD1a_BC2).*

4 Palaeo-hydrogeological modelling

Modelling of palaeo-hydrogeology was based on models developed as part of SR-Can F1.2 as shown in the conceptual model in Figure 4-1.

The parameter settings and the sensitivities considered in this study are summarised in Table 4-1. Both ECPM models (based on an underlying stochastic DFN model) and CPM (homogeneous models within defined sub-domains) were considered. The models were gradually developed in a stepwise manner with the objective of increasing consistency with the observed conditions at the site. Major new requirements of the modelling exercise were to:

- Include the high transmissivity cage feature near the surface (at least in the foot wall of ZFMNE00A2).
- Ensure a match to the pore-water Chloride with appropriate uncertainties.
- Ensure a match to the ratio Br/Cl since this gives an indication of the transition in origin of saline groundwaters from marine to Brine.

Having made changes to meet these requirements, the model should ideally match the original F1.2 calibration targets: Cl, $\delta^{18}O$ and more qualitatively, Mg. However, in seeking a match the approach taken was to vary parameters and settings one at a time so as to understand the behaviour of the system to individual parameters rather than treat the problem as a curve fitting exercise. Initially, both CPM and ECPM models were used in this exercise, but eventually sensitivity studies focussed on models based on ECPM since it was felt this was more representative of the fractured rock at Forsmark.

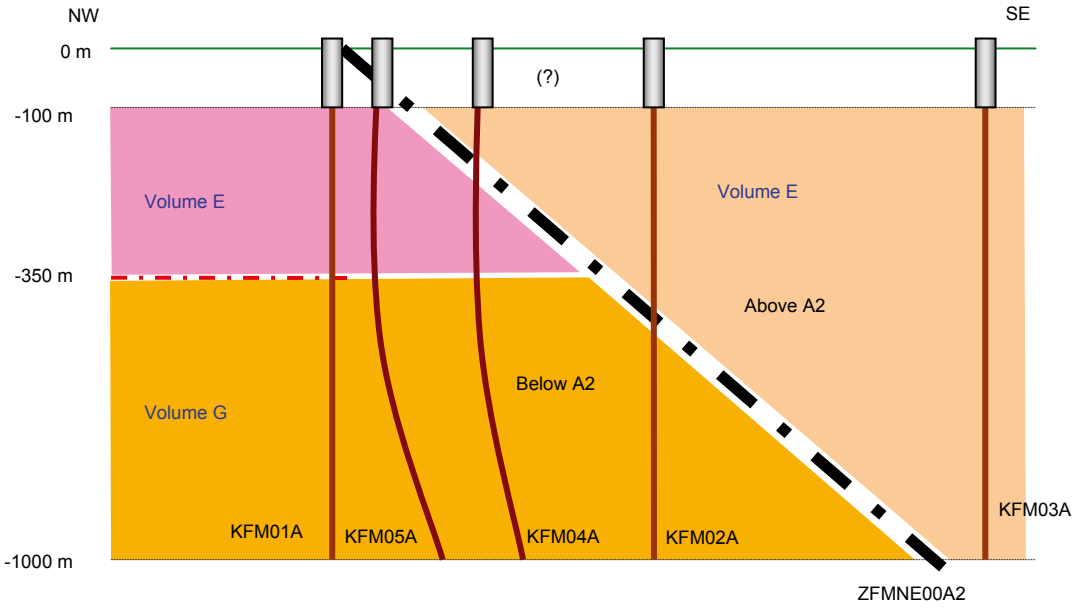

Figure 4-1. *Schematic cross-section taken from the SR-Can F1.2 ECPM model. Volume E was based on the DFN derived from KFM03A; Volume G had the same DFN as Volume E, but with a transmissivity 10 times lower. A homogeneous CPM model was used for the HRD outside of RFM029 $K=5 \cdot 10^{-9}$ m/s.*

Table 4-1. Summary of hydraulic parameters and conditions used in SR-Can F1.2 base case model with an indication of the possible range of alternative parameters that have been considered here in sensitivity studies.

Parameter	Calibration value	Range
Model domain	Regional model – about 15 km (SW-NE) × 11 km (NW-SE) is the minimum	Trim model out to sea beyond major "medium confidence" ZFMNE0486 north of Singö DZ
Grid resolution	50 m necessary in site-scale 100 m on regional-scale	25 m on the site-scale
Initial condition	Full Glacial 0–500 m; then linear gradient to no Glacial, full Brine at –2,000 m; full Brine below –2,000 m	Brine –400 m to –1,500 m in foot wall, –500 m to –2,300 m
Top surface flow BC	Topography	A specified infiltration of 180 mm/year
Top surface waters	Ancylus Ice Lake (Glacial), Littorina Sea (Marine), Baltic Sea/Precipitation with land-rise (Marine diluting with /Rain 1960/);	Use modified meteoric water based on HFM03. Used modern winter meteoric water as an alternative for Glacial water e.g. Ancylus Lake
ECPM model Hydraulic conductivity (K) based on Hydro-DFN	Calibrated on short interval PSS and PFL data This had block-scale properties of K50% ~$4 \cdot 10^{-10}$ m/s, K10% = $1 \cdot 10^{-11}$ m/s Minimum fracture radius = 4 m	Reduce minimum fracture radius = 5.6 m for smaller grid elements. Perform 3 realisations
CPM model Hydraulic conductivity (K)	Based on PFL, mainly KFM01A K=$1 \cdot 10^{-11}$ m/s in Volume G	
Depth dependence	Based on rock domain model for HRD	
Kinematic HRD porosity $n_{et,block}$	Based on DFN value, $t=0.5T^{0.5}$ (t is fracture transport aperture, T is transmissivity)	
Matrix porosity n_m	$4 \cdot 10^{-3}$	
Defromation zone model	Alternative model for Forsmark stage 1.2 (cf. Figure 2-5)	Add horizontal zone in RFM029; or horizontal zone in A2 foot wall; Remove 2 sub-vertical zones
HCD hydraulic properties	HCD3 = depth dependency but with local conditioning to PSS 100 m data	Change T of zones intersecting KFM03A
Kinematic HCD porosity n_{et}	Based on $t=5T^{0.5}$	
FWS, a_r, for RMD	0.25 m^2m^{-3}	0.1–0.16 m^2m^{-3} based on PFL data
Intrinsic diffusion coefficient in matrix D_e	$5 \cdot 10^{-13}$ m^2s^{-1}	

4.1 Original ECPM and CPM models

A complete list of simulation cases and their names is given in Table 4-2 as well an indication of what sensitivity each case trying to quantify. These names are referred to in the caption of each of the following figures showing results. Again, the names are made up several portions each describing a different facet of the model such as HCD, HRD, HSD, boundary and initial conditions.

Table 4-2. List of cases and simulation names considered in the calibration on F2.1 hydrogeochemistry.

Case description	Test effects of	Simulation case name
Original SR-Can ECPM model with topographic head boundary condition	Baseline ECPM	SC_HCD3_AC_HRD3A2_T_HSD1_BC1_local50
Original SR-Can CPM model with topographic head boundary condition	Baseline CPM	SC_HCD3_AC_HRDDT_HSD1_BC1_local50
ECPM model with alternative Glacial reference water composition	Glacial water composition	SC21_HCD3_AC_HRD3A2_T_HSD1_BC1_RefW2
ECPM model with alternative Glacial and Meteoric reference water compositions	Glacial and meteoric water compositions	SC21_HCD3_AC_HRD3A2_T_HSD1_BC1_RefW3
ECPM model with alternative Glacial and Meteoric reference water compositions, and 0.16 m^2/m^3 flow wetted surface	Flow wetted surface	SC21_HCD3_AC_HRD3A2_T_FWS_HSD1_BC1_RefW3
CPM model with alternative Glacial reference water composition and near-surface high T feature	Cage feature	SC21_HCD3_AC_HRDDT3_HSD1_BC1_RefW2
CPM model with alternative Glacial reference water composition, flux boundary condition, and near-surface high T feature	Cage feature with flux boundary condition	SC21_HCD3_AC_HRDDT3_HSD1_BC2_RefW2
ECPM model with alternative Glacial and Meteoric reference water compositions, flux boundary condition, near surface high T feature ($T=2\cdot10^{-3}$ m^2/s), and 0.16 m^2/m^3 flow wetted surface	Cage feature transmissivity	SC21_HCD3_AC_HRD3A2_T4_FWS_HSD1_BC2_RefW3
ECPM model with alternative Glacial and Meteoric reference water compositions, flux boundary condition, near surface high T feature ($T=1\cdot10^{-3}$ m^2/s), and 0.16 m^2/m^3 flow wetted surface	Cage feature transmissivity	SC21_HCD3_AC_HRD3A2_T5_FWS_HSD1_BC2_RefW3
ECPM model with alternative Glacial and Meteoric reference water compositions, flux boundary condition, near surface high T feature ($T=1\cdot10^{-3}$ m^2/s), a high $T=1\cdot10^{-3}$ m^2/s top 1 m soil layer, and 0.16 m^2/m^3 flow wetted surface	Cage feature transmissivity and run-off in soil	SC21_HCD3_AC_HRD3A2_T5_FWS_HSD1a_BC2_RefW3
ECPM model with alternative Glacial and Meteoric reference water compositions, flux boundary condition, near surface high T feature, and 0.1 m^2/m^3 flow wetted surface	Flow wetted surface	SC21_HCD3_AC_HRD3A2_T5_FWS2_HSD1_BC2_RefW3
ECPM model with alternative Glacial and Meteoric reference water compositions, flux boundary condition, near surface high T feature ($T=1\cdot10^{-3}$ m^2/s), DZ's ZFMNE1188 and ZFMNW1194 removed, and 0.16 m^2/m^3 flow wetted surface	Hydraulic significance of deformation zones near KFM01A	SC21_HCD4_AC_HRD3A2_T5_FWS_HSD1_BC2_RefW3
ECPM model with alternative Glacial and Meteoric reference water compositions, flux boundary condition, near surface high T feature ($T = 1\cdot10^{-3}$ m^2/s) in the foot wall of A2, a high $T=1\cdot10^{-3}$ m^2/s top 1 m soil layer, modified T in 3 DZ's intersecting KFM03A and 0.16 m^2/m^3 flow wetted surface	Hydraulic conductivity of deformation zones in KFM03A	SC21_HCD5_AC_HRD3A2_T5foot_FWS_HSD1a_BC2_RefW3
ECPM model 1 st realisation with alternative Glacial and Meteoric reference water compositions, flux boundary condition, near surface high T feature ($T=1\cdot10^{-3}$ m^2/s), and 0.16 m^2/m^3 flow wetted surface	Stochastic Hydro-DFN model of background rock	SC21_HCD3_AC_HRD3aA2_T5_FWS_HSD1_BC2_ReW3
ECPM model 2nd realisation with alternative Glacial and Meteoric reference water compositions, flux boundary condition, near surface high T feature ($T=1\cdot10^{-3}$ m^2/s), and 0.16 m^2/m^3 flow wetted surface	Stochastic Hydro-DFN model of background rock	SC21_HCD3_AC_HRD3bA2_T5_FWS_HSD1_BC2_RefW3
ECPM model 3rd realisation with alternative Glacial and Meteoric reference water compositions, flux boundary condition, near surface high T feature ($T=1\cdot10^{-3}$ m^2/s), and 0.16 m^2/m^3 flow wetted surface	Stochastic Hydro-DFN model of background rock	SC21_HCD3_AC_HRD3cA2_T5_FWS_HSD1_BC2_RefW3

Case description	Test effects of	Simulation case name
ECPM model with alternative Glacial and Meteoric reference water compositions, flux boundary condition, near surface high T feature, 0.16 m^2/m^3 flow wetted surface, and 5% residual Brine in the initial condition	Initial condition	SC21_HCD3_AC_HRD3A2_T5_FWS_HSD1_BC2_IC2_RefW3
ECPM model with alternative Glacial and Meteoric reference water compositions, flux boundary condition, near surface high T feature in the foot wall of A2, a high $T=1\cdot10^{-3}$ m^2/s top 1 m soil layer, 0.16 m^2/m^3 flow wetted surface, and with a different initial condition in the foot wall and hanging walls of ZFMNE00A2	Initial condition	SC21_HCD3_AC_HRD3A2_T5foot_FWS_HSD1a_BC2_IC3_RefW3
ECPM model on a refined 25 m local-scale grid with alternative Glacial and Meteoric reference water compositions, flux boundary condition, near surface high T feature ($T=1\cdot10^{-3}$ m^2/s), and 0.16 m^2/m^3 flow wetted surface	Grid refinement	CAGE_HCD3_AC_HRD3A2_T5_FWS_HSD1_BC2_RefW3
ECPM model of individual component transport with alternative Glacial and Meteoric reference water compositions, flux boundary condition, near surface high T feature ($T=1\cdot10^{-3}$ m^2/s) in the foot wall of A2, a high $T=1\cdot10^{-3}$ m^2/s top 1 m soil layer, modified T in 3 DZ's intersecting KFM03A and 0.16 m^2/m^3 flow wetted surface	Horizontal extent of cage feature	Comp_HCD5_AC_HRD3A2_T5foot_FWS_HSD1a_BC2_RefW3

As a baseline comparison for the variant cases, the distributions of Chloride for the original ECPM and CPM models used in SR-Can F1.2 are given in Figure 4-2 and Figure 4-3. For both model implementations, the onset of saline water is over 100 m too deep compared to the data.

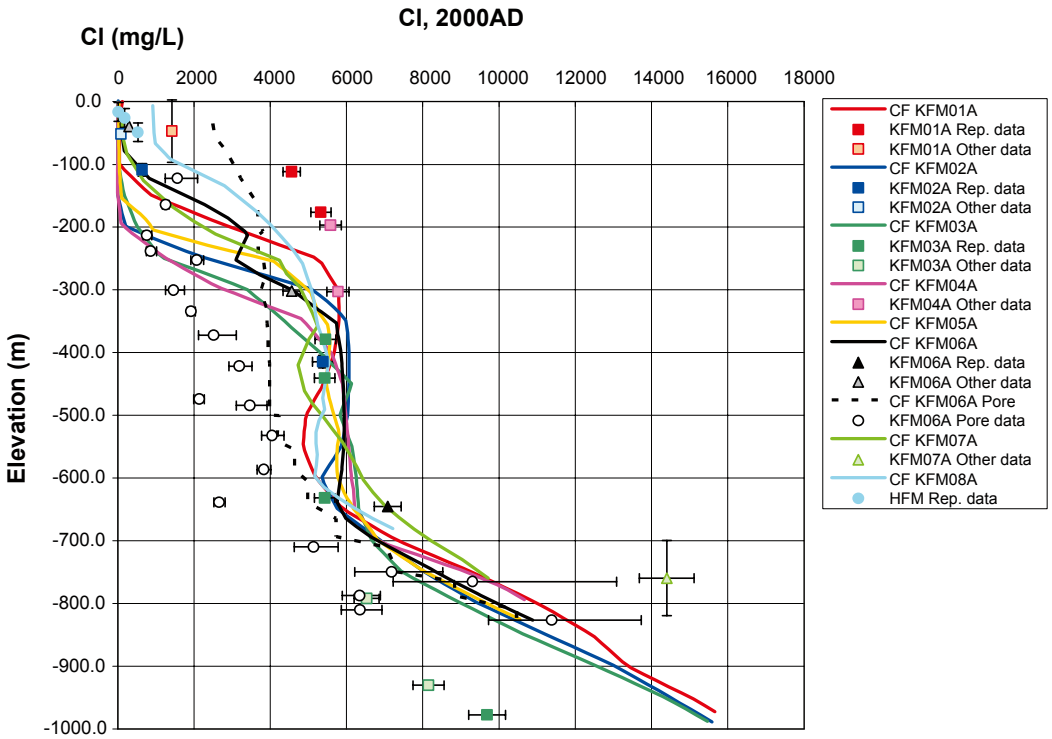

Figure 4-2. *Comparison of Cl with F2.1 data for the original ECPM model from SR-Can (SC21_HCD3_AC_HRD3A2_T_HSD1_BC1_local50).*

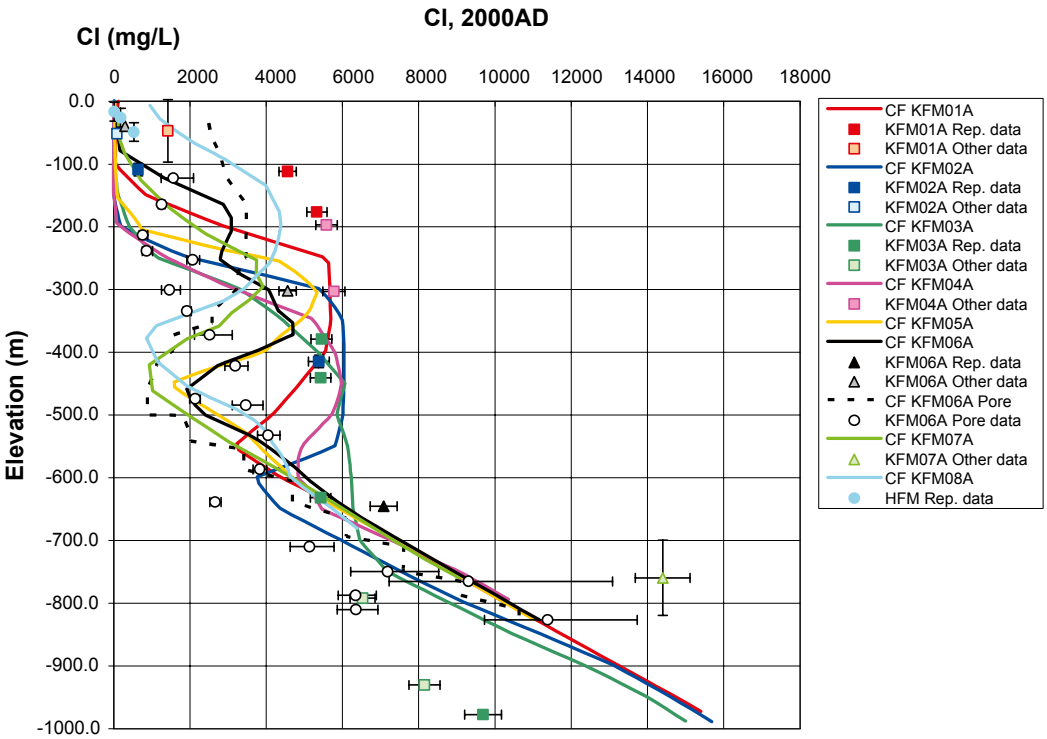

Figure 4-3. *Comparison of Cl with F2.1 data for the original CPM model from SR-Can (SC_HCD3_AC_HRDDT_HSD1_BC1_local50).*

These types of figures can be compared with the conceptual discussions summarised in Figure 2-16. There, individual data points are grouped according to the fracture domain in which they are located. Broadly, KFM03A and the top 500 m of KFM02A correspond to the hanging wall of ZFMNE00A2 (i.e. fracture domain FFM03), KFM07A and KFM04A correspond to the border of rock domain RFM0029, and the remaining samples belong to the foot wall of ZFMNE00A2 (i.e. fracture domain FFM01 and FFM02).

4.2 Alternative reference waters

The first step was to use alternative reference water compositions to show how uncertainty in the end-members can explain some of the differences between the model and data. Groundwater from HFM03 was used as representative of near-surface modified meteoric water to improve HCO_3 mainly, but also some other ions. This corresponds to rain water being modified by very rapid reactions taking place in organic matter at the surface. The alternative Glacial water was based on winter snow melt which has a reduced $\delta^{18}O$ ratio. Possible interpretations of the results in Figure 4-4 to Figure 4-7 are that prior to the Littorina phase, the sea water composition contained water from low temperature precipitation, and that meteoric water is modified by near-surface organic materials. Clearly, Figure 4-4 and Figure 4-5 suggest the change in composition of the Glacial reference water gives an improved match, but hydrochemical interpretation of the result is complex. We are not necessarily implying that the Glacial water is in fact winter snow-melt. All we conclude, is that freshwater existing at mid-depths down to about 700 m and this some glacial component, but may be a mix of Glacial melt-water from the last ice-age and older freshwater. Figure 4-6 and Figure 4-7 demonstrate a dramatic improvement in using a composition for meteoric water based on the groundwater sample in HFM03, which is termed as being representative of 'dilute granitic water'. The modelled pulse of high HCO_3 shows consistency with the measured profile.

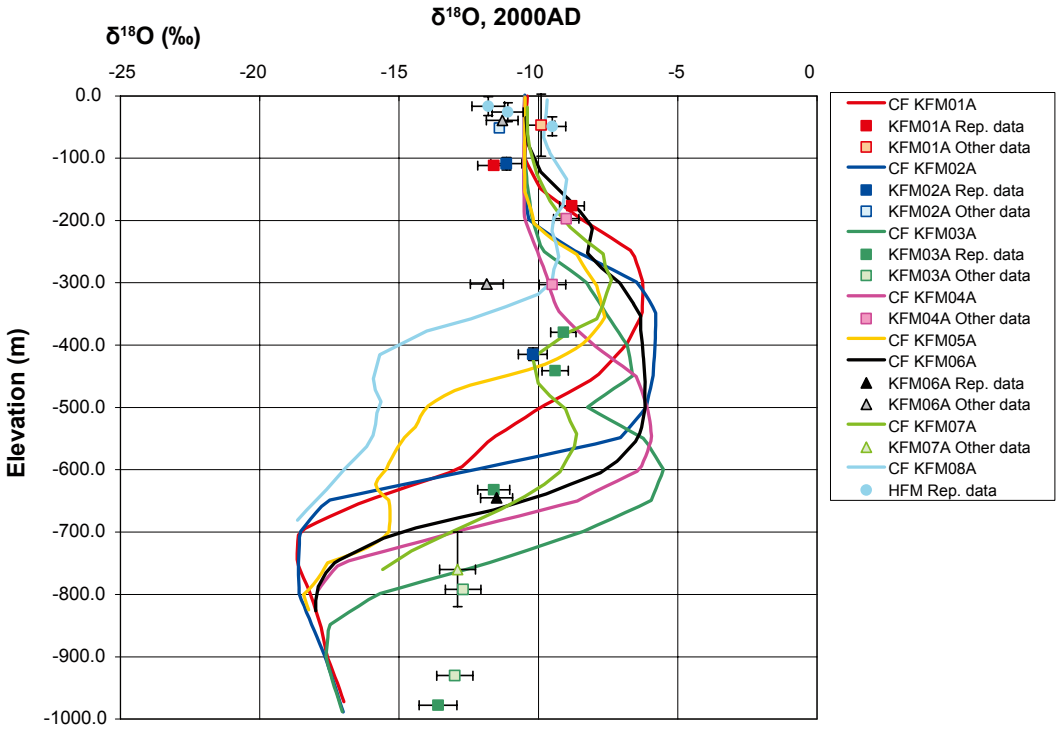

Figure 4-4. *Comparison of δ18O with F2.1 data for the original ECPM model from SR-Can (SC21_HCD3_AC_HRD3A2_T_HSD1_BC1_local50).*

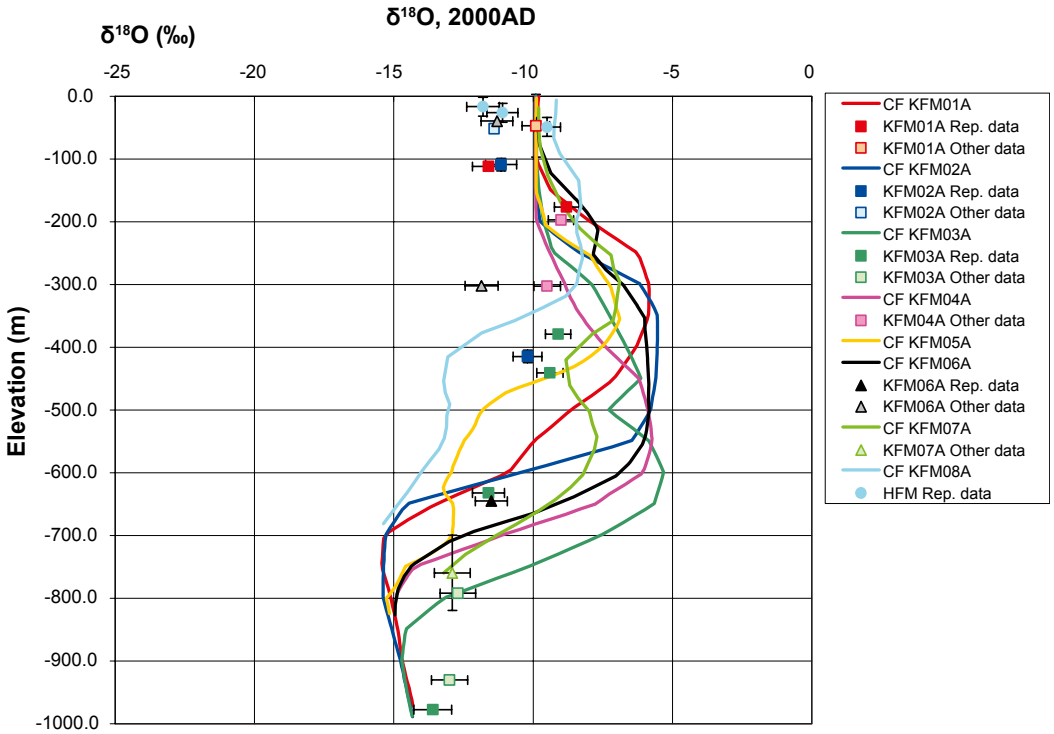

Figure 4-5. *Comparison of δ18O with F2.1 data for the ECPM model with modified reference waters (SC21_HCD3_AC_HRD3A2_T_HSD1_BC1_RefW2).*

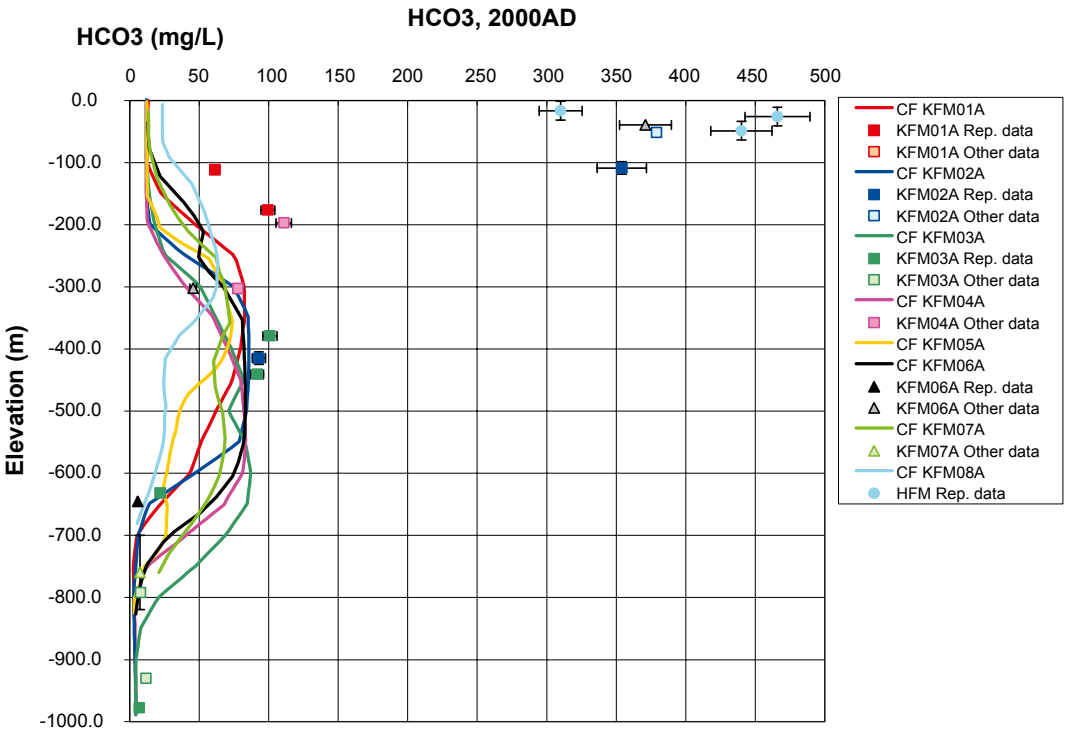

Figure 4-6. *Comparison of HCO_3 with F2.1 data for the original ECPM model from SR-Can (SC21_HCD3_AC_HRD3A2_T_HSD1_BC1_local50).*

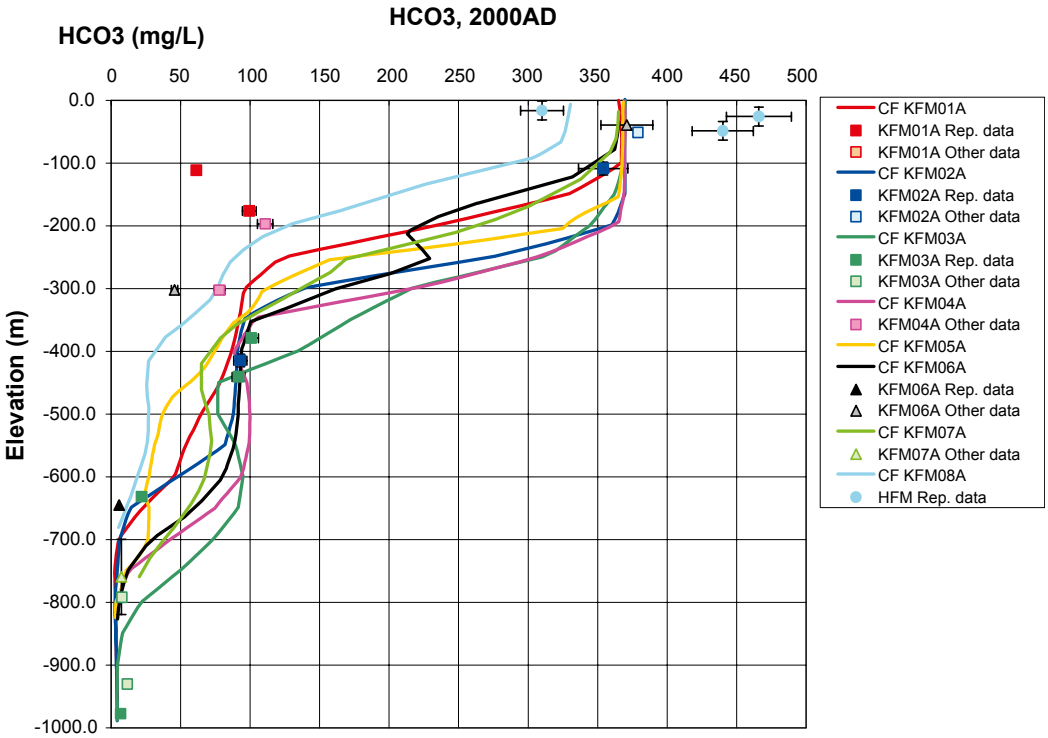

Figure 4-7. *Comparison of HCO_3 with F2.1 data for the ECPM model with modified reference waters (SC21_HCD3_AC_HRD3A2_T_HSD1_BC1_RefW2).*

4.3 Flow wetted surface

The flow wetted surface, a_r, is the amount of water conducting fracture surface (counting both walls of a fracture) area per unit volume and hence equates to twice the connected fracture intensity (2 $P32_c$). The parameter is used to control the effectiveness of diffusion in to the rock matrix from the surfaces of water-bearing fractures in which advective transport of tracers takes place. To simplify the model parameterisation, a uniform value of a_r,is used throughout the model even for the ECPM model, although it would be possible to have a spatially varying parameter based on the underlying DFN. The original model had an a_r of 0.25 m^2/m^3, or equivalent to an average conductive fracture spacing of 8 m. For F2.1, pore water data was only available for KFM06A. Since the pore-water chloride is too high in Figure 4-2, a_r was reduced to 0.16 m^2/m^3, or equivalent to an average conductive fracture spacing of 12 m to get the improvement seen in Figure 4-8 (see the dashed line for KFM06A compared to the circles to show the measured data). This is approximately the maximum value to get a match. The minimum was found to be about 0.1 m^2/m^3, as shown in Figure 4-9, although this is a variant on a much later model in the sequence of model development.

4.4 Surface boundary condition

As described in Section 2.3.3, site conditions suggest a system of high transmissivity near the surface which tends to flatten the driving head in the candidate area. As illustrated in the simulation of point-water heads in Chapter 3, to include a horizontal cage feature of high transmissivity, it is imperative to change the top surface boundary condition from one of topographic head to a specified flux.

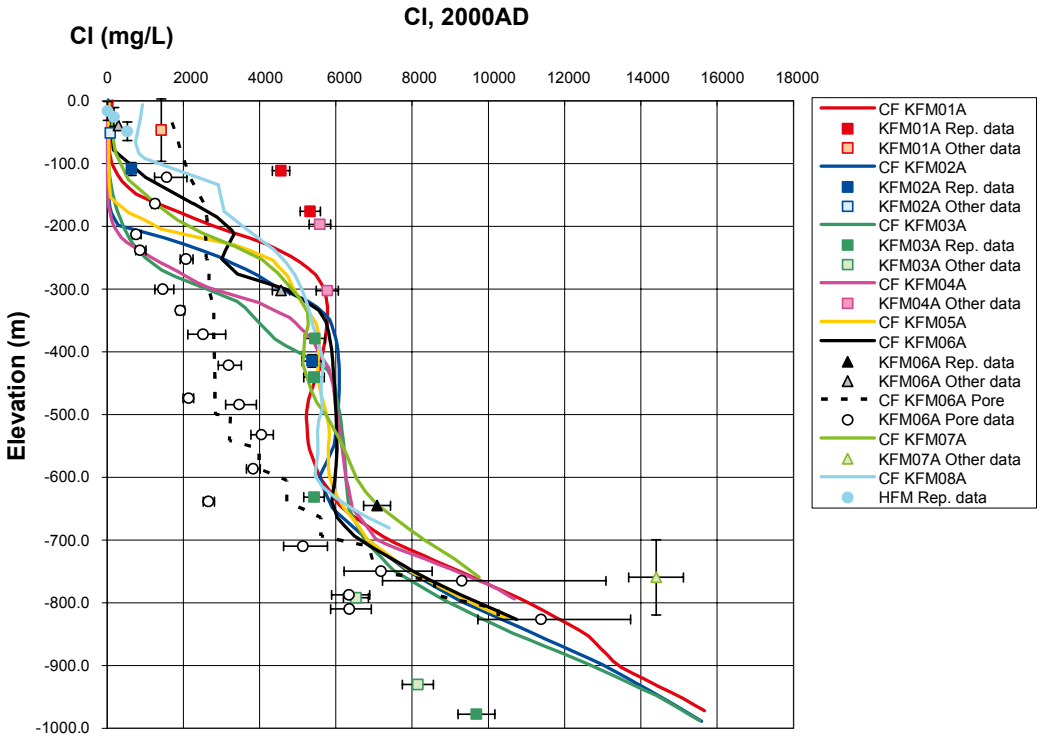

Figure 4-8. *Comparison of Cl with F2.1 data for the ECPM model with lower flow wetted surface, 0.16 m^2/m^3 (SC21_HCD3_AC_HRD3A2_T_FWS_HSD1_BC1_RefW2).*

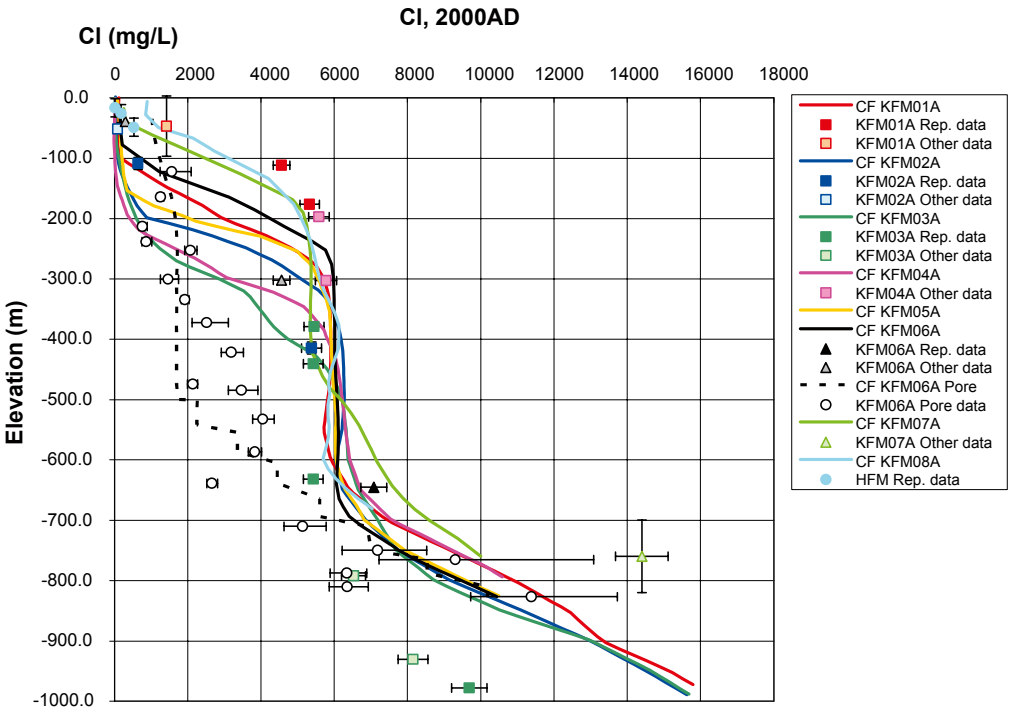

Figure 4-9. *Comparison of Cl with F2.1 data for the ECPM model with the lowest flow wetted surface, 0.1 m^2/m^3, near-surface high T feature and flux boundary condition on top (SC21_HCD3_AC_HRD3A2_T5_FWS2_HSD1_BC2_RefW3).*

The flux specified is based on a P-E of 180 mm/year, though as suggested in Chapter 3 not all of this may infiltrate the bedrock. Figure 4-10 and Figure 4-11 show one example based on the homogeneous CPM model of how much difference a flux boundary condition makes in reducing flow at depth for a model with high transmissivity near the surface. Salinity occurs about 100 m higher up in many boreholes for the case with a flux boundary condition in Figure 4-11. Clearly, it is more representative of site conditions to include a high transmissivity cage feature near the surface and use a flux based boundary condition, otherwise salinity is flushed too deep and the driving head gradient is over-predicted, see Chapter 3. Hence, for all subsequent simulations a flux based boundary condition was used.

4.5 Near surface high transmissivity system

The next stage was to add in a high transmissivity system near the surface within the candidate area. The first case considered was for a case where a high transmissivity cage feature of $2 \cdot 10^{-3}$ m^2/s throughout RFM029 which based on Chapter 3 gave a good match to the near-surface heads without changing the bedrock infiltration by adjusting the soil properties. The results for this case are shown for the ECPM model in Figure 4-12. Comparing this with the equivalent results for a CPM model in Figure 4-11, the results are felt to be less good for the CPM model, and so only the ECPM model based on an underlying DFN was used for the subsequent simulations.

The next pair of cases used a lower transmissivity cage feature of $1 \cdot 10^{-3}$ m^2/s more consistent with the measured flow rates in the percussion drilled boreholes. Figure 4-13 shows the case with just a high transmissivity in the near-surface horizontal feature, while Figure 4-14 shows the case with the addition of high horizontal transmissivity in the top 1 m of soil. The second of these cases was the one that gave the most consistency with the observed heads in Chapter 3, and for this calibration also seems to give the best results.

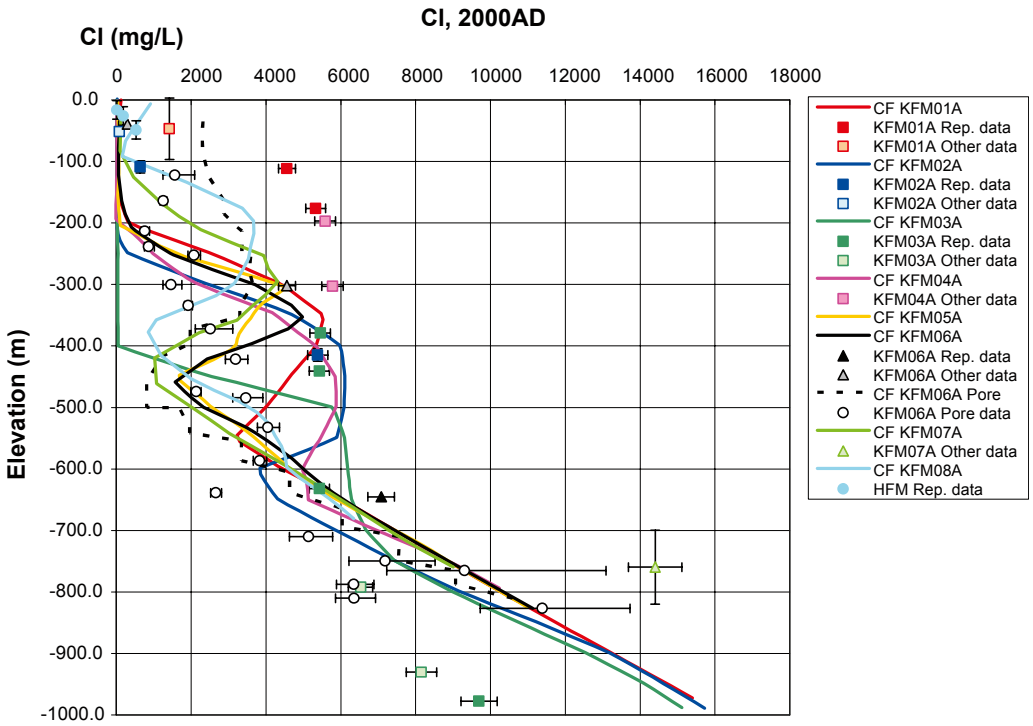

Figure 4-10. *Comparison of Cl with F2.1 data for the CPM model with a near-surface high T feature ($T=2\cdot10^{-4}$ m²/s) and topography boundary condition on top (SC21_HCD3_AC_HRDDT3__HSD1_BC1_ RefW2).*

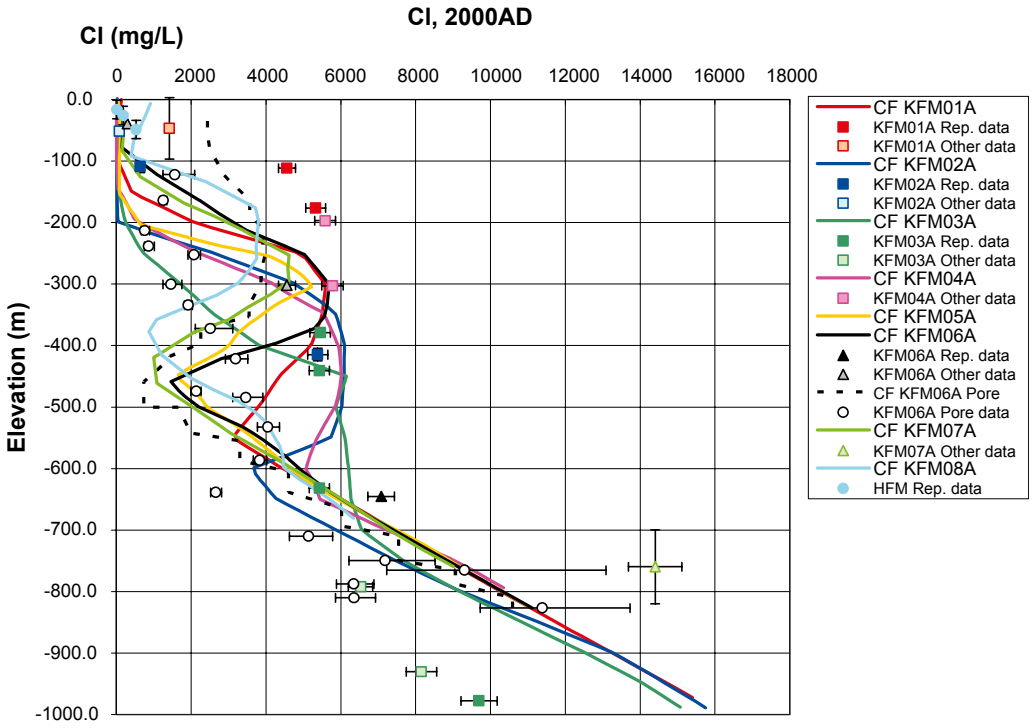

Figure 4-11. *Comparison of Cl with F2.1 data for the CPM model with a near-surface high T feature ($T=2\cdot10^{-4}$ m²/s) and flux boundary condition on top (SC21_HCD3_AC_HRDDT3_HSD1_BC2_RefW2).*

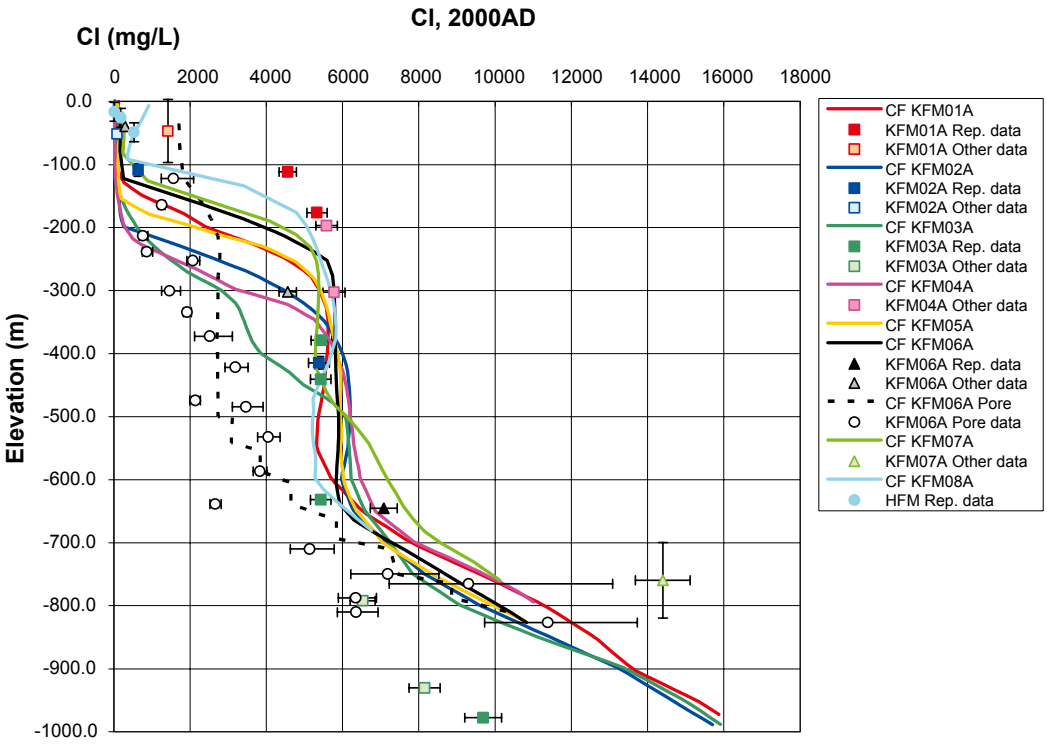

Figure 4-12. *Comparison of Cl with F2.1 data for the ECPM model with a near-surface high T feature ($T=2\cdot10^{-3}$ m^2/s), flow wetted surface 0.16 m^2/m^3, and flux boundary condition on top (SC21_HCD3_AC_HRD3A2_T4_FWS_HSD1_BC2_RefW3).*

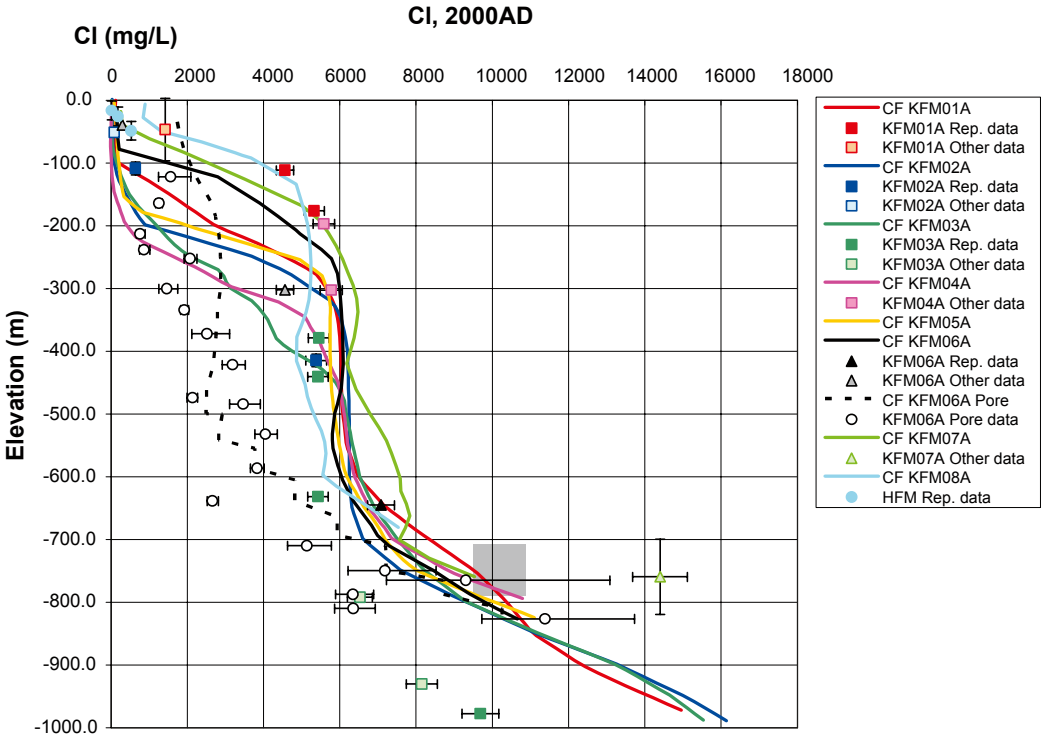

Figure 4-13. *Comparison of Cl with F2.1 data for the ECPM model with a near-surface high T feature ($T=1\cdot10^{-3}$ m^2/s), flow wetted surface 0.16 m2/m3, and flux boundary condition on top (SC21_HCD3_AC_HRD3A2_T5_FWS_HSD1_BC2_RefW3).*

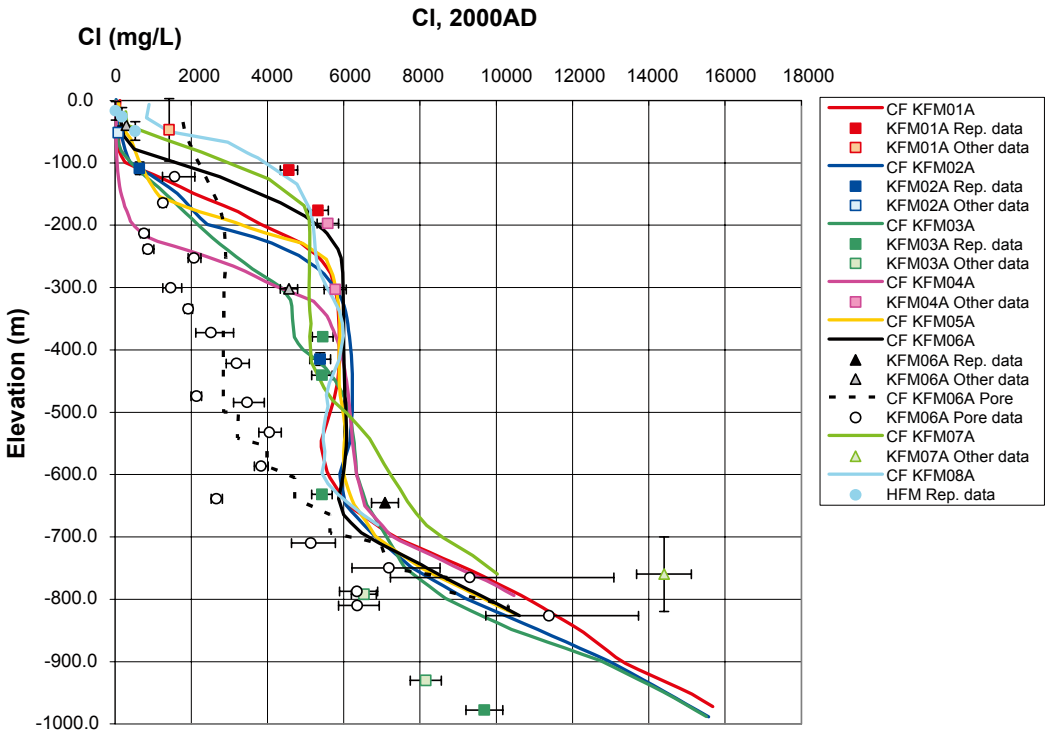

Figure 4-14. *Comparison of Cl with F2.1 data for the ECPM model with a near-surface high T feature ($T=1\cdot10^{-3}$ m²/s), flow wetted surface 0.16 m²/m³, a high $T=1\cdot10^{-3}$ m²/s top 1 m soil layer, and a flux boundary condition on top (SC21_HCD3_AC_HRD3A2_T5_FWS_HSD1a_BC2_RefW3).*

In judging the quality of the fit, it needs to be commented that for F2.1 there is little data available from the new boreholes KFM06A, KFM07A and KFM08A, and hence the comparison is necessarily subjective. We have assumed that the data suggests that the salinity in each of the boreholes broadly follows a similar pattern as suggested by the entire observed data set apart from a few notable differences such as the lower salinity near the surface in KFM02A, the higher salinity at depth in KFM07A and lower salinity at depth in KFM03A. It is not clear at this stage whether these represent general spatial trends or merely localised conditions in a particular borehole or the deformation zone from which water has been sampled. Therefore, the interpretation put on Figure 4-14 is that Cl predicted by the model in KFM06A, KFM07A and KFM08A are in good agreement with the overall trend. These boreholes are not intersected by ZFMNE00A2, whereas the boreholes from which we have good data, KFM01A and KFM04A give Cl deeper than in the model. It is suggested this may be due to having too higher transmissivity contribution from the DZ's, both sub-vertical and ZFMNE00A2, in the upper sections of these 2 boreholes.

4.6 Deformation zone model

Figure 4-13 and Figure 4-14 may offer some insight into why the predicted Cl profile in KFM01A and KFM04A are deeper than the observed values while the predicted Cl in KFM06A, KFM07A and KFM07A reach the right sort of values, 4,000–6,000 mg/L, located within 1 km to the north-west. KFM01A, KFM04A and KFM05A are all intersected by the gently dipping ZFMNE00A2 in the upper section, whereas KFM06A, KFM07A and KFM08A are not. Hence, the main hypothesis for the poor prediction of the Cl profile in KFM01A and KFM04A is that transmissivity of ZFMNE00A2 prescribed in the vicinity of these two boreholes is too

high, suggesting either the geometry, depth dependency function or the heterogeneity of ZFMNE00A2 have not been well represented, at least locally. Another contributing factor is that there are vertical zones, ZFMNE1188 and ZFMNW1194, located very close and parallel to these 2 boreholes. These are lineaments of uncertain hydraulic importance. To quantify the effect of these two zones, a case was run with them completely removed. The results in Figure 4-15 compared with Figure 4-13 show that the Cl profile moves up only slightly in KFM01A and KFM04A without these two zones. Hence, they may be part of the story, but the geometry and transmissivity of ZFMNE00A2 is the key to improve the Cl prediction here. This motivates a more detailed study of the hydraulic properties of ZFMNE00A2 once the stage 2.2 structural model is available.

Another case was considered to try to improve the match in KFM03A by reducing the transmissivity in ZFMNE00A4, ZFMNE00A7 and ZFMNE00B1 to give more consistency with the values seen in the KFM03A PSS 100 m data. The effect is limited to KFM03A since this is the only borehole that intersects these DZ's and is illustrated by Figure 4-16. The mix of marine and Glacial is clearly improved by the change. This is an illustration of how important the assignment of transmissivities of the deformation zones is.

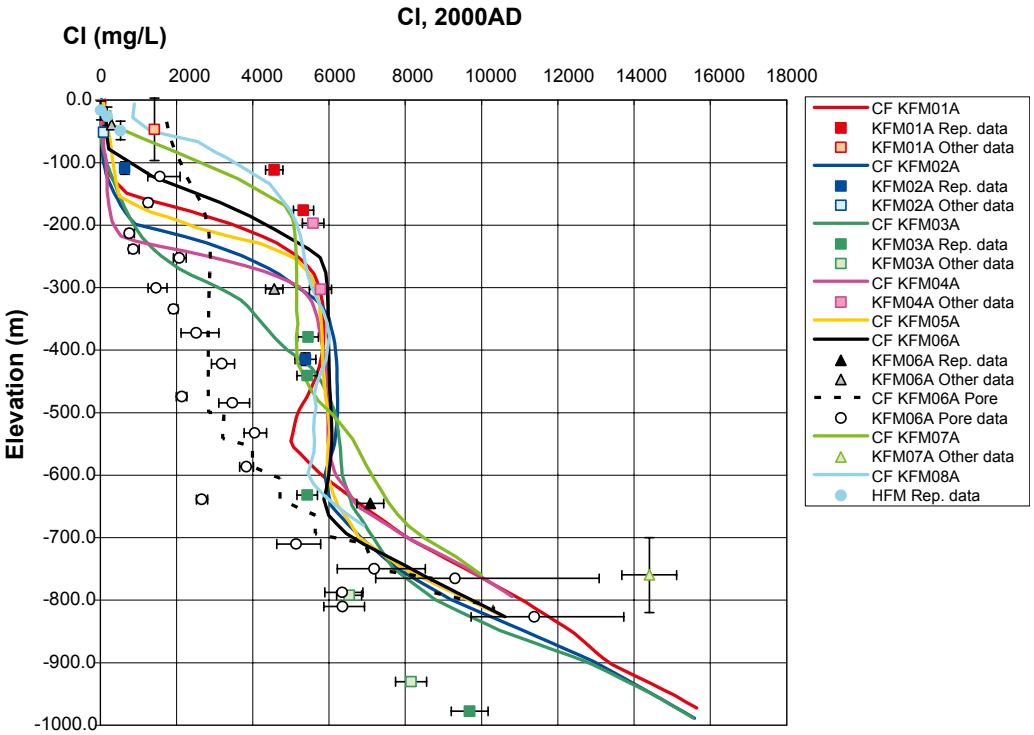

Figure 4-15. *Comparison of Cl with F2.1 data for the ECPM model with a near-surface high T feature ($T=1{\cdot}10^{-3}$ m^2/s), flow wetted surface 0.16 m^2/m^3, DZ's ZFMNE1188 and ZFMNW1194 removed, and a flux boundary condition on top (SC21_HCD4_AC_HRD3A2_T5_FWS_HSD1a_BC2_RefW3).*

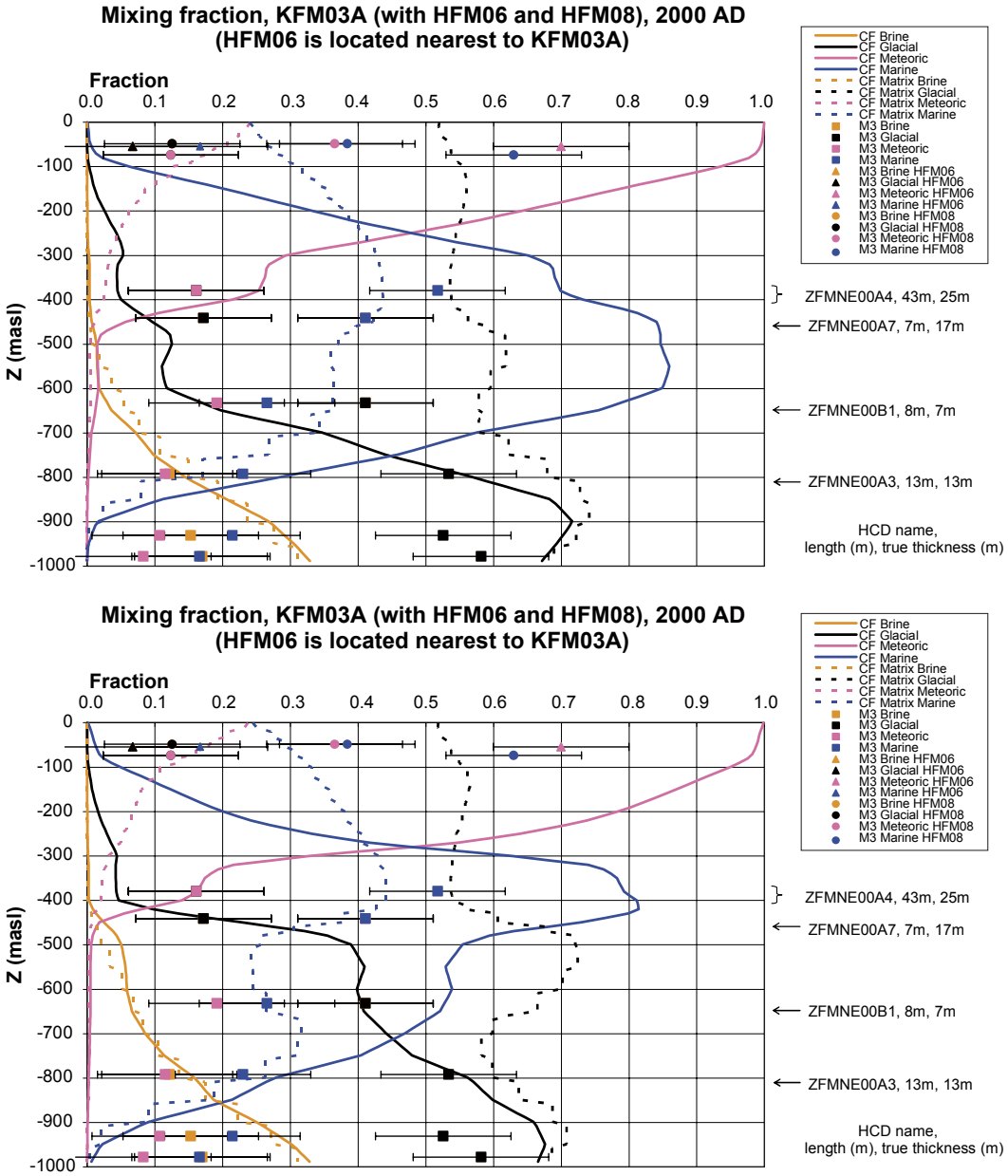

Figure 4-16. *Effect on reference water fractions in KFM03A by reducing the transmissivity of 3 deformation zones. Top: the ECPM model with a near-surface high T feature ($T=1\cdot10^{-3}$ m^2/s), a high transmissivity 1 m soil layer, flow wetted surface 0.16 m^2/m^3, and a flux boundary condition on top (SC21_HCD3_AC_HRD3A2_T5_FWS_HSD1a_BC2_RefW3). Bottom: the same model with the transmissivity of 3 DZ's reduced (SC21_HCD4_AC_HRD3A2_T5_FWS_HSD1a_BC2_RefW3).*

4.7 Stochastic DFN

In previous SDM and SR-Can studies only single realisations of the regional Hydro-DFN have been considered because it was found that the properties of the HCD have a greater control on the system than do those of the HRD. Here, it was thought useful to quantify the difference in predicted hydro-geochemistry for a few realisations of the underlying Hydro-DFN model.

The methodology for obtaining properties from a regional DFN model was updated slightly to follow some of the ideas implemented for L1.2 site descriptive modelling /Hartley et al. 2006b/. The methodology involves the following steps:

1. Generate a stochastic realisation of the fracture network according to the Hydro-DFN prescription according a division of the rock into appropriate hydraulic or fracture domains.
2. Perform a connectivity analysis on the regional-scale to identify which fractures form part of the connected network, by which mean there is a path by which water can percolate through from the boundaries of the model to reach the fracture, and remove those fractures which are isolated.
3. Perform upscaling to derive equivalent continuum porous medium properties the represent the fracture properties within each grid cell based on flow and connectivity simulations.

Step 2. was the additional step performed here than was not included in the original F1.2 methodology. The purpose is to avoid over-estimating the hydraulic conductivity on by including fractures that form a connected network on the scale of a grid cell, but not on the regional-scale. In addition, a lower truncation on the sive of fractures was used of 5.6 m radius in the embedded local-scale and 14 m in the regional-scale. The results of 3 realisations are shown in Figure 4-17 to Figure 4-19.

The differences are of sufficient magnitude to suggest multiple realisations should be performed in the latter stages of a calibration, but single realisations are probably sufficient to understand the general sensitivities of the system. They also show that the HRD has very little effect on KFM01A and KFM04A, confirming that it is the HCD that control hydro-geochemistry in these two boreholes.

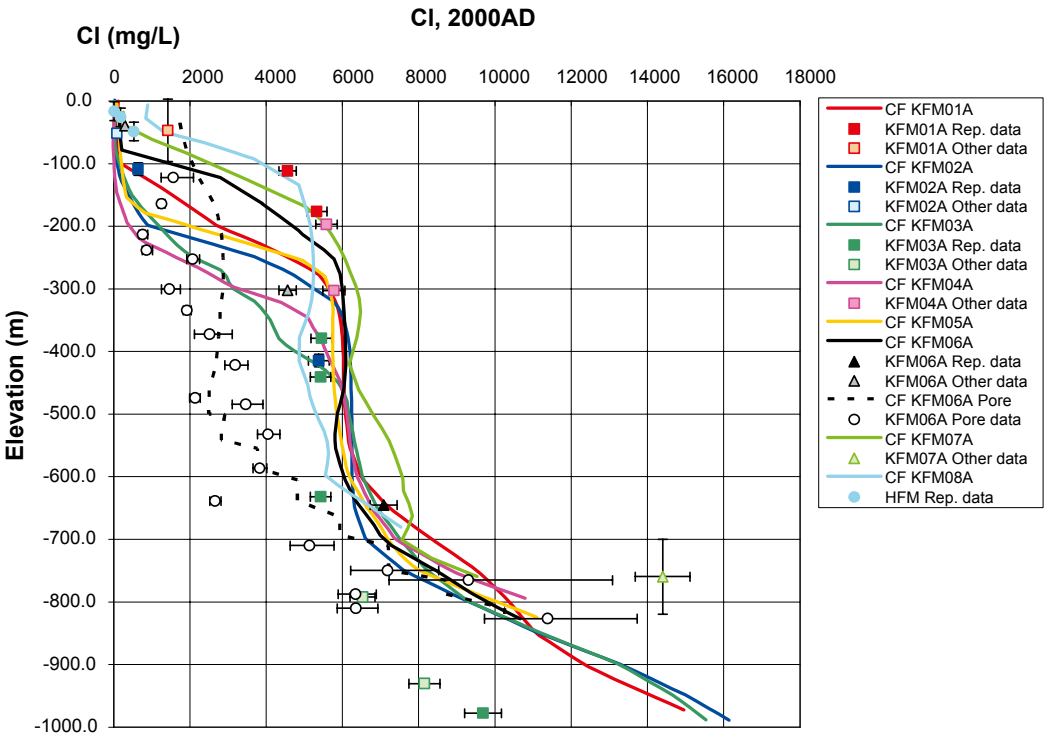

Figure 4-17. *Comparison of Cl with F2.1 data for realisation 1 of the ECPM model with a near-surface high T feature ($T=1{\cdot}10^{-3}$ m^2/s), flow wetted surface 0.16 m^2/m^3, and flux boundary condition on top (SC21_HCD3_AC_HRD3aA2_T5_FWS_HSD1_BC2_RefW3).*

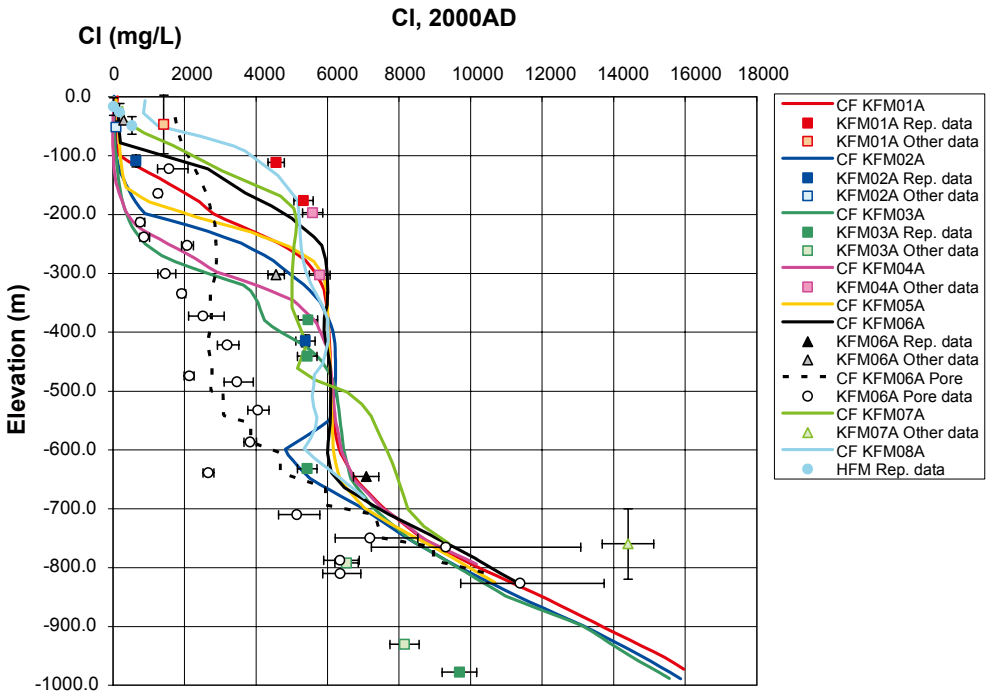

Figure 4-18. *Comparison of Cl with F2.1 data for realisation 2 of the ECPM model with a near-surface high T feature ($T=1\cdot10^{-3}$ m^2/s), flow wetted surface 0.16 m^2/m^3, and flux boundary condition on top (SC21_HCD3_AC_HRD3bA2_T5_FWS_HSD1_BC2_RefW3).*

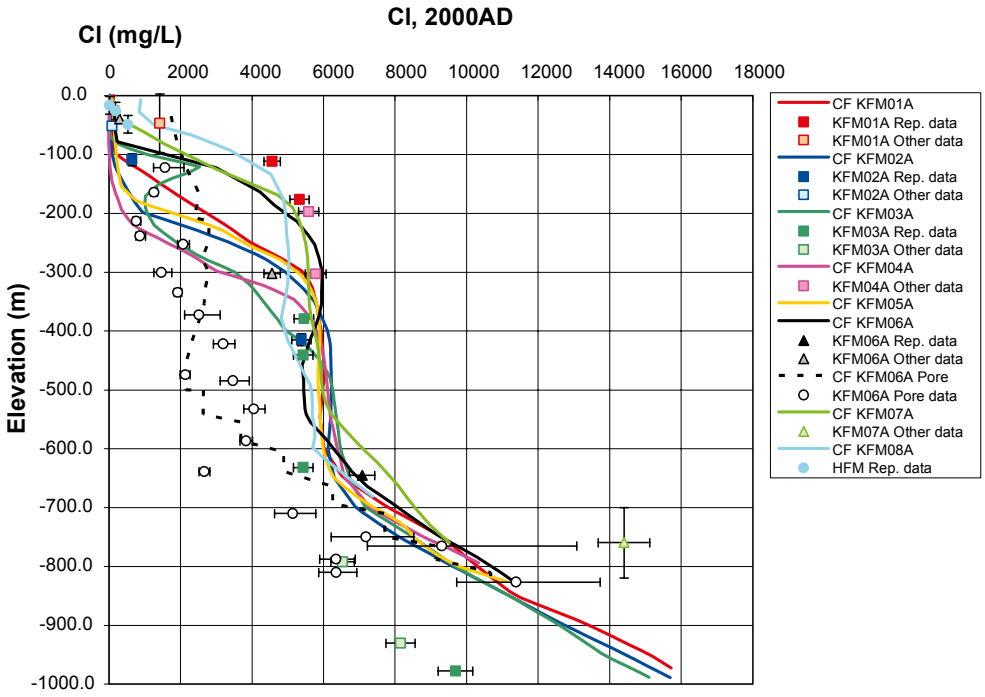

Figure 4-19. *Comparison of Cl with F2.1 data for realisation 3 of the ECPM model with a near-surface high T feature ($T=1\cdot10^{-3}$ m^2/s), flow wetted surface 0.16 m^2/m^3, and flux boundary condition on top (SC21_HCD3_AC_HRD3cA2_T5_FWS_HSD1_BC2_RefW3).*

4.8 Initial condition

The initial conditions for hydro-geochemistry for the start of the simulations at 8,000 BC are uncertain. It is thought that Glacial water infiltrates to large depths mixing with the Brine. The original initial conditions were pure Glacial above –500 m, a linear variation from zero to full Brine at –2,100 m. One conceptual issue that arises is that this initial condition gives approximately the right behaviour for Cl (and Br/Cl as will be seen later) arising from Brine, but gives too little Ca and too much Mg. In the case of Ca, it is only present in groundwater samples at the types of concentrations only specified for the Brine end-member, and so if one is seeking a mechanism to explain the Ca concentrations purely based on mixing, then some diluted Brine water needs to be retained higher up in the bedrock. Similarly, some Brine higher up may improve the match for Na, Mg and SO4. Therefore, a numerical experiment was tried with 5% Brine in both the fracture and matrix systems initially. The amount of Brine cannot be too high otherwise the Cl concentration becomes too high. The comparative results for Ca concentrations for the case with a near-surface high T feature ($T=1\cdot10^{-3}$ m^2/s), flow wetted surface 0.16 m^2/m^3 are shown for the original and modified initial conditions in Figure 4-20 and Figure 4-21, respectively. As can be seen the improvement is marginal with only slightly more Ca in some more boreholes, since the Brine is mostly flushed out of the top 500 m of bedrock. Note: the Cl concentration in the fracture system is also relatively insensitive to this change in initial condition, but the Cl concentration in the matrix becomes too high, which means that if there were some residual Brine high up in the system, then a lower value of flow wetted surface around 0.1 m^2/m^3 needs to be used to reduce the diffusion of Littorina Cl in the matrix. (The Cl in the matrix pore-water is presently of uncertain origin).

Another variant on the initial condition was considered with a different initial profile in the foot wall of ZFMNE00A2 (only inside RFM029) to the rest of the model domain. In the foot wall, groundwater was set to pure Glacial above –400 m, a linear variation from zero to full Brine at –1,500 m. Outside the depth for maximum Brine was lowered slightly to –2,300 m. The motivation was to try to explain the difference in Cl seen in KFM03A a few kilometres to the east in the hanging wall of ZFMNE00A2 and the much more elevated salinity observed in KFM07A. The initial profile of Brine specified in the variant is shown in Figure 4-22 and Figure 4-23.

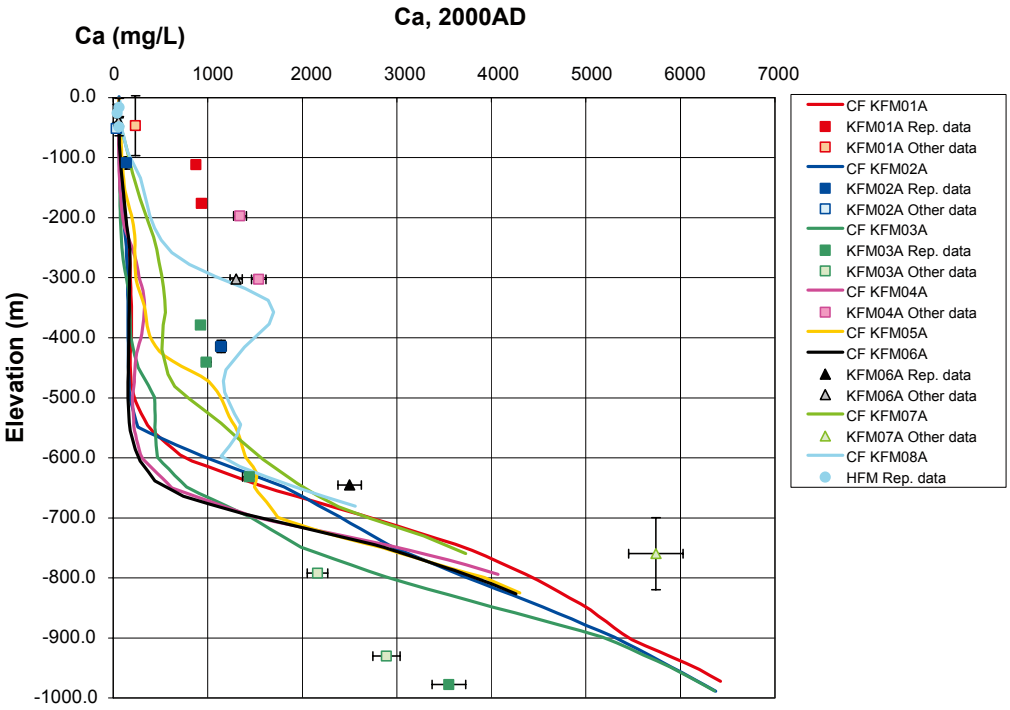

Figure 4-20. *Comparison of Ca with F2.1 data for the ECPM model with a near-surface high T feature ($T=1\cdot10^{-3}$ m^2/s), flow wetted surface 0.16 m^2/m^3, and flux boundary condition on top (SC21_HCD3_AC_HRD3A2_T5_FWS_HSD1_BC2_RefW3).*

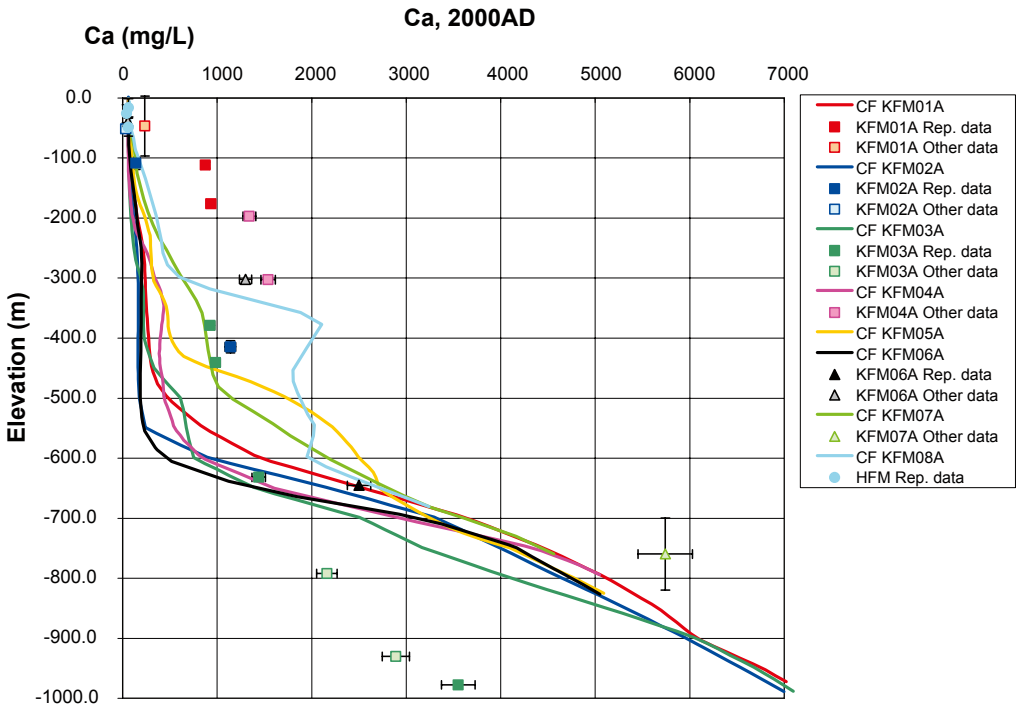

Figure 4-21. *Comparison of Ca with F2.1 data for the ECPM model with a near-surface high T feature ($T=1\cdot10^{-3}$ m^2/s), flow wetted surface 0.16 m^2/m^3, flux boundary condition on top and 5% residual Brine in the initial condition (SC21_HCD3_AC_HRD3A2_T5_FWS_HSD1_BC2_IC2_RefW3).*

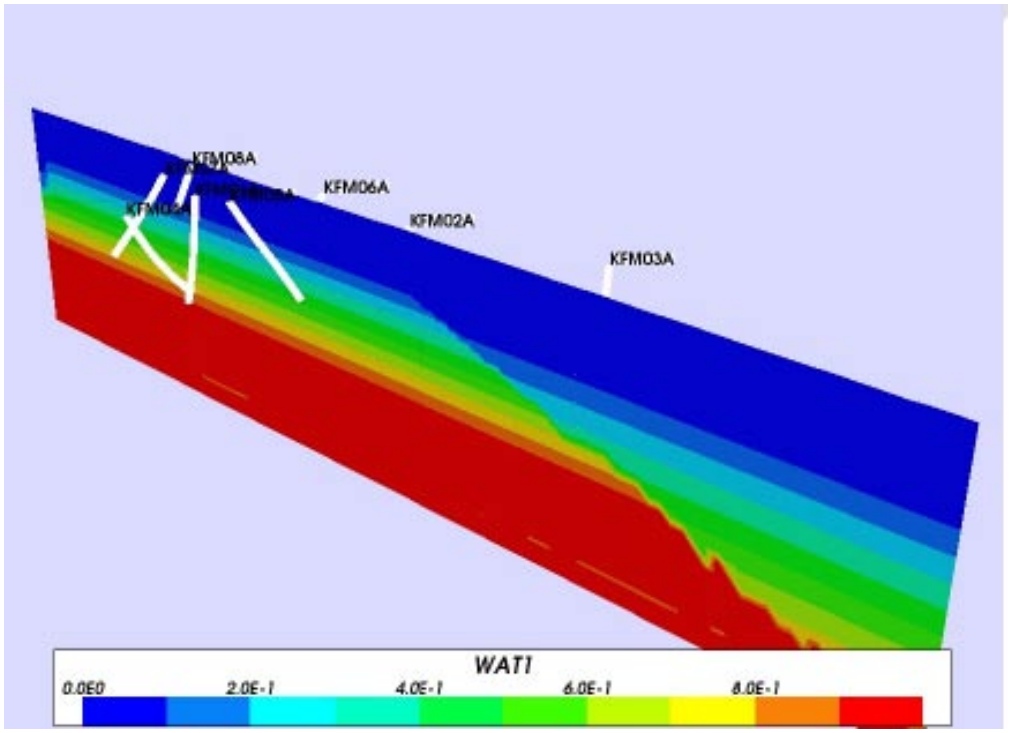

Figure 4-22. *Brine at 8,000 BC on a NW-SE slice for a case with a different initial condition in the foot wall and hanging walls of ZFMNE00A2 (SC21_HCD3_AC_HRD3A2_T5foot_FWS_HSD1a_BC2_IC3_RefW3).*

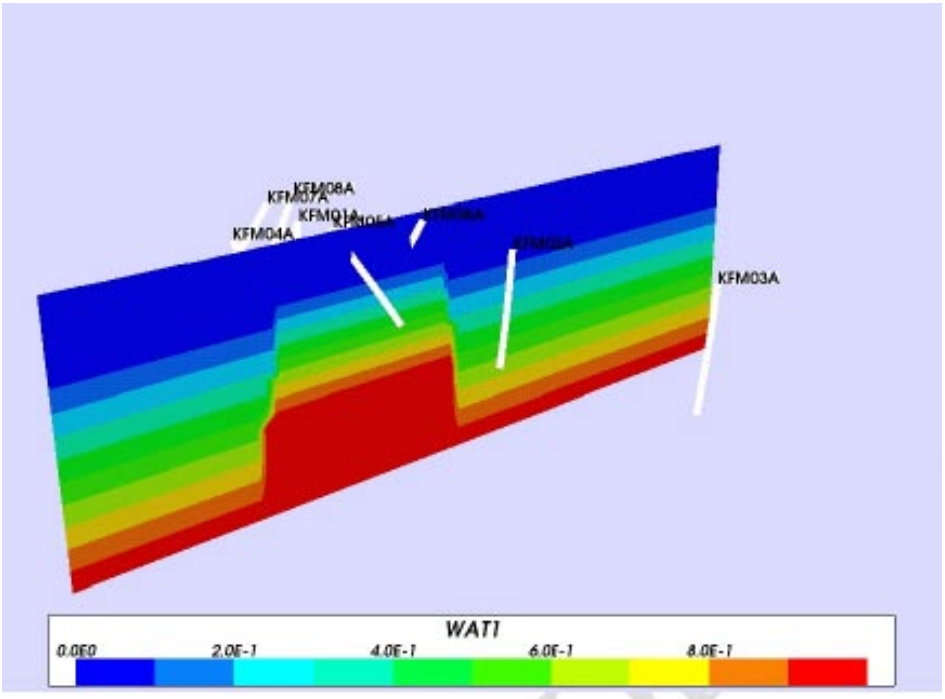

Figure 4-23. *Brine at 8,000 BC on a SW-NE slice for a case with a different initial condition in the foot wall and hanging walls of ZFMNE00A2 (SC21_HCD3_AC_HRD3A2_T5foot_FWS_HSD1a_BC2_IC3_RefW3).*

However, it was found that these rapid spatial changes in salinity were quickly smoothed out in the simulations simply due to the weight of Brine as shown in Figure 4-24 after a mere 2,000 years of simulation. This is because a column of Brine about 25 m high induces an equivalent head difference of 1 m, so the initial condition specified results in an equivalent head difference of about 32 m, and hence a large driving force to smooth out such variations.

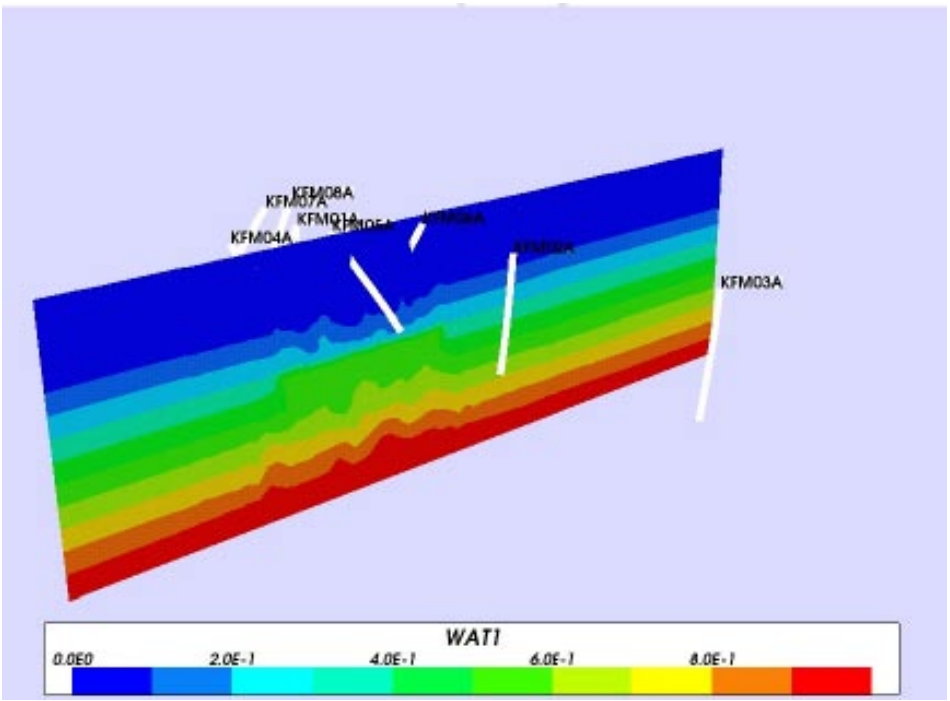

Figure 4-24. *Brine at 6,000 BC on a SW-NE slice for a case with a different initial condition in the foot wall and hanging walls of ZFMNE00A2 (SC21_HCD3_AC_HRD3A2_T5foot_FWS_HSD1a_BC2_ IC3_RefW3).*

The predictions for Cl concentration are shown in Figure 4-25 showing that the profile at depth in KFM03A is improved, but all other profiles have also been flushed more deeply due to the lower Brine specified in the hanging wall and the tendency to smooth out large variations in Brine levels. This effect can only be reduced by having much lower hydraulic conductivity (and fracture connectivity) at depths below about –600 m such the hydraulic system becomes compartmentalised. Otherwise one has to conclude that the differences in salinity seen in KFM03A and KFM07A must be localised measurement effects perhaps due to drawing water preferentially from depth in the case of KFM07A and nearer the surface in KFM03A, i.e. the samples do not reflect the natural in-situ hydro-geochemistry distribution.

4.9 Discretisation

The intention had been to use a 25 m local-scale embedded grid for the palaeo-hydrogeology models also, but this was not possible for all simulations due to a lack of computer resources prior to August 2006. A few calculations were performed on a 25 m to check the effect. Comparing Figure 4-26 and Figure 4-13 for two equivalent cases, the differences are slight.

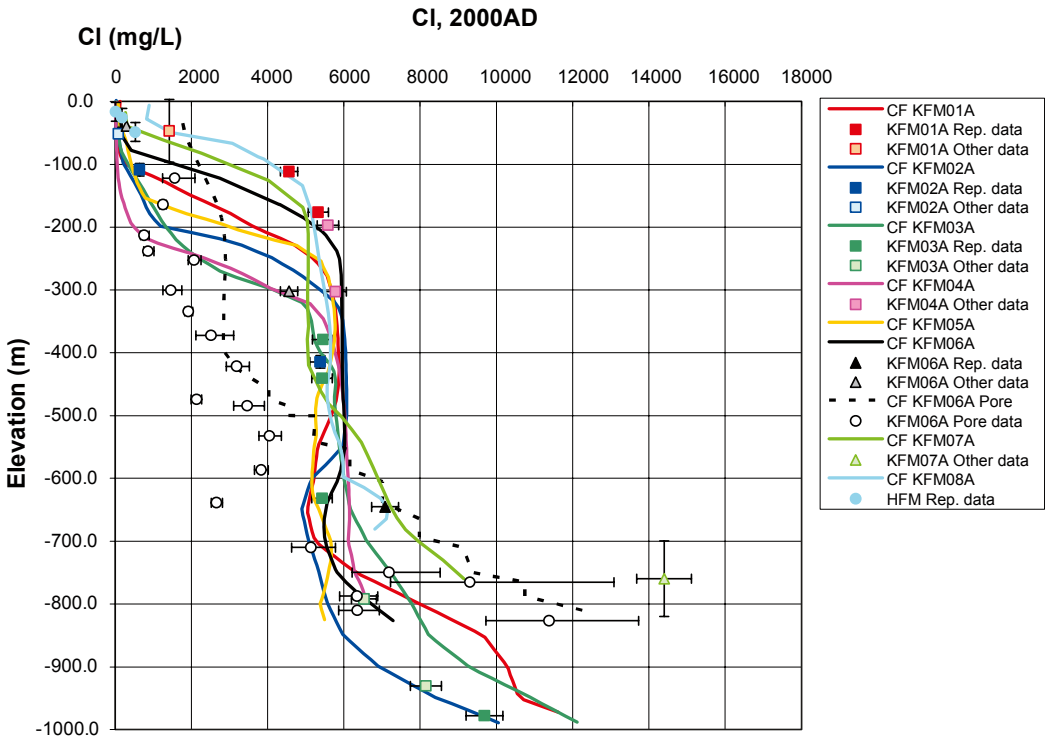

Figure 4-25. *Comparison of Cl with F2.1 data for the ECPM model with a near-surface high T feature ($T=1\cdot10^{-3}$ m^2/s) in the foot wall of A2, flow wetted surface 0.16 m^2/m^3, flux boundary condition on top and a different initial condition in the foot wall and hanging wall of ZFMNE00A2 (SC21_HCD3_AC_HRD3A2_T5foot_FWS_HSD1a_BC2_IC3_RefW3).*

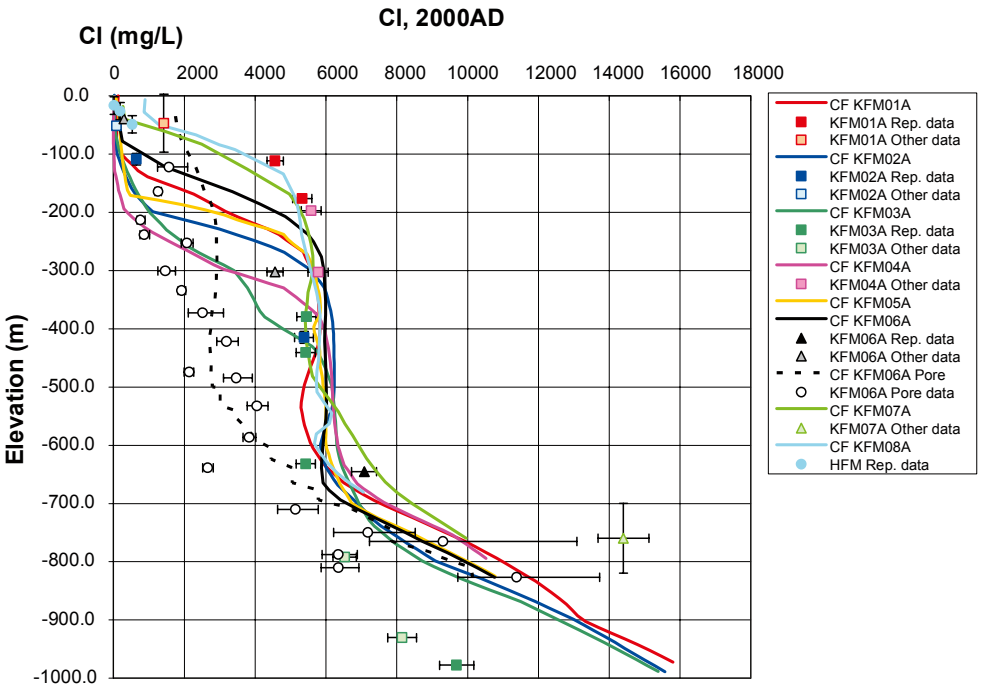

Figure 4-26. *Comparison of Cl with F2.1 data for the ECPM model with a near-surface high T feature ($T=1\cdot10^{-3}$ m^2/s), flow wetted surface 0.16 m^2/m^3, flux boundary condition on top and 25 m local-scale grid (CAGE_HCD3_AC_HRD3A2_T5_FWS_HSD1_BC2_RefW3).*

4.10 Other ions and Br/Cl

In this section we present the calibration for the key groundwater constituents used in the palaeo-hydrogeology: Cl, $\delta^{18}O$, and Mg together with a new calibration target based on the ratio of Br/Cl. The ratio Br/Cl is used to differentiate saline water of ancient Brine origin from that of marine origin since the ratio of Br/Cl is about double that for waters of Brine origin compared to marine. Since both Bromide and Chloride are judged to be conservative tracers, it is considered that the ratio Br/Cl is a more reliable indicator of salinity origin than Mg, which is subject to other processes than just mixing. Br was added to the composition table of each reference water in the numerical simulations. Figure 4-27 to Figure 4-30 show the distributions of Cl, Br/Cl, $\delta^{18}O$ and Mg in the core drilled boreholes for one of the better matched cases with a near-surface cage feature ($T=1\cdot10^{-3}$ m^2/s) in the foot wall of ZFMNE00A2, flow wetted surface 0.16 m^2/m^3, a high $T=1\cdot10^{-3}$ m^2/s top 1 m soil layer, and a flux boundary condition on top. Figure 4-28 compares the modelled and observed ratio of Br/Cl showing a transition from marine to Brine derived at about –600 m. This agrees well with the simulations, although the data suggest higher values of Br in the Brine water. The $\delta^{18}O$ plot shows the model predicts a transition to some glacial water at –600 m. Many of the boreholes suggest a lower $\delta^{18}O$ ratio associated with the Littorina pulse than is observed in the data. Perhaps this suggests that the Marine water that has entered the bedrock near the coast is actually a diluted mixture of Baltic water and terrestrial water from snow melt. This motivates more careful attention to the chemical composition of marine water close to the shore that infiltrates the bedrock. It is likely that the coastal water is itself a mixing zone for Baltic, rain and snow-melt waters. Mg is generally over-predicted in most boreholes. Using the alternative definition for marine water, based on the current Baltic, rather than the modelled Littorina water, will only improve this by about 6%.

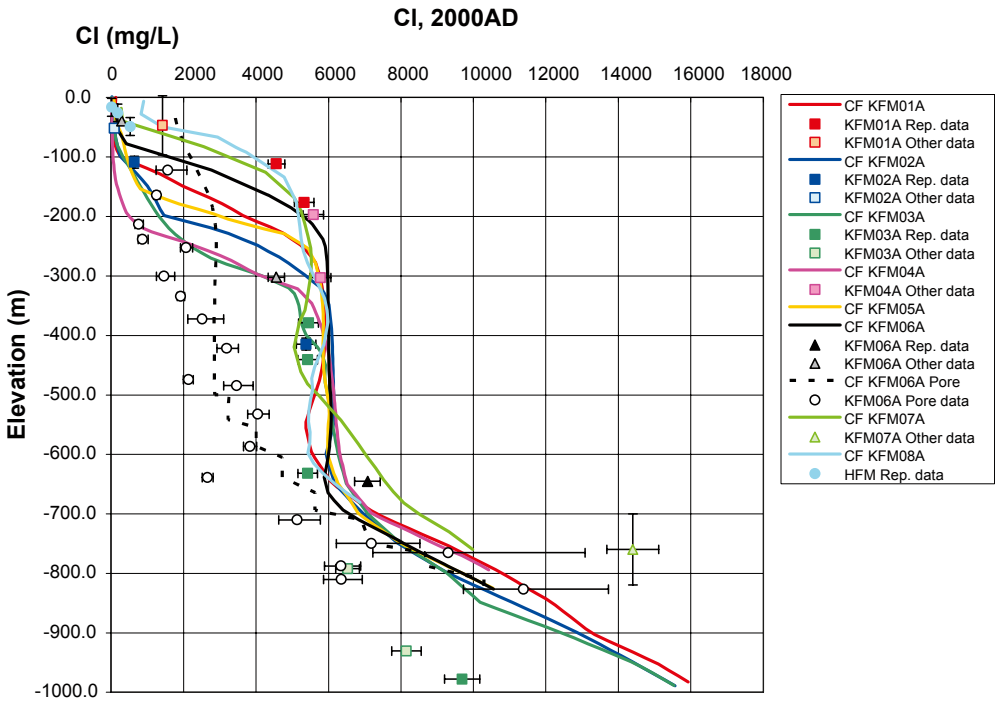

Figure 4-27. *Comparison of Cl with F2.1 data for the ECPM model with a near-surface high T feature ($T=1\cdot10^{-3}$ m^2/s) in the foot wall of A2, flow wetted surface 0.16 m^2/m^3, a high $T=1\cdot10^{-3}$ m^2/s top 1 m soil layer, and a flux boundary condition on top (SC21_HCD3_AC_HRD3A2_T5foot_FWS_HSD1a_BC2_RefW3).*

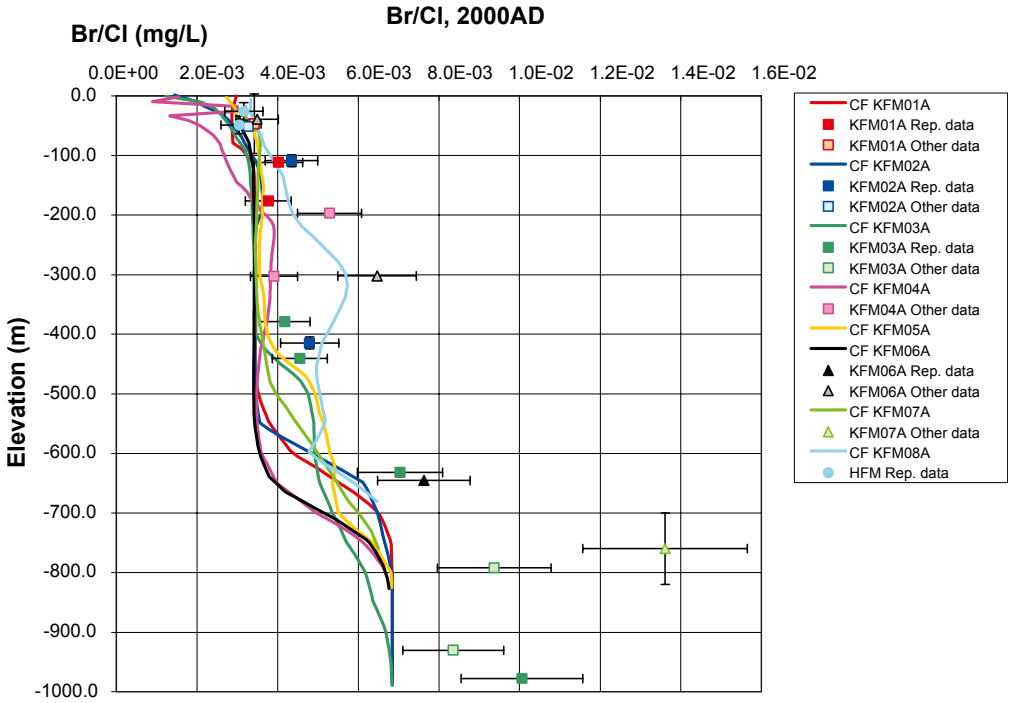

Figure 4-28. *Comparison of Br/Cl with F2.1 data for the ECPM model with a near-surface high T feature ($T=1\cdot10^{-3}$ m^2/s) in the foot wall of A2, flow wetted surface 0.16 m^2/m^3, a high $T=1\cdot10^{-3}$ m^2/s top 1 m soil layer, and a flux boundary condition on top (SC21_HCD3_AC_HRD3A2_T5foot_FWS_HSD1a_BC2_RefW3).*

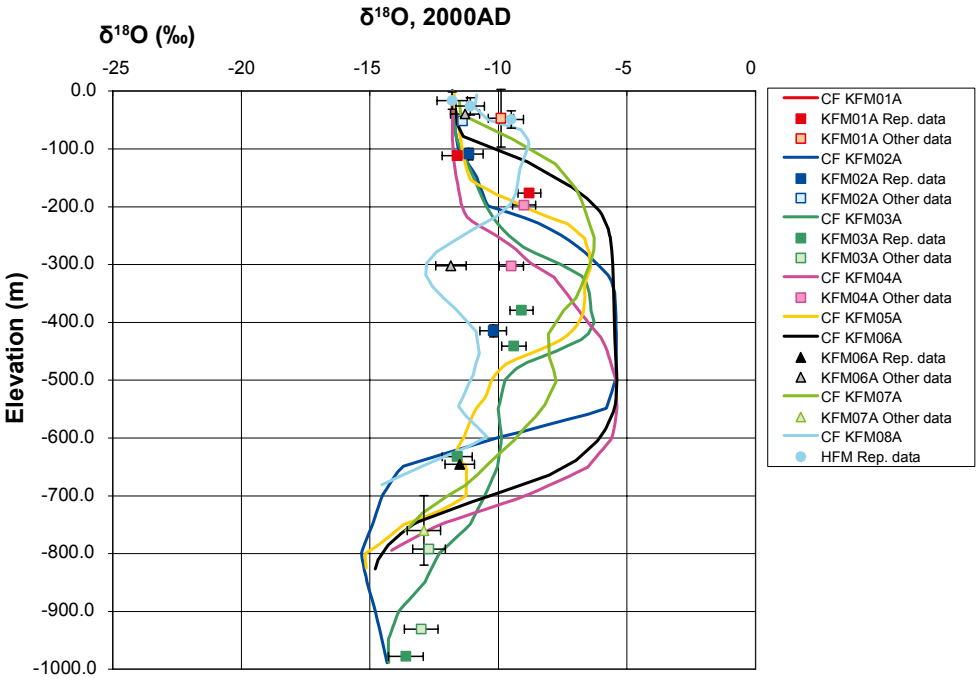

Figure 4-29. *Comparison of $\delta^{18}O$ with F2.1 data for the ECPM model with a near-surface high T feature ($T=1\cdot10^{-3}$ m²/s) in the foot wall of A2, flow wetted surface 0.16 m²/m³, a high $T=1\cdot10^{-3}$ m²/s top 1 m soil layer, and a flux boundary condition on top (SC21_HCD3_AC_HRD3A2_T5foot_FWS_HSD1a_BC2_RefW3).*

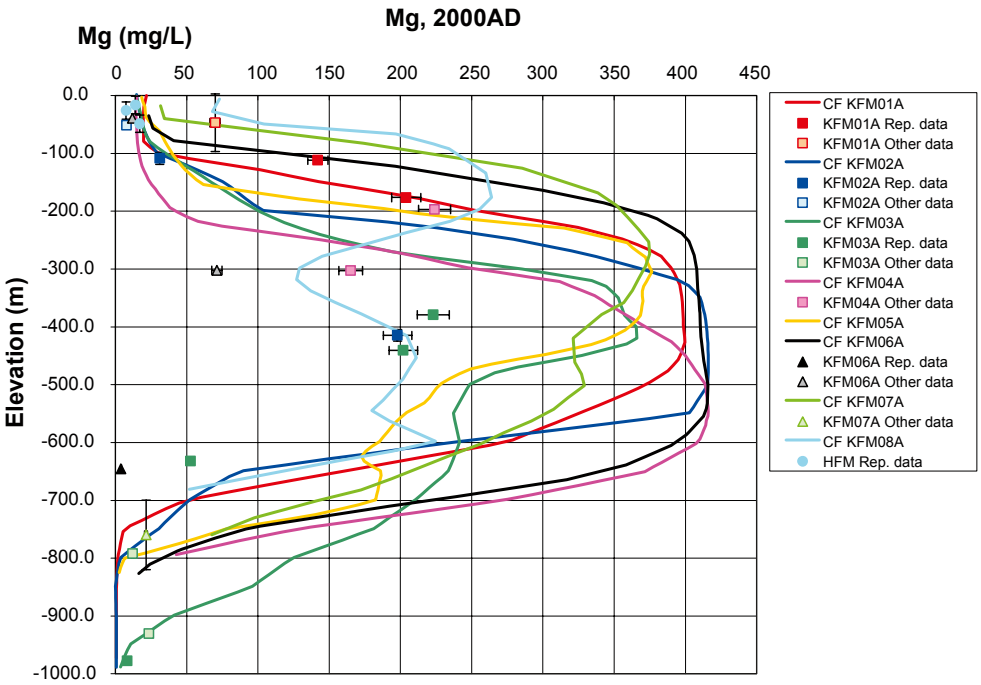

Figure 4-30. *Comparison of Mg with F2.1 data for the ECPM model with a near-surface high T feature ($T=1\cdot10^{-3}$ m²/s) in the foot wall of A2, flow wetted surface 0.16 m²/m³, a high $T=1\cdot10^{-3}$ m²/s top 1 m soil layer, and a flux boundary condition on top (SC21_HCD3_AC_HRD3A2_T5foot_FWS_HSD1a_BC2_RefW3).*

4.11 Alternative modelling methodology based on transport of individual ions

For all the results shown so far in this report, coupled flow and solute transport calculations have been based on the concept of transporting fractions of reference waters. This necessarily assumes all hydro-geochemical components are conservative, i.e. only subject to mixing. Although this may be a valid approximation for key components such as Chloride, it is less valid for many of the components. Still, it remains a useful method for understanding the mixing of various types of groundwater that have been present in the system for a long time or entered more recently from the surface. To relax the assumption of conservative transport, one needs to transport the groundwater components individually, but still account for coupled variable-density flow. To demonstrate this option, a simulation case was performed with each component transported individually, but based on equivalent initial and boundary conditions for each ion as for the reference water case. The effect of reactions was neglected in this case to test the results are equivalent to ones for reference water transport under conservative conditions. The results for Chloride and Br/Cl ratio are shown in Figure 4-31 and Figure 4-32 and can be compared to Figure 4-27 and Figure 4-28. The results are very similar, as they should be. There are some differences which are thought to result from the particular time-stepping scheme used, and would be expected to diminish for a smaller time-step size. This option could be used in the up-coming to consider non-conservative processes for some components as necessary.

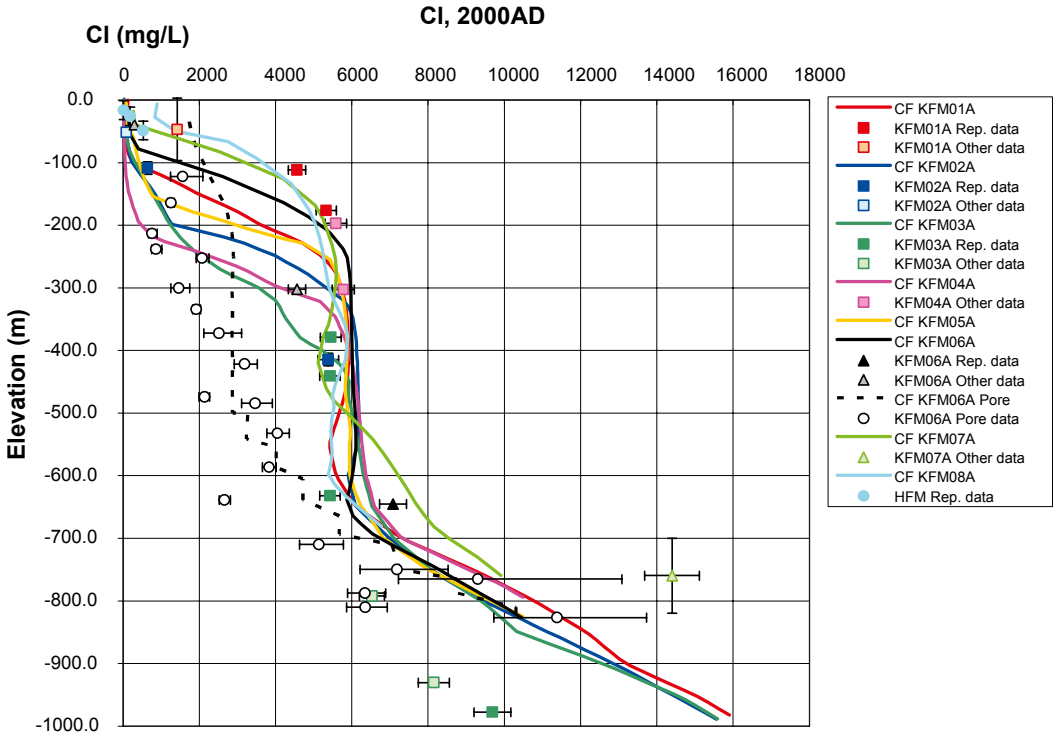

Figure 4-31. *Comparison of Cl with F2.1 data for the ECPM model of individual component transport with a near-surface high T feature ($T=1{\cdot}10^{-3}$ m^2/s) in the foot wall of A2, flow wetted surface 0.16 m^2/m^3, a high $T=1{\cdot}10^{-3}$ m^2/s top 1 m soil layer, and a flux boundary condition on top (Comp_HCD3_AC_HRD3A2_T5foot_FWS_HSD1a_BC2_RefW3).*

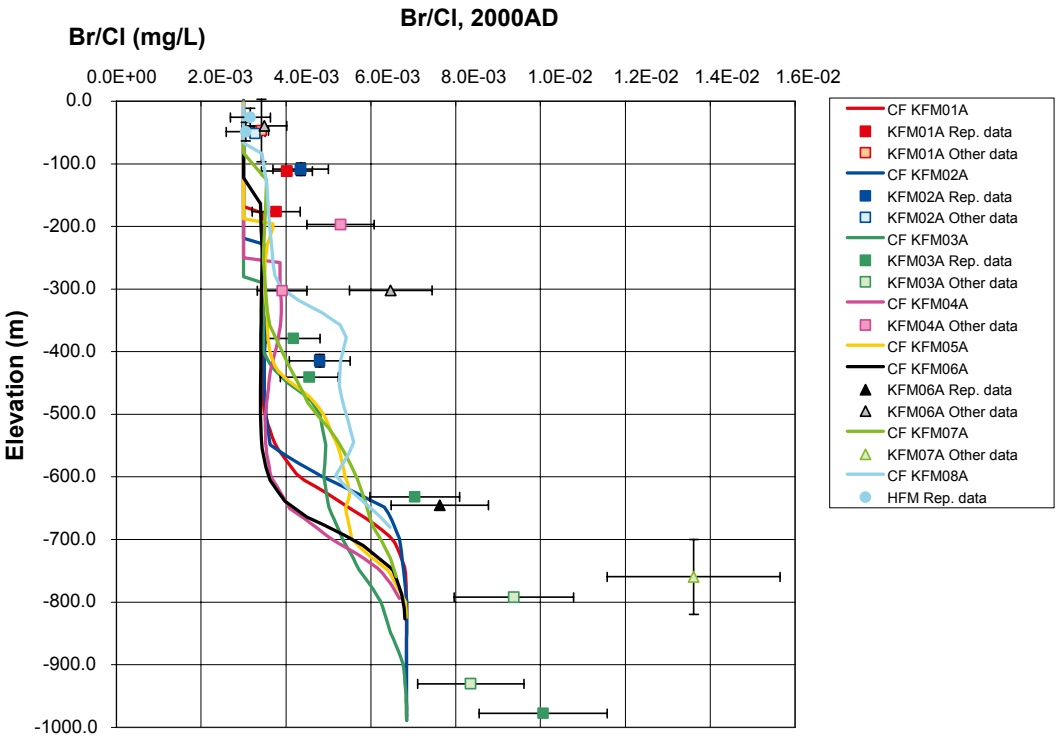

Figure 4-32. *Comparison of Br/Cl with F2.1 data for the ECPM model of individual component transport with a near-surface high T feature ($T=1{\cdot}10^{-3}$ m^2/s) in the foot wall of A2, flow wetted surface 0.16 m^2/m^3, a high $T=1{\cdot}10^{-3}$ m^2/s top 1 m soil layer, and a flux boundary condition on top (Comp_HCD3_AC_HRD3A2_T5foot_FWS_HSD1a_BC2_RefW3).*

4.12 Conclusions

The objectives sought in this study were to achieve a reasonable match to the updated F2.1 hydro-geochemistry data while updating the hydrogeological conceptual model to better reflect the observed site conditions, primarily the hydraulic cage feature. In seeking a match, the approach taken was to vary parameters and settings one at a time so as to understand the behaviour of the system to individual parameters rather than treat the problem as a curve fitting exercise. Based on this, the following findings and suggestions are made:

- A number of improvements to the calibration can be made by varying the composition of the reference waters within the ranges of alternative definitions defined by ChemNet. The alternative Glacial composition based on snow-melt reduces the over-prediction of $\delta^{18}O$. Partly this is just an observation relating to the uncertainty in Glacial water composition, but also may provoke a conceptual debate as to whether Glacial water is actually a mixture of true glacial melt-water and ancient meteoric water originating during or at the end of the last ice age. The use of a “dilute groundwater” for meteoric water improves the match to bicarbonate in particular, and some other ions near surface. This suggests a modification of the composition of meteoric water due to fast reactions with organic material in the very near-surface. The alternative Brine is little different from the original, apart from a lower sulphate composition which would improve the match at large depths for SO_4. The alternative Littorina is based on modern Baltic water. If this were ‘concentrated’ to be of the same salinity as the Littorina and used as a reference water, then it would give some improvement to several ions, but only of the order of 5%, which is not sufficient to account for the discrepancies between modelled and measured ions such as Na.

- The flow-wetted surface, a_r, which controls RMD appears to be constrained by the pore-water Cl to lie in a range of around 0.1–0.16 m^2/m^3, equivalent to a spacing between water conducting fractures of about 12–20 m. These conclusions are subject to some sensitivity to the initial condition assumed. For example, if it were assumed there is some residual Brine left in the system at the beginning of the temperate period, then low values of flow wetted surface are appropriate. Measurements of Br/Cl in the pore-water, if possible, would shed some light on the origin of the salinity in the matrix.
- It is imperative that future calculations be performed with flux type boundary condition, but there remains some uncertainty has to how much of P-E really enters the bedrock. The results suggest a considerable amount of run-off or very near-surface groundwater flow.
- A transmissivity of around $1 \cdot 10^{-3}$ m^2/s for the system of high T horizontal features in the candidate area seems appropriate and coupled with a flux boundary condition gives us optimism for getting a realistic conceptual integration of the surface hydrology, bedrock hydrogeology and hydro-geochemistry.
- Predicted salinity in KFM06A, KFM07A and KFM08A broadly follows the pattern suggested by the entire observed data set, though there is very little data in these boreholes.
- KFM01A and KFM04A give Cl deeper than in the model which is thought to be due to having too high a transmissivity contribution from the DZ's, mainly ZFMNE00A2, in the upper sections of these 2 boreholes. Possibly, the sub-vertical zones ZFMNE1188 and ZFMNW1194 have limited hydraulic significance, and ZFMNE00A2 has too high a transmissivity near the surface.
- The above suggests the hydraulic properties of ZFMNE00A2 are key to the understanding large parts of the site, and so deserves individual analysis.
- Changing the transmissivity in the deformation zones is the key for any calibration exercise as illustrated by the sensitivity of Littorina and Glacial waters to changing the transmissivity of sub-horizontal zones that intersect KFM03A.
- Multiple realisations of the Hydro-DFN give differences that are of sufficient magnitude to suggest multiple realisations should be performed in the latter stages of a calibration, but single realisations are probably sufficient to understand the general sensitivities of the system. They also show that the HRD has very little effect on KFM01A and KFM04A, confirming that it is the HCD that control hydro-geochemistry in these two boreholes.
- It was found difficult to explain the lower levels of Na, higher levels of Ca, and lower levels of Mg in the data relative to the model based on the current conceptual model and considering mixing alone. The only possibility to improve the match for these ions without considering reactive chemistry might be to use a much more complex mixture of reference waters in the initial condition and surface waters, e.g. the water infiltrating from the Baltic has been a mixture of Marine and snow-melt together with some residual Brine in the matrix and low flow wetted surface.
- Changing the initial condition for the Brine/Glacial transition zone in different sub-domains to try to explain the difference between salinity in KFM03A and KFM07A proved hard to sustain such global differences over thousands of years due to the buoyancy force induced by rapid spatial changes in salinity. Hence, the difference in deep salinity distribution between KFM03A and KFM07A is as yet unexplained. Possible hypothesise are that the hydraulic system is very discontinuous and hence compartmentalised, or that the salinity profile measured in KFM03A is a localised feature, and possibly a recent change induce by drilling. More analysis on the fracture connectivity should improve the understanding of the connectivity of the deep roc.
- A finer discretisation improves the match slightly and should be used in future, at least for the upper rock.
- Using Br/Cl ratio to differentiate saline water of ancient Brine origin from that of marine origin has been successful and suggests a transition from marine derived salinity to Brine derived at about –600 m.
- Overall the model predictions for many chemical components has been improved based on the numerical implementation of the new conceptual model described in Chapter 2, and further potential improvements have been demonstrated by exploring sensitivities to the compositions of the reference waters and initial conditions within reasonable bounds.

5 Interference test modelling

The interference test was performed in July 2005 with groundwater abstraction from the percussion drilled borehole HFM01, and monitoring in 13 percussion drilled boreholes and 8 core drilled boreholes. Some monitoring boreholes were packed-off into sections while the rest were open-hole measurements. The test and its interpretation is reported in /Gokall-Norman et al. 2005/. The test lasted about 20 days of pumping before the start of recovery, but unfortunately the test was perturbed by precipitation after about 15 days of pumping. This makes the test more difficult to interpret and model since there are in fact 3 transient processes influencing heads during the test. The first arises because the system is essentially unconfined, and prior to the tests, there had been little precipitation, and so heads were gradually falling in a heterogeneous manner according to hydraulic properties, depth and distance to sea and lakes. The second is the effect of the pumping test reducing heads, and the third is the precipitation event after 15 days causing heads to recover in some boreholes. In theory, the effects unrelated to pumping could have been accounted for and removed from the interpreted response to pumping. However, this was not done in the interpretation by /Gokall-Norman et al. 2005/ which makes a quantitative model calibration with the interpreted drawdowns less exact.

5.1 Visualisation of responses in observation boreholes

Figure 5-1 to Figure 5-3 show the responses to the interference test in the monitoring boreholes. The figures reveal that the drawdown spreads easily within the upper rock to the north, south and west, but is transmitted less well to the east and to depth apart from a moderate response of about 0.1–0.3 m (the higher value based on the drawdown before precipitation) transmitted to the intersection of KFM02A and ZFMNE00A2 at about –500 m elevation and over 1 km away. This suggests some strong heterogeneity in hydraulic properties. The responses appear consistent with the updated conceptual model. Hence, the conceptual model developed in Section 2.3.3 and implemented in Chapter 3 and Chapter 4 was used to illustrate and test the performance of the model in predicting the HFM01 interference test.

5.2 Model simulations

Single-hole interpretations of HFM01 gave a transmissivity at HFM01 over a 168 m section of $7.3 \cdot 10^{-5}$ m^2/s or an average hydraulic conductivity of 4.2 10^{-7} m/s. /Gokall-Norman et al. 2005/ interpreted transmissivities from the transient evaluation of the interference test between different pairs of boreholes of between 2.2 and $4.1 \cdot 10^{-4}$ m^2/s or an average hydraulic conductivity around HFM01 of between 1.3–$2.4 \cdot 10^{-6}$ m/s, which is rather consistent with the geometric mean hydraulic conductivity for the percussion drilled boreholes of $4 \cdot 10^{-6}$ m/s given in Table 3-3. /Gokall-Norman et al. 2005/ give storativities of between 4–$6 \cdot 10^{-5}$, or equivalent to a specific storage coefficient of around $(2–4) \cdot 10^{-7}$ m^{-1}. A quick analysis of the data against a radial flow model yielded a transmissivity of about $3.6 \cdot 10^{-4}$ m^2/s confirming the results of /Gokall-Norman et al. 2005/.

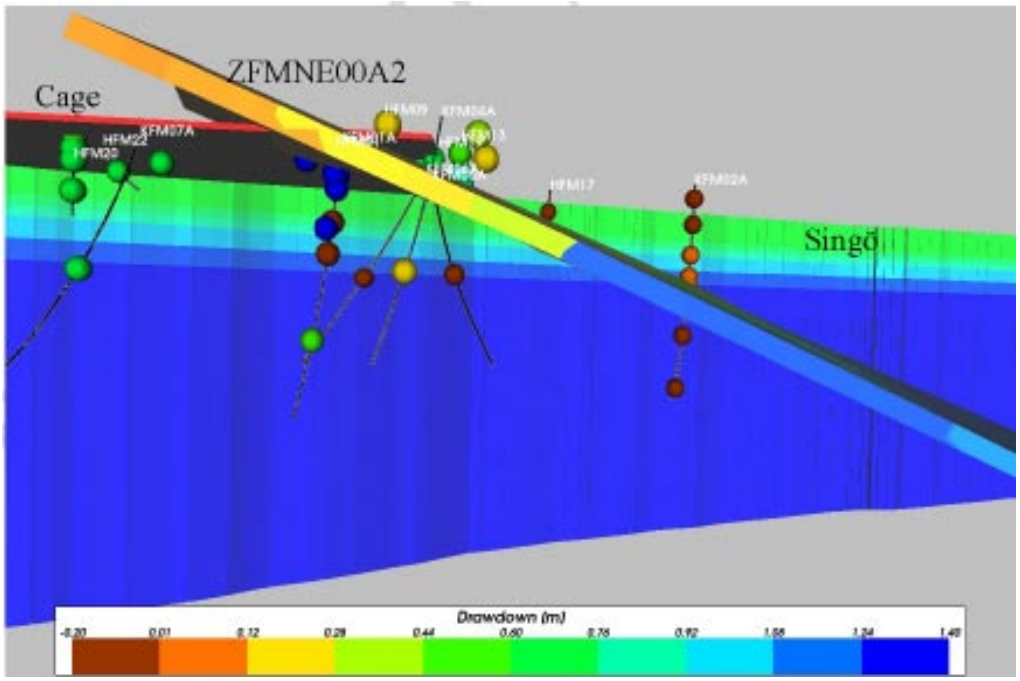

Figure 5-1. *Visualisation of drawdown at end of pumping seen in observation boreholes for a view from the south-west showing the vertical Singö deformation zone, ZFMNE00A2, and the hydraulic cage feature. The drawdowns are shown by spheres coloured by the size of drawdown. The abstraction is at HFM01 in the centre.*

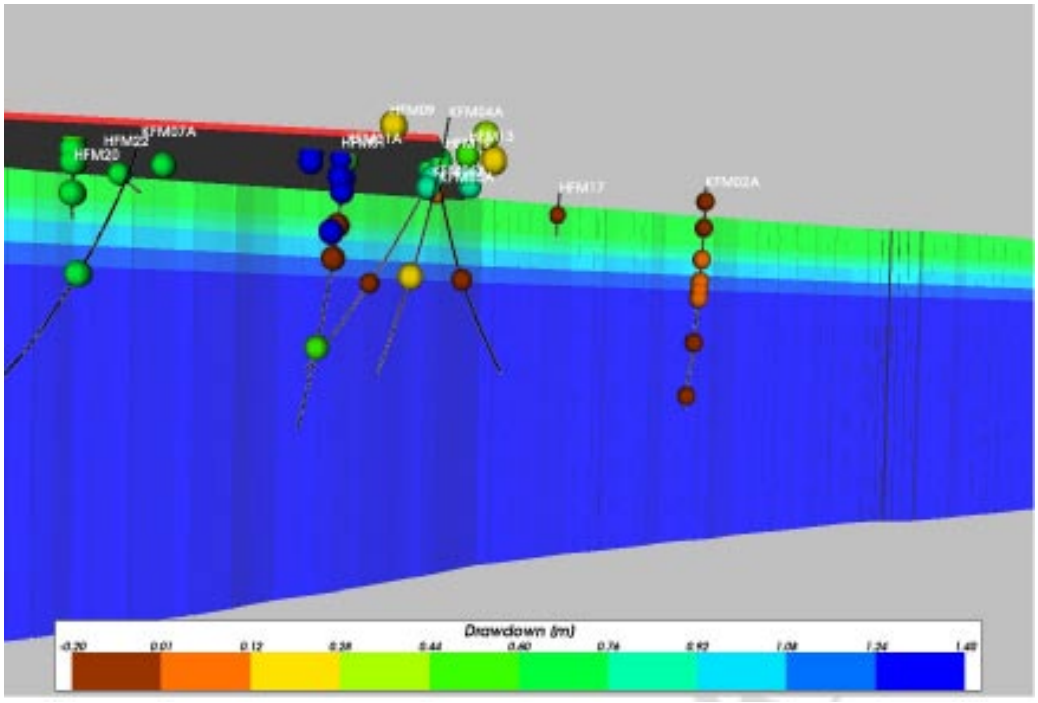

Figure 5-2. *Visualisation of drawdown at end of pumping seen in observation boreholes for a view from the south-west showing the vertical Singö deformation zone, and the hydraulic cage feature. The drawdowns are shown by spheres coloured by the size of drawdown. The abstraction is at HFM01 in the centre.*

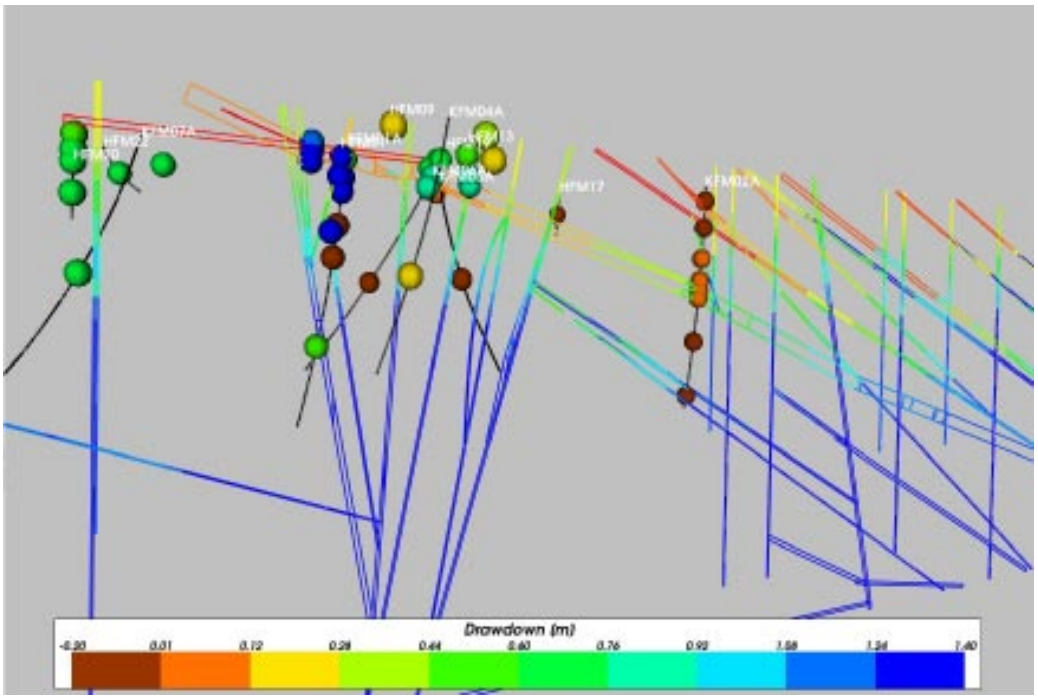

Figure 5-3. *Visualisation of drawdown at end of pumping seen in observation boreholes for a view from the south-west showing a slice through the structural model on a section N115E with DZ's coloured by log transmissivity. The drawdowns are shown by spheres coloured by the size of drawdown. The abstraction is at HFM01 in the centre.*

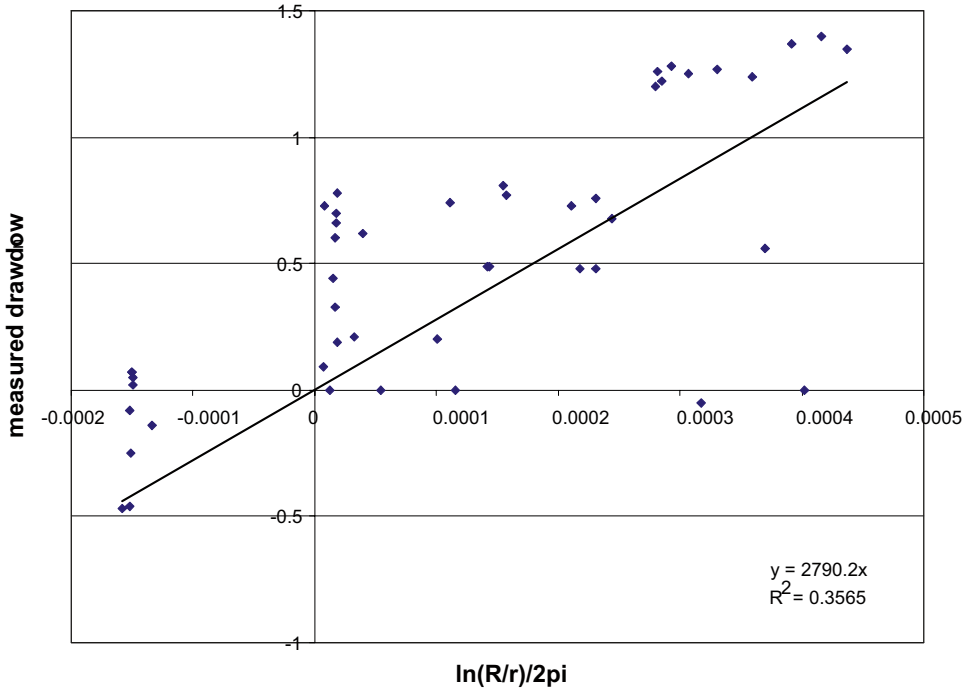

Figure 5-4. *Interpretation of measured drawdown against a radial flow model with radius of influence 1,000 m. Giving a transmissivity of about (3–4)·10^{-4} m^2/s.*

The same model used in Chapter 3 with a 25 m local refinement was used here to simulate the interference test. A number of assumptions had to be made to represent appropriate boundary conditions during the pumping phase as this was found to be an important issue. The initial condition was based on a steady-state calculation with an infiltration of 180 mm/year and no pumping. The boundary conditions were then modified to a much lower infiltration of only 10 mm/year to represent the dry period between the start of pumping and the first 15 days of the test when there was little or no precipitation. Also, pumping was switched on at a flux of 89 L/min which was distributed down the borehole according to the length multiplied by hydraulic conductivity in the elements intersected by the borehole. Transient simulations of the first 15 days of the test were performed to simulate the period prior to precipitation. The models were based on case 'CAGE_SS_HCD3_AC_HRD3A2_T5foot_HSD1a_BC2' from Chapter 3, which has a top 1 m soil layer of $T=1\cdot10^{-3}$ m^2/s, and horizontal cage feature $T=1\cdot10^{-3}$ m^2/s in the foot wall of ZFMNE00A2, although HCD properties were modified slightly based on the best simulation case in Chapter 4, which has a lower transmissivity in 3 DZ's that intersect KFM03A, but this is far from HFM01. The specific storage coefficients derived from some limited calibration of the model were $2\cdot10^{-3}$ m^{-1} in the HSD, and $5\cdot10^{-7}$ m^{-1} in the bedrock. Some initial simulations used fully saturated models which resulted in high flows from the high conductivity soil around the top of HFM01. To avoid this unphysical behaviour, the model was modified to use a Van-Genuchten unsaturated model that effectively 'switches off' finite-elements that become de-saturated by abstraction. A number of cases were considered in the modelling, but only four cases of interest are mentioned here to demonstrate the behaviour of the system. These focussed on varying the contrast in hydraulic properties between the HCD and HRD as shown in Table 5-1.

Examples of the simulated drawdown after 15 days of pumping are shown for the case with a reduced hydraulic conductivity in the HRD in Figure 5-5 to Figure 5-7 for a NW-SE vertical slice and 2 horizontal slices at different depths. It should be noted in these simulations that most of the changes occur due to the pumping at HFM01, but there is also some transient change due to infiltration being drastically reduced to simulate the 'dry period' when the test was performed in July 2005 which also gives a reduction in head around the top of KFM02A where there are several sub-horizontal zones. The simulations show that the drawdown in HFM01 spreads out rapidly along the hydraulic cage feature to the west of ZFMNE00A2, as well as being transmitted rapidly to depth along ZFMNE00A2 to the lower section of KFM02A. The transmission of the drawdown to depth is generally poor except where there are sub-vertical DZ's. These results are generally consistent with the observed drawdown. In the model, the hydraulic cage is limited to a 20 m thick feature centred on an elevation of –25 m this gives an interesting compartmentalisation of the drawdown response as shown in Figure 5-7 for a slice at an elevation of –65 m. In the field, the drawdown distribution spreads out more like that shown in Figure 5-6 to depths of at least 100 m, which suggests the hydraulic cage as made up of several extensive sub-horizontal features in the top 100–200 m. Still, the modelling suggests the right sort of compartmentalisation of the drawdown and the results could be simulated by developing a more realistic representation of the hydraulic cage feature. The case shown here is one with a reduced hydraulic conductivity of 1/10th in the bedrock from base case model. This was found to be important to get a good match; otherwise the pressure pulse was spread out in a more spatial uniform way than suggested by the data. Cross-plots of measured versus modelled drawdowns in the borehole sections for the four cases listed in Table 5-1 are given in Figure 5-8 to Figure 5-11. The best results were obtained with a reduced conductivity in both the HCD and HRD, although it should be remarked that better matches could be obtained by 'fine-tuning' the specific storage also.

Table 5-1. List of cases and simulation names considered in the calibration on the 2005 HFM01 interference test.

Case	Simulation case name
Model based on head and chemistry calibration with unsaturated flow	CAGE_TRANS_HCD3foot_AC_HRD3A2_T5s_HSD1b_BC2_p_SINK
Case with hydraulic conductivity of HRD reduced by 1/10	CAGE_TRANS_HCD3foot_AC_HRD3A2_T5.2s_HSD1b_BC2_p_SINK
Case with hydraulic conductivity of HCD reduced by 1/4	CAGE_TRANS_HCD3.3foot_AC_HRD3A2_T5s_HSD1b_BC2_p_SINK
Case with hydraulic conductivity of HCD reduced by a 1/4 and HRD reduced by 1/10	CAGE_TRANS_HCD3.3foot_AC_HRD3A2_T5.2s_HSD1b_BC2_p_SINK

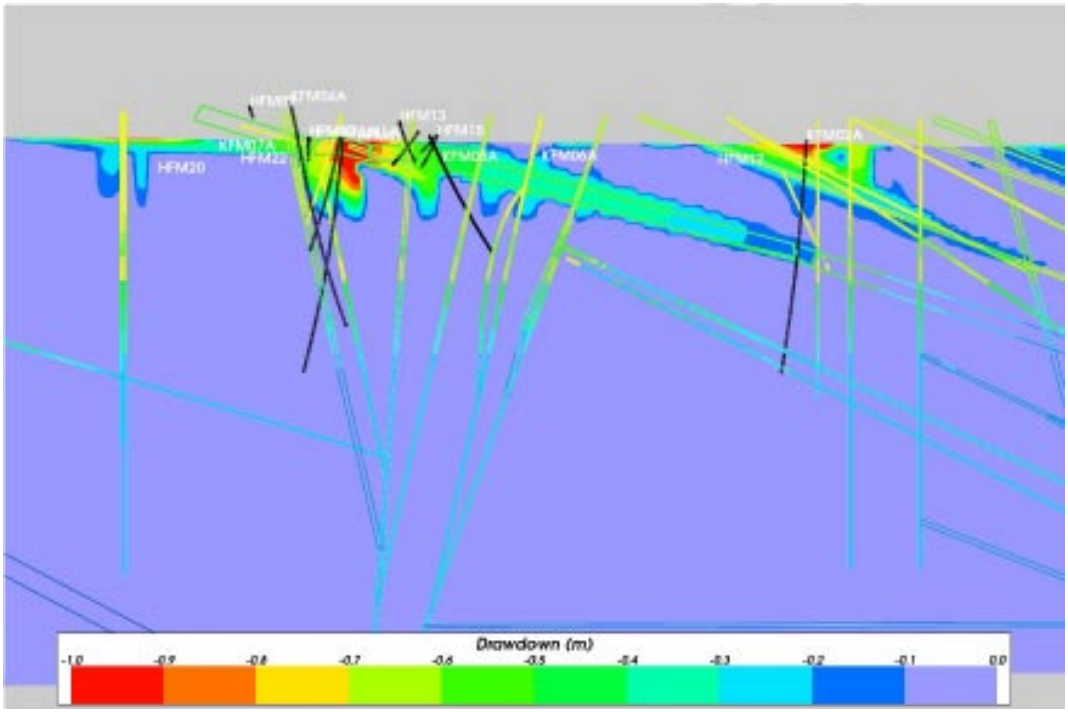

Figure 5-5. *Simulation of drawdown after 15 days created by interference test in HFM01 (and 'dry period') on a NW-SE vertical slice through HFM01 and showing the drawdown transmitted along ZFMNE00A2. Case with lower hydraulic conductivity in HRD (CAGE_TRANS_HCD3foot_AC_HRD3A2_T5.2s_HSD1b_BC2_p_SINK).*

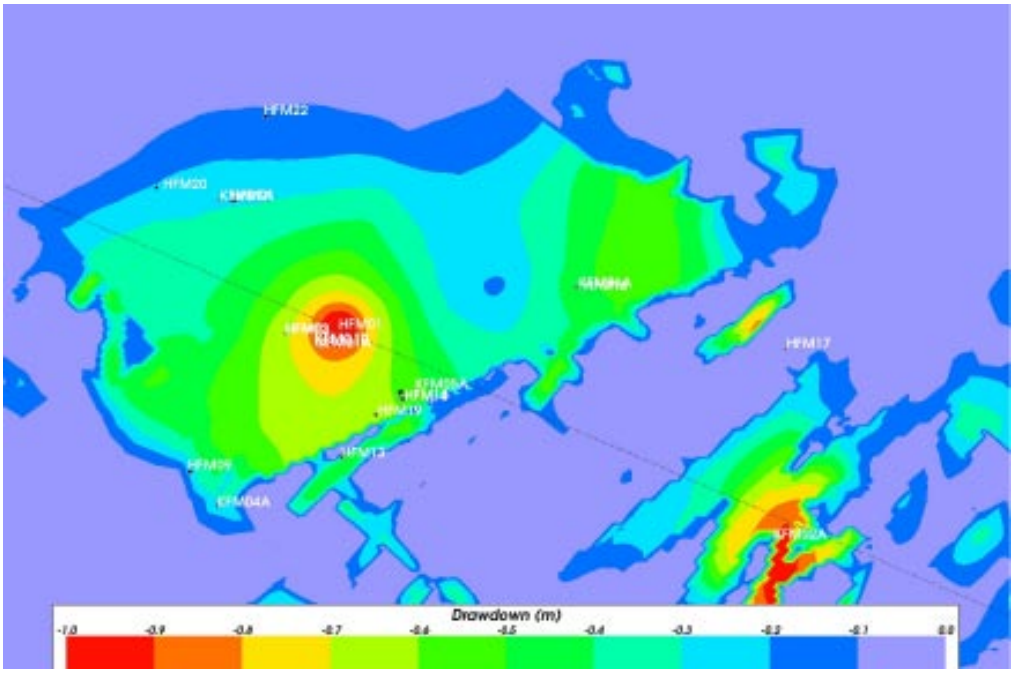

Figure 5-6. *Simulation of drawdown after 15 days created by interference test in HFM01 (and 'dry period') on a horizontal slice at –25 m through the horizontal cage feature and showing the drawdown in the foot wall of ZFMNE00A2. Case with lower hydraulic conductivity in HRD (CAGE_TRANS_HCD-3foot_AC_HRD3A2_T5.2s_HSD1b_BC2_p_SINK).*

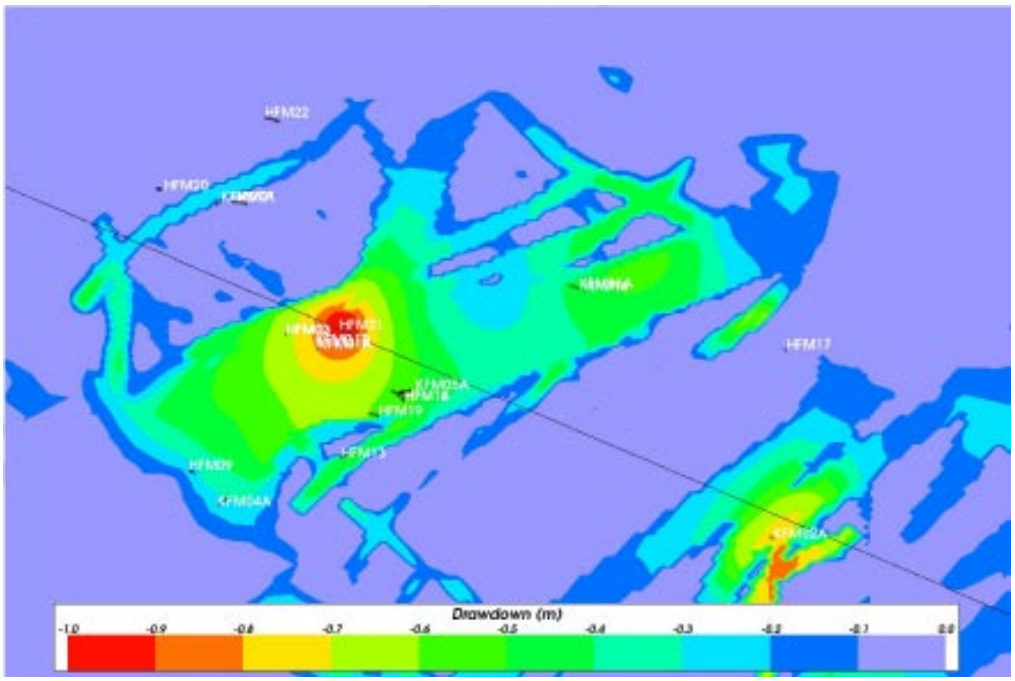

Figure 5-7. *Simulation of drawdown after 15 days created by interference test in HFM01 (and 'dry period') on a horizontal slice at –65 m through the horizontal cage feature and showing the drawdown in the foot wall of ZFMNE00A2. Case with lower hydraulic conductivity in HRD (CAGE_TRANS_HCD-3foot_AC_HRD3A2_T5.2s_HSD1b_BC2_p_SINK).*

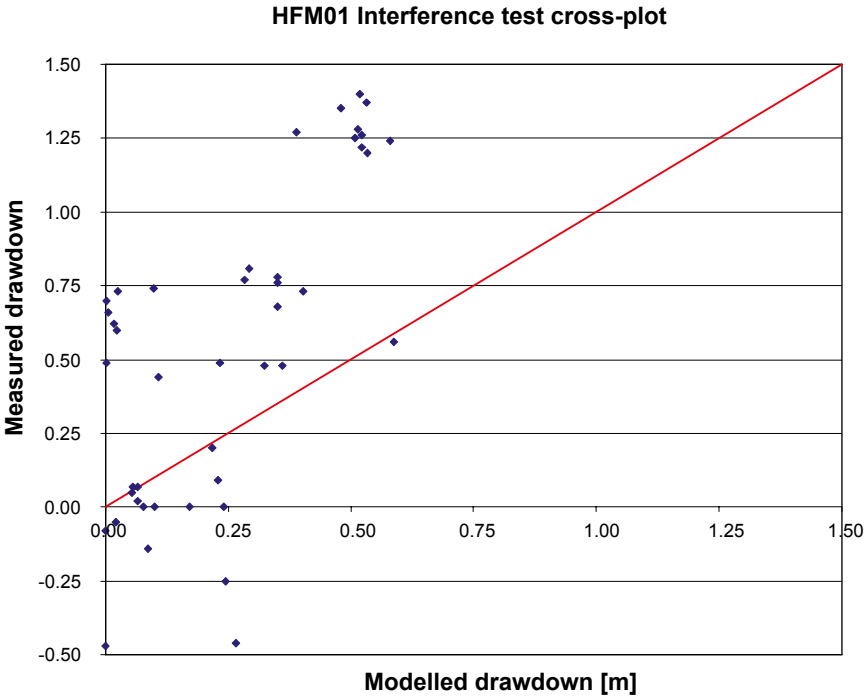

Figure 5-8. *Cross-plot of measured drawdown at the end of pumping versus the modelled drawdown after 15 days in HFM01. Base case (CAGE_TRANS_HCD3foot_AC_HRD3A2_T5s_HSD1b_BC2_p_SINK).*

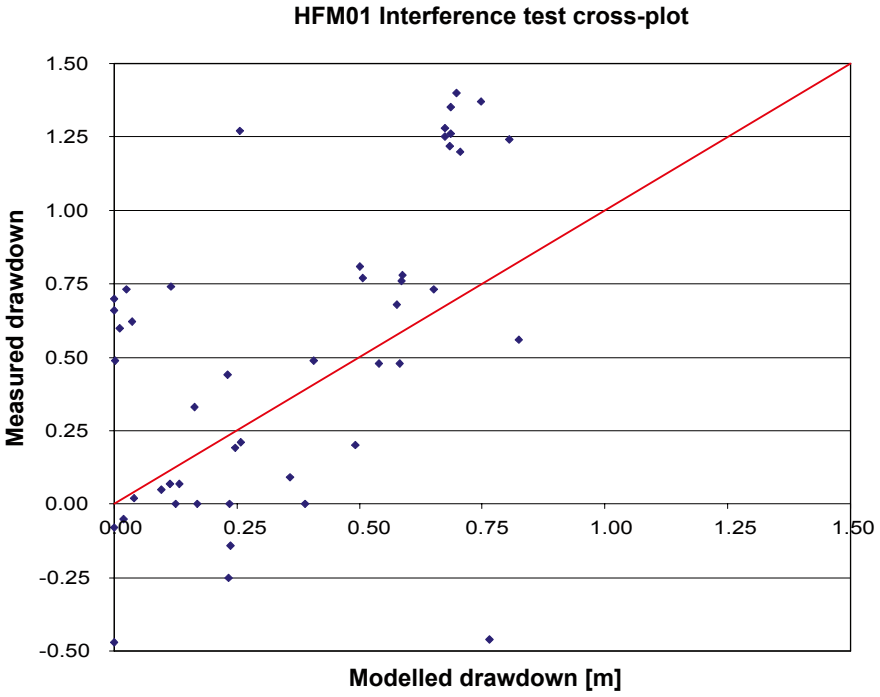

Figure 5-9. *Cross-plot of measured drawdown at the end of pumping versus the modelled drawdown after 15 days in HFM01. Case with lower hydraulic conductivity in HRD (CAGE_TRANS_HCD-3foot_AC_HRD3A2_T5.2s_HSD1b_BC2_p_SINK).*

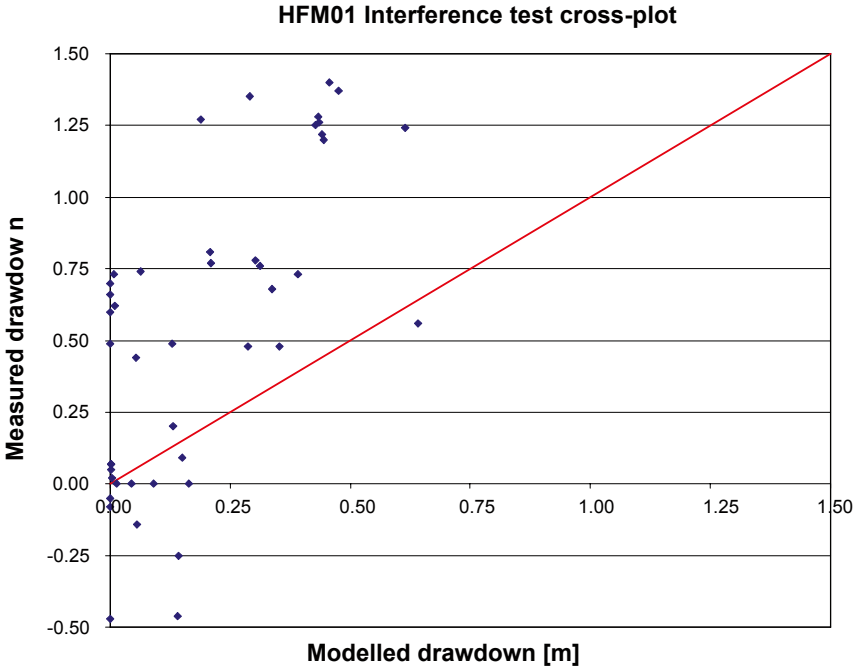

Figure 5-10. *Cross-plot of measured drawdown at the end of pumping versus the modelled drawdown after 15 days in HFM01. Case with lower hydraulic conductivity in HCD (CAGE_TRANS_HCD3.3foot_AC_HRD3A2_T5s_HSD1b_BC2_p_SINK).*

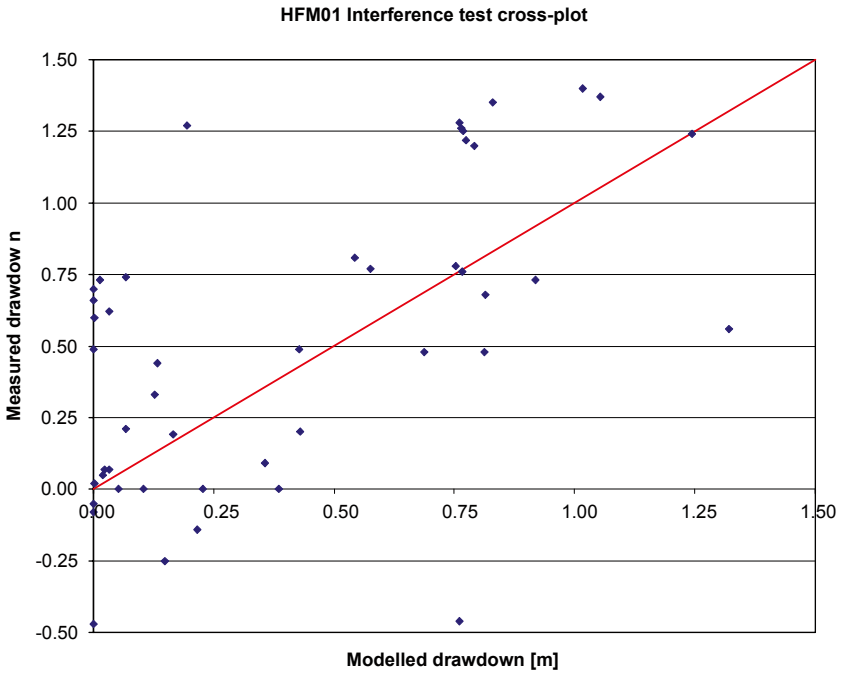

Figure 5-11. *Cross-plot of measured drawdown at the end of pumping versus the modelled drawdown after 15 days in HFM01. Case with lower hydraulic conductivity in HRD and HCD (CAGE_TRANS_HCD3.3foot_AC_HRD3A2_T5.2s_HSD1b_BC2_p_SINK).*

5.3 Conclusions

- One achievement of this study was to show that the same ECPM type model developed for calibrating against near-surface heads and palaeo-hydrogeology could also be used for interpreting the interference test, and therefore demonstrate consistency of the site conceptual model developed in Chapter 2 with disparate forms of site data using a single hydrogeological model, which makes the explanation of how we build confidence more straightforward.
- The values of transmissivities and storativities interpreted here give high hydraulic diffusion coefficients as interpreted in Section 2.3.3, and are of similar magnitude to those interpreted in /Gokall-Norman et al. 2005/. Here, a uniform specific storage coefficient was used of $5 \cdot 10^{-7}$ m^{-1} in the bedrock, for simplicity. In future studies, a specific storage coefficient will be based on summing the fracture storativity within each grid cell over the connected fractures in that cell, and using an empirical relationship between storativity and transmissivity S=function(T).
- It is noted that the interpretation of interference tests should be performed carefully with the aim of removing the effect of any ongoing transient processes such as natural drainage during dry periods or precipitation.
- The transient simulations performed here demonstrate consistency with field data on how pressure disturbances are transmitted. The hydraulic response is dominated by the hydraulic cage feature and the deformation zones, in particular ZFMNE00A2.
- Preliminary results suggest a higher contrast between the deformation zones and background rock than was used in F1.2 to give a very discrete transmission of pressure changes. This needs to be explored in future studies of bedrock properties based on PFL-f, PFL-s and PSS tests in more recent hydraulic tests.

6 References

Berggren M, 1998. Hydraulic conductivity in Swedish bedrock estimated by means of geostatistics, Thesis Report Series 1998:9, Royal Institute of Technology, Stockholm.

Carlsson A, 1979. Characteristic features of a superficial rock mass in southern central Sweden – Horizontal and subhorizontal fractures and filling material. Striae 11.

Darcel C, Davy P, Bour O, De Dreuzy J-R, 2006. Discrete fracture network for the Forsmark site. SKB R-06-79, Svensk Kärnbränslehantering AB.

Edelman J H, 1947. Over de berekening van grondwaterstromingen, Thesis, Technische Hogeschool Delft.

Follin S, Stigsson M, Svensson U, 2005. Regional hydrogeological simulations for Forsmark – numerical modelling using DarcyTools. Preliminary site description Forsmark area – version 1.2. SKB R-05-60, Svensk Kärnbränslehantering AB.

Follin S, Stigsson M, Svensson U, 2007. Sensitivity of the connected open fracture surface area per unit volume to the orientation, size and intensity of Poissonian discrete fracture network (DFN) models. SKB R-07-28, Svensk Kärnbränslehantering AB.

Gentzschein B, Levén J, Follin S, 2006. A comparison between well yield data from the site investigation in Forsmark and domestic wells in northern Uppland. SKB P-06-56, Svensk Kärnbränslehantering AB.

Gokall-Norman K, Ludvigson J-E, Jönsson S, 2005. Hydraulic interference test in borehole HFM01. Forsmark site investigation. SKB P-05-236, Svensk Kärnbränslehantering AB.

Hartley L, Hoch A, Hunter F, Jackson P, Gylling B, Marsic N, 2005. Regional hydrogeological simulations – Numerical modelling using CONNECTFLOW, Preliminary site description Simpevarp subarea – version 1.2. SKB R-05-12, Svensk Kärnbränslehantering AB.

Hartley L, Hoch A, Jackson P, Joyce S, McCarthy R, Rodwell W, Marsic N, 2006a. Groundwater flow and transport modelling during the temperate period for the SR-Can assessment – Forsmark area – version 1.2. SKB R-06-98, Svensk Kärnbränslehantering AB.

Hartley L, Cox I, Hunter F, Jackson P, McCarthy R, Gylling B, Marsic N, 2006b. Regional Hydrogeological Simulations– Numerical Modelling Using CONNECTFLOW, Preliminary site description, Laxemar subarea – version 1.2. SKB R-06-23, Svensk Kärnbränslehantering AB.

Juston J, Johansson P-O, Levén J, Tröjbom M, Follin S, 2007. Analysis of meterological, hydrological and hydrogeological monitoring data. SKB R-06-49, Svensk Kärnbränslehantering AB.

La Pointe P, Olofsson I, Hermanson J, 2005. Statistical model of fractures and deformation zones for Forsmark. Preliminary site description Forsmark area – version 1.2. SKB R-05-26, Svensk Kärnbränslehantering AB.

Larsson-McCann S, Karlsson A, Nord M, Sjögren J, Johansson L, Ivarsson M, Kindell S, 2002. Meteorological, hydrological and oceanographical information and data for the site investigation program in the communities of Östhammar and Tierp in the northern part of Uppland. SKB TR-02-02, Svensk Kärnbränslehantering AB.

Levén J, Carlberg T, Follin S, 2006. Compilation and visualisation of cross discipline borehole data using WellCad. SKB P-06-55, Svensk Kärnbränslehantering AB.

Ludvigson J-E, Jönsson S, 2003. Hydraulic interference tests. Boreholes HFM01, HFM02 and HFM03. Forsmark site investigation. SKB P-03-35, Svensk Kärnbränslehantering AB.

Påsse T, 1997. A mathematical model of past, present and future shore level displacement in Fennoscandia. SKB TR-97-28, Svensk Kärnbränslehantering AB.

Rhén I, Bäckblom G, Gustafson G, Stansfors R, Wikberg P, 1997. Äspö HRL – Geoscientific evaluation 1997/2. Results from pre-investigations and detailed characterisation, Summary report. SKB TR-97-03, Svensk Kärnbränslehantering AB.

SKB 2004. Preliminary site description Forsmark area – version 1.1. SKB R-04-15, Svensk Kärnbränslehantering AB.

SKB 2005a. Preliminary site description Forsmark area – version 1.2. SKB R-05-18, Svensk Kärnbränslehantering AB.

SKB 2005b. Preliminary safety evaluation for the Forsmark area based on data and site descriptions after the initial site investigation stage. SKB TR-05-16, Svensk Kärnbränslehantering AB.

SKB 2005c. Preliminary site description Simpevarp subarea – version 1.2. SKB R-05-08, Svensk Kärnbränslehantering AB.

SKB, 2006a. Site descriptive modelling Forsmark stage 2.1 – Feedback for completion of the site investigation including from safety assessment and repository engineering. SKB R-06-38, Svensk Kärnbränslehantering AB.

SKB 2006b. Long-term safety for KBS-3 repositories at Forsmark and Laxemar – a first evaluation, Main report of the SR-Can project. SKB TR-06-09, Svensk Kärnbränslehantering AB.

SKB 2006c. Hydrogeochemical evaluation of the Forsmark site, modelling stage 2.1 – issue report. SKB R-06-69, Svensk Kärnbränslehantering AB.

SKB 2006d. Preliminary site description Laxemar subarea – version 1.2. SKB R-06-10, Svensk Kärnbränslehantering AB.

SKI 2005. Need for Confirmatory Testing of Upscaled Flow and Transport Models, INSITE Report TRD-05-08, Statens Kärnkraftsinspektion.

Streltsova T D, 1988. Well testing in heterogeneous formations. John Wiley & Sons.

Waber H N, Smellie J, 2005. Borehole KFM06A characterisation of pore water. Part I: Diffusion experiments, Forsmark site investigation. SKB P-05-196, Svensk Kärnbränslehantering AB.

Werner K, Johansson P-O, Brydsten L, Bosson E, Berglund S, Tröjbom M, Nyman H, 2007. Recharge and discharge of near-surface groundwater in Forsmark. Comparison of classification methods. SKB R-07-08, Svensk Kärnbränslehantering AB.

Westman P, Wastegård S, Schoning K, Gustafsson B, Omstedt A, 1999. Salinity change in the Baltic Sea during the last 8,500 years: evidence, causes and models. SKB TR-99-38, Svensk Kärnbränslehantering AB.